## *Rovibrational, excitation of molecules by atoms*

Kirkpatrick, D. J. O.

# ROVIBRATIONAL EXCITATION OF MOLECULES BY ATOMS

by

D.J.O. KIRKPATRICK, B.Sc.



A thesis submitted to the University of Durham for the Degree of Doctor of Philosophy

JANUARY, 1983

ACKNOWLEDGEMENTS

I wish to express my sincere gratitude to my supervisor, Dr. D.R. Flower, for his guidance, assistance and encouragement throughout my graduate studies. I would also like to thank Prof. B.H. Bransden for accepting me as a graduate student at Durham, and for his interest in this work and the benefit of his knowledge and experience on numerous occasions.

I am grateful to all those who have assisted me during this work, in particular Drs. D. Dewangan, C. Noble, R. Shingal, T. Scott and J.V. Major and my fellow graduate students, G. Danby and C. Newby, for many helpful discussions and advice.

I would also like to thank the SERC for the provision of a studentship, and of the grant which made possible the use of the CRAY-1 computer.

Finally, I am very grateful to Mrs. M. Chipchase for her efficient and patient typing of the manuscript.

## ABSTRACT

The results of close coupling (CC) and infinite order sudden (IOS) approximation calculations of cross sections for rovibrational excitation of both para and ortho $H_2$ by He are presented. Large discrepancies are found between the present CC results and those of Lin and Secrest (1979) and Lin (1979). The $v = 0 \rightarrow 1$ vibrationally inelastic cross sections are found to differ from those of Lin by factors attaining four orders of magnitude close to the $v = 1$ excitation threshold. Also, structure in the variation of both vibrationally elastic and inelastic cross sections with energy, reported by Lin and Secrest, and Lin, is absent in the present results.

The present CC results are found to be in good quantitative agreement with the coupled states calculations of Alexander and McGuire (1976). Agreement with the IOS calculations is only qualitative but improves with increasing collision energy, consistent with the progressive failure of the energy sudden component of the IOS approximation as the collision energy falls.

The values of the vibrational relaxation rate coefficient calculated from the CC results fall below the experimental data of Audibert et al. (1976) at low temperature. This is most probably due to the relatively poor description of the $H_2$ + He system employed, in particular the interaction potential of Gordon and Secrest (1970).

The CC results are employed to investigate the accuracy of two energy sudden factorisation schemes. The factorisation which includes off-energy-shell effects is shown to be more

accurate than that which does not. However, neither scheme produces cross sections which obey detailed balance.

The present IOS results are in good agreement with the adiabatic distorted wave IOS calculations of Bieniek (1980) at low energy. However, as the collision energy increases significant discrepancies appear. For $H_2$ + He it appears that at energies sufficiently high for the IOS approximation to be valid the use of adiabatic distorted wave techniques is not valid.

Exploratory IOS calculations of rovibrational excitation of $H_2$ by $H^+$ are reported and discussed. There appears to be evidence that the comparison between theoretical and experimental values of rovibrational cross sections presented by Schinke et al. (1980) and Schinke (1980) is distorted by their restricted numerical methods and faults in their basis wavefunctions.

CONTENTS

# CHAPTER I

# INTRODUCTION

## 1. Molecular Processes in Astrophysics

Astronomical observations have established that a significant amount, and considerable variety, of molecular species are contained in the interstellar medium. Although some molecules have been discovered by their absorption of visible (CH, $CH^+$ and CN) or ultraviolet ($H_2$ and CO) starlight, by far the majority have been detected in the radio region of the spectrum, usually in emission. The molecules are generally found in comparatively dense, extended regions. Also, the most dense molecular clouds are regions of active star formation. Molecular processes are not only important in the evolution of these clouds, but also offer a means of determining their composition and physical conditions (temperature, density, etc.).

The abundance of a given molecular species represents the competition between the chemical processes responsible for its formation and destruction. Formation of a molecule by collisions between atoms requires that energy must be carried away by a third party, in order to form a bound state. In the low densities present in the interstellar gas a three-body collision is extremely improbable. However, in radiative association, the energy is carried away by an emitted photon. There is also the role played by interstellar dust grains. Although these grains are probably chemically inert, molecular reactions may occur on these surfaces at essentially every collision between a grain and an atom. The destruction of interstellar molecules is due to the absorption of photons.

Direct photodissociation can occur when the energy of the photon is larger than the binding energy of the molecule. However lower energy photons can produce dissociation by exciting the molecules to an intermediate state which subsequently dissociates (such as in predissociation, spontaneous radiative dissociation and photoionisation). The various processes responsible for the formation and destruction of interstellar molecules, and the relative importance of each, are discussed in the reviews of Dalgarno (1975) and Watson (1974).

The only available information about these regions is their spectra, i.e. the radiation added to or subtracted from the radiation field along the line of sight. The spectra will be determined by the spontaneous emission and absorption of photons by the molecules, caused by their interaction with the radiation field (see e.g. Green (1974)). However, if the cloud is in equilibrium with a radiation field, the number of photons emitted will equal the number absorbed. Therefore, no spectral lines will be observed, since there is no net gain or loss of photons along the line of sight. The energy transfer mechanism which disturbs this equilibrium by causing transitions is molecular collisions. The actual spectra observed will depend on the relative rates of collisional and radiative processes occurring in the clouds, which in turn depend on the cloud's composition and physical conditions. Therefore, if we have sufficient knowledge of the processes of spectral line formation, this can be used in conjunction with the observed spectra to infer the physical conditions present in the clouds.

The temperature in molecular clouds is generally $\lesssim$ 100K. At such low temperatures, collisional excitation of vibrational levels (other than the ground state) is extremely improbable. For example, the energy separation between the ground and first excited vibrational state of $H_2$ corresponds to a temperature of $\simeq$ 5000K. However, excited vibrational levels can be populated by the passage of a shock wave, where the density and temperature are high for a short time (Aannestad and Field (1973), Hollenbach and Shull (1977)). Another mechanism is by absorption of high energy photons (Black and Dalgarno (1976)). There is also the possibility that the process responsible for the formation of the molecules may produce highly excited rovibrational states. However the formation process occurs only once during the lifetime of the molecule , whereas the other excitation processes would be expected to occur more frequently. Such excitation processes produce differing energy level populations, and hence the relative intensities of the observed spectral lines can be employed to infer which process is most likely to have caused the vibrational excitation (see e.g. Gautier et al. (1976)). If a shock wave is responsible for the excitation, the location of the vibrational emission region can help to determine the origin of the shock. Also, details of the emission spectra can establish the velocity of propagation of the shock wave (see e.g. Simon et al. (1979)).

Interstellar clouds lose energy by the conversion of kinetic energy into energy of excitation of the cloud constituents. The excited atoms and molecules subsequently emit photons which eventually escape from the cloud. Rotational transitions in molecules play an important role in such

cooling processes. Also, various atomic and molecular processes, involving the absorption of interstellar ultraviolet radiation, are important sources of heat in the clouds, along with other sources such as cosmic rays and the dissipation of turbulence. Full accounts of the various processes responsible for the cooling and heating of interstellar clouds are presented by Dalgarno and McCray (1972), Field (1974) and Flower (1983).

Cooling and heating processes will develop various thermal and pressure gradients which effect the dynamical evolution of the cloud and may indeed trigger its collapse to the point where star formation occurs.

Rovibrational excitation cross sections are required not only to interpret the observed molecular spectra, but also to derive the energy loss from molecular clouds. A good, overall view of molecular processes in interstellar clouds is presented by Dalgarno (1975).

## 2. Cross Sections and Rate Coefficients

The probability that a molecule will change energy levels by energy transfer during a collision, and that the projectile will be scattered in a given direction, is expressed in terms of a differential cross section. This will depend on the initial ($\gamma$) and final ($\gamma'$) quantum numbers of the transition and also on the relative collision velocity $\underset{\sim}{v}$. If we take the origin of co-ordinates at the target and consider the projectile approaching along the z-axis (Figure 1) the differential cross section for a collision velocity $\underset{\sim}{v}$, is given by

$\frac{d\sigma}{d\Omega}(\gamma \to \gamma'; \theta, \phi | v)$ = (number of particles giving rise to transitions $\gamma \to \gamma'$ deflected into solid angle $d\Omega(\theta, \phi)$, per unit time, per unit flux)

which has the units of area. I.2.1

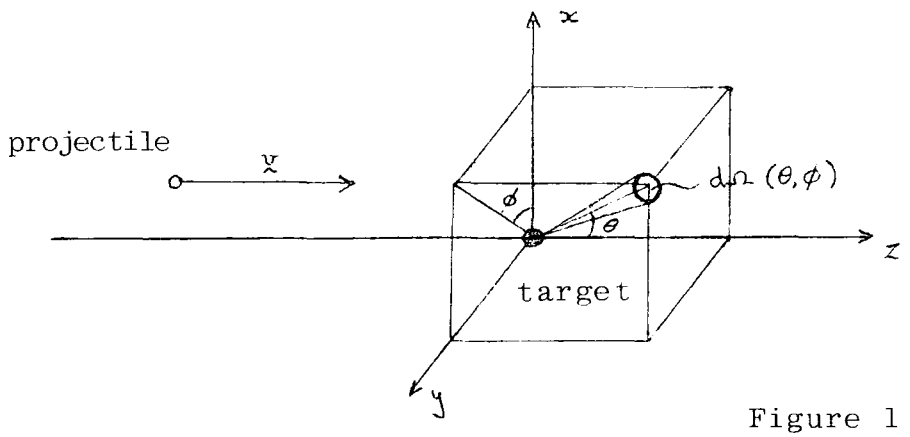


Figure 1

The experimental determination of differential cross sections is not generally performed in the centre of mass reference frame (for example, the target may be at rest). To compare experiment with theory it is necessary to convert what is actually observed in the laboratory frame to what would have been observed in the centre of mass frame. Since the observation of scattered flux is done with macroscopic apparatus this is a purely classical problem.

The total (or integrated) cross section is the integral of the differential cross section over all angles

$$\sigma(\gamma \to \gamma' | v) = \int \frac{d\sigma}{d\Omega}(\gamma \to \gamma'; \theta, \phi | v)\, d\Omega \qquad \text{I.2.2}$$

which also has the units of area. The total cross section is the total number of particles deflected into any angle per unit flux, per unit time, which cause transitions $\gamma \to \gamma'$.

Since unit flux is one particle per unit area, per unit time, the total cross section represents the effective area presented by the target which gives rise to transitions $\gamma \rightarrow \gamma$. Similarly, the differential cross sections $\frac{d\sigma}{d\Omega}(\gamma \rightarrow \gamma'; \theta, \phi | v)$ is the effective area of the target which gives rise to transitions $\gamma \rightarrow \gamma'$ and deflections into the solid angle $d\Omega(\theta, \phi)$. If we construct a circular region of area $\sigma(\gamma \rightarrow \gamma' | v)$ at the target and perpendicular to the projectile - target relative velocity, then a transition will occur if and only if the projectile passes through this circle (Figure 2).

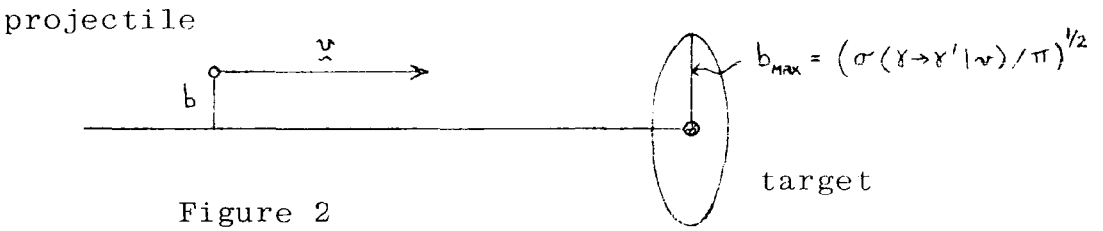


Figure 2

The cross section defines an effective interaction radius, $b_{max}$, such that a transition $\gamma \rightarrow \gamma'$ will occur if the projectile approaches closer to the target than $b_{max}$.

The rate at which transitions $\gamma \rightarrow \gamma'$ occur is given by the flux of particles through the area $\sigma(\gamma \rightarrow \gamma' | v)$

$$k_{\gamma \rightarrow \gamma'}(v) = n v \sigma(\gamma \rightarrow \gamma' | v) \qquad \text{I.2.3}$$

where n is the number density of the projectiles. In general, there will be a distribution of collision velocities $f(v)$, hence

$$k_{\gamma \rightarrow \gamma'} = n \int_0^\infty v \sigma(\gamma \rightarrow \gamma' | v) f(v) dv \qquad \text{I.2.4}$$

The usual form of $f(v)$ is the Maxwell velocity distribution at temperature T

$$f(v) \equiv f(v,T) = 4\pi\left(\frac{\mu}{2\pi kT}\right)^{3/2} v^2 \exp\left(-\mu v^2/2kT\right) \qquad \text{I.2.5}$$

where $\mu$ is the reduced mass of the collision and k is Boltzmann's constant. Using $E = \frac{1}{2}\mu v^2$, we can obtain the expression in terms of an averaging over E, the initial collision energy of the system in molecular state $\gamma$ . Taking n = 1, this gives

$$k_{\gamma\to\gamma'}(T) = \left(\frac{8kT}{\mu\pi}\right)^{1/2}\left(\frac{1}{kT}\right)^2 \int_0^\infty E\,\sigma(\gamma\to\gamma'|E)\exp\left(-E/kT\right)dE \qquad \text{I.2.6}$$

## 3. Experimental Determination of Cross Sections

The experimental determination of cross sections consists of basically two complementary categories of experiment - molecular beam and bulk relaxation experiments. Molecular beam experiments can measure particular state to state rovibrational cross section but are limited by technical difficulties. Many of these limitations are not encountered in bulk relaxation experiments, however such techniques can only measure rate constants.

In a molecular beam scattering experiment, two beams of particles intersect each other. The pressure in the beams and apparatus is kept very low ( $\sim 10^{-6}$ torr) so that the two beams do not undergo collisions except in the region of intersection. A detector, which can be rotated about this scattering region, measures the intensity of the scattered particles as a function of the scattering angle. Essentially there are two different techniques which can be employed to

detect inelastic scattering; state-selection and energy change methods. In an ideal state-selection experiment the molecules are prepared in a definite quantum state before scattering and then analysed in their final state by an appropriate filter which permits only molecules in the desired state to reach the detector. Such experiments use the focussing properties of electric fields but, however, are only applicable in special cases, such as TF$\ell$, which has a large dipole moment. Alternatively, various spectroscopic techniques can be employed to measure the distribution of states before and after the collision. However, in this case there are difficulties in the interpretation of the data. In contrast, the energy change method is universally applicable, although the resolution is not so high. In this method the inelastic events are detected indirectly by making use of energy conservation. If both beams are monoenergetic and well collimated, then the conversion of translational to internal energy in an inelastic collision will result in a change in the relative velocity. This can be observed by a small change in the laboratory velocity of both scattered particles. The intensity of molecules with an altered velocity is then a measure of the inelastic cross section.

Beam scattering experiments in their present state of development suffer from several disadvantages. State-selection experiments are only applicable to special cases and the lower resolution of energy change methods makes the measurement of state to state rovibrational cross sections extremely difficult, esepcially for neutral beams. The use

of ions in molecular beam experiments has the significant advantages that they are easily accelerated to high energies, where vibrational excitation occurs, and are also easily energy analysed and detected. Therefore beam experiments can resolve individual rovibrational cross sections in systems such as $H_2 + H^+$, due to the large rotational constant of $H_2$ and the ease of detection and energy analysis of $H^+$. Also beam experiments are only sensitive to fairly large transition probabilities of the order of 1%, whereas at ordinary temperatures, vibrational transitions may be determined by probabilities of the order of $10^{-4}$.

The limitations of beam experiments are not encountered in bulk relaxation experiments. Relaxation experiments have the common feature of disturbing a system from its equilibrium distribution and measuring the rate of return to equilibrium. Examples of such experiments are laser Raman excitation, sound absorption, nuclear magnetic resonance spin-lattice relaxation and double-resonance spectral techniques.

In laser Raman excitation, Raman active molecules are stimulated by a short laser pulse to the first vibrational level in a low temperature gas cell. As the molecules relax to the ground state via collisions there is a small temperature increase of the order of a few degrees, which leads to a density change which can be monitored. This method has the advantage that non-polar molecules (e.g. $N_2$ and $H_2$) can be excited into a defined vibrational state in a low temperature bath.

In sound absorption experiments the attenuation of ultrasonic waves is measured as a function of distance travelled in a gas. Part of this attenuation comes from converting

translational energy into internal rovibrational molecular energy, and hence rate coefficients can be measured.

In nuclear magnetic spin-lattice relaxation, a non-thermal distribution of nuclear spin states is created by magnetic fields and pulses of resonant radiofrequencies. The rate of return to equilibrium is then monitored. The return to equilibrium occurs mainly by the coupling of nuclear spin and molecular rotation. Therefore collisions which change the rotational state will also thermalise the nuclear spin states, and one measures the rotational relaxation rates weighted by the coupling constants, which are known.

In double resonance a non-thermal distribution of rotational states is established by pumping with strong radiation at a resonant frequency which disturbs the populations of the resonant levels. This anomalous distribution is then transferred to other levels by collisional excitation. The resulting variation in the populations of other levels is detected by noting the change in intensity in other transitions. These changes in intensity are related to the relative rates of collisional transfer between all the levels.

An account of these and other experimental methods for the measurement of rovibrational cross sections and rate constants is given in the reviews of Oka (1973) and Toennies (1976).

## 4. Theoretical Determination of Cross Sections

The calculation of rovibrational cross sections requires the solution of the Schrodinger equation describing the collision. This calculation is simplified by use of the Born-Oppenheimer approximation which uncouples nuclear and

electronic motion. The electrons are much lighter than the nuclei and therefore move much more rapidly so that we may expect them to adiabatically adjust to the instantaneous position of the nuclei. Therefore, the calculation divides conveniently into two separate problems - determination of the interaction potential due to the electronic motion, and calculation of the collision dynamics of the nuclei on this potential surface.

(a) Interaction Potential

The interaction potential between an atom A and a diatomic molecule BC, approximated as a vibrating rotor, is given by

$$V(\underset{\sim}{R},\underset{\sim}{r}) = E_{A+BC}(\underset{\sim}{R},\underset{\sim}{r}) - E_{BC}(r) - E_A \qquad \text{I.3.1}$$

Where $\underline{R}$ is the position vector of atom A relative to the centre of mass of the molecule BC, and $\underline{r}$ lies along the internuclear axis of BC. $E_{A+BC}(\underline{R}, \underline{r})$ is the total electronic energy of the total system for position vectors $\underline{R}$ and $\underline{r}$, and $E_{BC}(r)$ and $E_A$ are the total energies of the isolated molecule and atom (i.e. for $R = \infty$ ).

Interaction potentials manifest themselves in a variety of static and dynamic phenomena, such as equilibrium structure of solids, sound absorption in gases, etc. Measurement of such phenomena can be used to experimentally determine interaction potentials. However, such methods rely on comparing experimental observations with predictions based on model potentials. Such models are necessarily inflexible and different experiments tend to sample different parts or averages of the potential. It is often found that a potential

which fits one type of experimental data is inadequate for another (see e.g. Shafer and Gordon (1973)).

The theoretical determination of interaction potentials is the quantum mechanical problem of calculating the total energy of the collection of nuclei and electrons of A and BC. Since the electronic motion is much faster than the nuclear motion, this reduces to determining the electronic energy as a function of fixed nuclear geometry (Born-Oppenheimer approximation). The major contributions to the energy are the kinetic energy of the electrons and the Coulomb interactions among the electrons and nuclei. Since the interaction energy is the difference between the total energy of the combined systems and that of the isolated systems, this can lead to large cancellations and subsequent loss of accuracy. In discussing the calculation of interaction potentials it is convenient to distinguish between long range, short range and intermediate distances.

At large distances, A and BC can be described as non-overlapping charge distributions, and the interaction reduces to the electrostatic problem of interacting permanent and induced multipole moments. This potential consists of three terms - the electrostatic energy due to the interaction of permanent multipole moments, the induction energy, due to the interaction of permanent moments with those induced in the other collision partner, and the dispersion energy. The dispersion energy is due to the correlation of electron motions and is especially important in neutral systems (i.e. no permanent multipole moments) where it is responsible for

the Van der Waals minimum. This long range potential will depend on the multipole moments and polarisabilities of the collision partners. Because the interaction is weak, it can be accurately represented as a perturbation of the separated systems. The interaction energy can then be calculated directly by perturbation techniques, avoiding the problem of cal-cellation.

At small distances, the A and BC charge distributions overlap strongly and the interaction becomes repulsive. In this region, the system is best described as a single molecule and molecular orbital techniques such as the Hartree-Fock method are applicable. In the Hatree-Fock, or self con-sistent field method, each electron is considered to move in the electrostatic field created by the other electrons. However to describe the motion of one electron requires solutions for all the other electrons which determine the electrostatic field. In practise, a reasonable guess is made at the solutions and these are used in the Hartree-Fock equations to produce new solutions which become the next initial guess. This process is repeated until the solutions are the same as the input - hence the name self consistent field.

The wavefunctions of the electrons, or orbitals, are expanded in some suitable set of basis functions. For molecular systems, orbitals centred on the various atoms are frequently employed. Hence the frequent notation SCF-LCAO for self consistent field-linear combination of atomic orbitals. Often, such LCAO are formed into molecular orbitals - hence the notation SCF-LCAO-MO.

The Hartree-Fock method does not allow for the instantaneous correlation of electron motions. The resulting contribution to the energy is called correlation energy. However, at short distances the correlation energy is much smaller than the electrostatic, hence the Hartree-Fock method is reliable.

At intermediate distances the long range attractive forces and the short range repulsive forces compete to form a potential well, and this is the most difficult region for which to obtain accurate interactions. The long range perturbation techniques fail as the charge distributions begin to overlap. Molecular orbital methods become unreliable because the correlation energy is comparable to the electrostatic interaction and varies rapidly with distance as the orbitals change from molecular to atomic in nature. Indeed, the dispersion energy, responsible for Van der Waals minima in neutral systems, is due entirely to correlation effects. In Hartree-Fock methods only one set, or configuration, of molecular orbitals is employed. However, in configuration interaction techniques, the wavefunctions employed are linear combinations of possible configurations, hence allowing a better description of the wavefunctions as they change from molecular to atomic. Such configuration interaction techniques explicitly take into account correlation effects. However, configuration interaction calculations require roughly an order of magnitude more computer time than a Hartree-Fock calculation. The configuration interaction method is also accurate at short and long range, although at long range ( $\gtrsim$ 10 a.u.) the cancellation between the total energy

of the system and that of the isolated collision partners causes severe numerical difficulties.

A full account of the various methods of calculating interaction potentials is presented in the book of Schaefer (1972).

(b) Collision Dynamics

Once the interaction potential has been determined, the equations describing the motion of the nuclei in this potential must be solved. This is referred to as scattering or collision theory, and quantum, classical and various semi-classical formulations are available.

(i) Quantum Methods

In the quantum mechanical description of inelastic collisions of atoms with diatomic molecules, the equation of motion of the nuclei is the time-independent Schrodinger equation containing the Hamiltonian of the total system. In the conventional close-coupling solution, a space fixed co-ordinate system is used and (for the case where the molecule is approximated as a vibrating rotor) the wavefunction of the total system is expanded in terms of basis states which are eigenfunctions of the total angular momentum $\underline{J}$ and the vibrational Hamiltonian. Since $\underline{J}$ is compounded from the rotational angular momentum $\underline{j}$, and the orbital angular momentum $\underline{\ell}$, each basis state is indexed by the rotational angular momentum, orbital angular momentum, and vibrational quantum numbers of $j$, $\ell$ and $v$. The Schrodinger equation is then reducd to a set of coupled second order differential equations where the potential interaction couples together all the basis states such that $\underline{j} + \underline{\ell} = \underline{J}$. Since $\underline{J}$ is conserved, the coupling

matrix is diagonal in the total angular momentum quantum number J, and is independent of its z-component, $J_z$, since the orientation of the total system in space is irrelevant. However, for large j, the number of coupled equations becomes extremely large due to the (2j + 1) possible values of $\ell$, and consequently their numerical solution becomes extremely time consuming. The computer time required to solve a system of N coupled, second order differential equations, such as the close coupling equations, varies as $N^{\alpha}$ where $\alpha$ is between 2 and 3. Therefore, for all but the simplest systems, some approximation must be employed which offers decoupling of the close-coupled equations.

Various angular momentum decoupling approximations are now in common use, such as the coupled-states, energy sudden, infinite order sudden and effective potential approximations. Essentially, in each of these approximations an additional symmetry is introduced into the system which results in the conservation of some angular momentum quantum number, hence uncoupling the equations. These approximations are derived by some simplified treatment of one or more terms of the total Hamiltonian, and therefore their validity will be determined by the relative importance of these terms in the collision.

A derivation of the full close-coupled equations and brief descriptions of the various approximation schemes and their regions of validity are contained in Chapter II.

(ii) Classical and Semi-classical Methods

Due to numerical difficulties, quantum treatments are usually restricted to low energies and light molecules for which relatively few quantum states are excited. At the

other extreme of high energies and almost continuous energy levels, a classical description of the collision is valid. Many systems fall between these two extremes, and therefore a semiclassical theory seems most appropriate.

In time-dependent close-coupling, or classical path approximations, the relative motion of the collision partners is treated classically and the internal motion of the molecule by quantum mechanics. One assumes that the relative motion can be described by a classical trajectory which is independent of the internal motion of the molecule. This trajectory is usually calculated by either ignoring the potential completely (straight line paths), or including only the spherically symmetric component. Once the trajectory has been determined it can be used to construct a time dependent interaction potential. The problem then consists of calculating the probability of rovibrational transitions due to this time dependent interaction exerted by the passing atom. The principal source of error in this approximation is that the back coupling from the target to the trajectory is necessarily neglected. Therefore, the use of classical trajectories is only valid if the inelastic transitions which occur do not significantly affect the relative motion. As in the quantum treatment of the collision, various simplified treatments of the internal motion can be employed, resulting in such methods as the time-dependent sudden, and time-dependent coupled states approximations. The time-dependent close-coupling method and the various approximations derived from it are reviewed in the articles of Balint-Kurti (1975) and Dickinson (1979).

A major drawback of a purely classical description of the collision is the neglect of quantum mechanical interference effects. However, these are accounted for in the classical S-matrix method of Miller (1974) and Marcus (1972), which is a generalisation of the semiclassical treatment of elastic scattering due to Ford and Wheeler (1959). In this approach, all possible trajectories leading from a given initial state to a given final state are identified. The corresponding S-matrix element can then be constructed by the quantum mechanical superposition of contributions, one from each trajectory, with the correct phase factor provided by the classical action of the trajectory. However, for a system with several degrees of freedom, the numerical effort involved in the search for all trajectories satisfying a given set of double-ended boundary conditions becomes prohibitively large. This problem can be reduced if only cross sections averaged over some quantum numbers are required (Miller (1971)).

The semiclassical strong-coupling correspondence principle method of Percival and Richards (1970) approximates the solution of the time-dependent close coupling equations using a classical description of the internal motion of the molecule, incorporating the use of classical perturbation theory to determine the change in classical action of the molecule during the collision. Although, physically, it is expected to be most successful for large quantum numbers, comparison with quantum calculations have shown satisfactory results for cross sections between low lying rovibrational states (see e.g. Clark (1977)). The computing time for such

calculations is largely independent of the quantum numbers involved and arbitrarily large quantum numbers can be easily handled, in contrast to quantum calculations. The strong-coupling correspondence principle has been fully discussed by Clark et al. (1977).

For vibrational excitation a frequently used semiclassical approximation is based on the correspondence between the classical and quantum forced harmonic oscillators. Exact classical trajectories are employed to obtain the classical energy transfer as a function of angle. Using the Poisson distribution predicted by the forced oscillator model, vibrational excitation probabilities can be calculated (Giese and Gentry (1974)).

For systems in which quantum mechanical interference and tunneling phenomena do not play a significant role, purely classical methods are applicable. The advantage of classical methods is that all the couplings are treated essentially exactly, without having to include large numbers of basis states as in a quantum mechanical treatment. Therefore, in contrast to quantum methods, the computer time required by a classical method is approximately independent of the energy. A major problem in obtaining results from a purely classical calculation, which can be compared to quantum results, is the procedure employed to quantise the continuous classical variables, such as angular momentum. For example, in rotational excitation, a widely used technique is to define a final classical angular momentum, $j_c\hbar$, through the energy

$$E = B j_c (j_c + 1)$$

where B is the rotational constant of the molecule, and then associate a final rotational quantum number $j_Q$ with $j_c$ by

$$j_Q = j' \qquad j' - \tfrac{1}{2}\alpha \leq j_c \leq j' + \tfrac{1}{2}\alpha$$

where $\alpha = 1$ for heteronuclear molecules, and $\alpha = 2$ for homonuclear molecules to allow for the $\Delta j = 2$ selection rule. Techniques for performing classical calculations have been reviewed by Bunker (1971).

# CHAPTER II

# QUANTUM THEORY OF MOLECULAR COLLISIONS

## 1. Introduction

This chapter is concerned with the quantum mechanical description of inelastic collisions of atoms with diatomic molecules. Once the interaction potential has been determined, the equations describing the dynamics of the nuclei in this potential must be solved. This can be achieved by the solution of the time-independent Schrodinger equation containing the full Hamiltonian, which can be reduced to the solution of a set of coupled, second order differential equations. This approach is generally referred to as the close coupling (CC) method, and is discussed in Section 2. However, for all but the simplest atom-molecule systems, the numerical effort involved in the solution of the CC equations is prohibitively large, even with modern fast computers. The complexity of the CC equations arises from the coupling between the rotational and orbital angular momenta. In recent years a number of approximations have been developed in which the angular momenta are partially or completely uncoupled. In Section 3.(a)-(c) we discuss the three main angular momentum decoupling approximations (the energy sudden, the coupled states and the infinite order sudden approximations), and their ranges of validity. A brief account of alternative quantum mechanical approximations (the L-dominant, decoupled L-dominant, effective potential and adiabatic distorted-wave , infinite order sudden approximations) is contained in Section 3(d).

## 2. Close-Coupling Theory

Considered below is the quantum-mechanical description of the collision between a structureless atom and a diatomic molecule approximated by a vibrating rotor.

A space-fixed co-ordinate system is used (figure 1) with $\underset{\sim}{r} = (r,\theta,\phi)$ lying along the internuclear axis of the molecule BC and $\underset{\sim}{R} = (R,\Theta,\Phi)$ is the position vector of the atom A relative to the centre of mass of the molecule. The angle between $\underset{\sim}{R}$ and $\underset{\sim}{r}$ is denoted by $\gamma$.

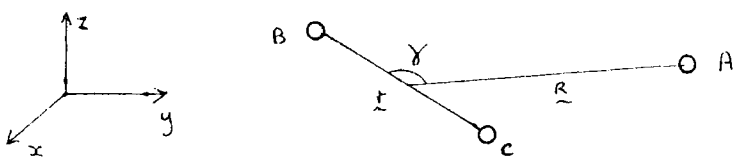


figure 1.

In this co-ordinate system the Schrodinger equation can be written

$$\left[ -\frac{\hbar^2}{2\mu R^2} \frac{\partial}{\partial R}\left(R^2 \frac{\partial}{\partial R}\right) + \frac{\hat{l}^2}{2\mu R^2} + H_{BC}(\underset{\sim}{r}) + V(\underset{\sim}{R},\underset{\sim}{r}) - E \right] \Psi(\underset{\sim}{R},\underset{\sim}{r}) = 0 \qquad \text{II.2.1}$$

where $\mu$ is the reduced mass of the atom-molecule system

$$\mu = \frac{m_A (m_B + m_C)}{m_A + m_B + m_C} \qquad \text{II.2.1a}$$

$H_{BC}(\underset{\sim}{r})$ is the Hamiltonian of the unperturbed molecule, E is the total energy and $V(\underset{\sim}{R},\underset{\sim}{r})$ is the interaction potential.

$$V(\underset{\sim}{R},\underset{\sim}{r}) \xrightarrow[R \to \infty]{} 0 \qquad \text{II.2.1b}$$

The standard approach to the solution of this equation is that due to Arthurs and Dalgarno (1960). Use is made of the conservation of the total angular momentum of the system in the collision.

$$\underset{\sim}{J} = \underset{\sim}{j} + \underset{\sim}{\ell} = \underset{\sim}{j}' + \underset{\sim}{\ell}' \qquad \text{II.2.2}$$

Where $\underline{j}$ is the rotational angular momentum of the molecule and $\underline{\ell}$ is the relative orbital angular momentum; primes denoting values after the collision. The boundary conditions of equation II.2.1 are

$$\Psi \xrightarrow[R \to 0]{} 0 \qquad \text{II.2.3a}$$

$$\Psi \xrightarrow[R \to \infty]{} e^{ik_{vj} z}\, \chi_{vj}(r)\, Y_{jm_j}(\hat{\underline{r}}) + R^{-1} \sum_{v'j'm_j'} f_{vjm_j \to v'j'm_j'}(\hat{\underline{R}})\, \chi_{v'j'}(r)\, Y_{j'm_j'}(\hat{\underline{r}})\, e^{ik_{v'j'} R} \qquad \text{II.2.3b}$$

II.2.3a is required as $R \to 0$ since $V(\underline{R}, \underline{r}) \to \infty$. The first term in II.2.3b corresponds to the incident plane wave describing the atom approaching along the positive z-direction and $\chi_{vj}(r) Y_{jm_j}(\hat{\underline{r}})$ are the rovibrational eigenstates of the molecule satisfying

$$\left( H_{BC} - \varepsilon_{vj} \right) \chi_{vj}(r)\, Y_{jm_j}(\hat{\underline{r}}) = 0 \qquad \text{II.2.4}$$

$\varepsilon_{vj}$ is the eigenenergy of the molecule in vibrational state v and rotational state j. The second term describes the scattered wave. Wavevector, $k_{vj}$, is defined by

$$k_{vj}^2 = \frac{2\mu}{\hbar^2} \left( E - \varepsilon_{vj} \right) \qquad \text{II.2.5}$$

The functions $f_{vjm_j \to v'j'm_j'}(\underline{R})$ are the scattering amplitudes from which the differential state-to-state cross sections can be obtained.

$$\sigma\left( vm_j \to v'j'm_j' ; \hat{\underline{R}} \right) = \frac{k_{v'j'}}{k_{vj}} \left| f_{vjm_j \to v'j'm_j'}(\hat{\underline{R}}) \right|^2 \qquad \text{II.2.6}$$

Since the total angular momentum J and its component along the space-fixed z-axis, M, are conserved, the most suitable expansion of the total wavefunction is in terms of

eigenstates of J,M given by

$$\mathcal{Y}^{JM}_{j\ell}(\hat{\underline{R}},\hat{\underline{r}}) = \sum_{m_j m_\ell} \langle j\ell m_j m_\ell | j\ell JM\rangle \, Y_{jm_j}(\hat{\underline{r}}) Y_{\ell m_\ell}(\hat{\underline{R}}) \qquad \text{II.2.7}$$

where $\langle j\ell m_j m_\ell | j\ell JM\rangle$ is a Clebsh Gordon coefficient. We expand the total wavefunction $\Psi^{JM}_{j\ell v}(\underline{R},\underline{r})$, corresponding to total angular momentum quantum numbers J and M and appropriate to the initial state specified by quantum numbers, $j,\ell,v$ as

$$\Psi^{JM}_{j\ell v}(\underline{R},\underline{r}) = R^{-1}\sum_{j'\ell'v'} U^{J j\ell v}_{j'\ell' v'}(R)\, \mathcal{Y}^{JM}_{j'\ell'}(\hat{\underline{R}},\hat{\underline{r}})\, \chi_{v'j'}(r) \qquad \text{II.2.8}$$

Substituting this into II.2.1 and using II.2.4 and the orthonormal properties of $\mathcal{Y}^{JM}_{j\ell}(\hat{\underline{R}},\hat{\underline{r}})$ and $\chi_{vj}(r)$

$$\iint \mathcal{Y}^{JM}_{j\ell}(\hat{\underline{R}},\hat{\underline{r}})\, \mathcal{Y}^{JM*}_{j'\ell'}(\hat{\underline{R}},\hat{\underline{r}})\, d\hat{\underline{R}}\, d\hat{\underline{r}} = \delta_{j\ell,j'\ell'} \qquad \text{II.2.9a}$$

$$\int \chi_{vj}(r)\, \chi^{*}_{v'j'}(r)\, dr = \delta_{vj,v'j'} \qquad \text{II.2.9b}$$

we obtain the following coupled differential equations satisfied by the radial functions $U^{J j\ell v}_{j'\ell' v'}(R)$.

$$\left[\frac{d^2}{dR^2} + k^2_{v'j'} - \frac{\ell'(\ell'+1)}{R^2}\right] U^{J j\ell v}_{j'\ell' v'}(R) = \sum_{v''j''\ell''} V^{J}_{v'j'\ell', v''j''\ell''}(R)\, U^{J j\ell v}_{j''\ell'' v''}(R) \qquad \text{II.2.10}$$

The coupling matrix elements are given by

$$V^{J}_{v'j'\ell', v''j''\ell''}(R) = \frac{2\mu}{\hbar^2}\iint \chi_{v'j'}(r)\, \mathcal{Y}^{JM}_{j'\ell'}(\hat{\underline{R}},\hat{\underline{r}})\, V(\underline{R},\underline{r})\, \mathcal{Y}^{JM*}_{j''\ell''}(\hat{\underline{R}},\hat{\underline{r}}) \times \chi^{*}_{v''j''}(r)\, d\hat{\underline{R}}\, d\hat{\underline{r}} \qquad \text{II.2.10a}$$

Since the orientation of the whole system in space is irrelevant, the coupling terms $V^J$ are independent of M, and hence also are the radial functions $U^J$. Almost invariably a single centre expansion of the potential is used.

$$V(\underline{R},\underline{r}) = \sum_{\lambda} v_\lambda(R,r)\, P_\lambda(\hat{\underline{r}}\cdot\hat{\underline{R}}) \qquad \text{II.2.11}$$

Giving

$$V^{J}_{v'j'l',v''j''l''}(R) = \frac{2\mu}{\hbar^2}\sqrt{\frac{f_\lambda(j'l',j''l'';J)}{\lambda}}\int \chi_{v'j'}(r)\, v_\lambda(R,r)\chi_{v''j''}(r)\, dr \qquad \text{II.2.12a}$$

$$f_\lambda(j'l',j''l'';J) = \iint Y^{JM}_{j'l'}(\hat{R},\hat{r})\, P_\lambda(\hat{r}.\hat{R})\, Y^{JM}_{j''l''}(\hat{R},\hat{r})\, d\hat{R}\, d\hat{r} \qquad \text{II.2.12b}$$

The angular integral $f_\lambda(j'l',j''l'';J)$ is a Percival Seaton coefficient (Percival and Seaton (1957)) which can be expressed in terms of 3-j and 6-j coupling terms.

As $R \to \infty$, $V^J \to 0$ and the solutions of II.2.10 with $V^J = 0$ are, for $k^2_{v'j'} > 0$ (Abramowitz and Stegun (1965)).

$$k_{v'j'}R\, j_{l'}(k_{v'j'}R) \qquad k_{v'j'}R\, n_{l'}(k_{v'j'}R) \qquad \text{II.2.13a}$$

where $j_{l'}(k_{v'j'}R)$ and $n_{l'}(k_{v'j'}R)$ are Spherical Bessel functions of the first and second kind. Alternatively the Spherical Hankel functions (sometimes known as Spherical Bessel functions of the third kind) of the first and second kind can be used.

$$h^{(1)}_l = j_l + i n_l \qquad h^{(2)}_l = j_l - i n_l \qquad \text{II.2.13b}$$

The boundary condition as $R \to \infty$ for $U^J$ can be written as a linear combination of $j_l$ and $n_l$ (or $h^{(1)}_l$ and $h^{(2)}_l$) or some mixture. A frequently used condition is

$$U^{Jjlv}_{j'l'v'} \xrightarrow[R\to\infty]{} 0 \qquad (k^2_{v'j'} \leqslant 0) \qquad \text{II.2.14}$$

$$U^{Jjlv}_{j'l'v'} \xrightarrow[R\to\infty]{} \left(-ik_{v'j'}R\, h^{(2)}_l(k_{v'j'}R)\right)\delta_{jlv,j'l'v'} - \left(\frac{k_{vj}}{k_{v'j'}}\right)^{1/2} S^J(jlv,j'l'v')\left(ik_{v'j'}R\, h^{(1)}_l(k_{v'j'}R)\right) \quad (k^2_{v'j'} > 0)$$

Also $U^{Jjlv}_{j'l'v'} \xrightarrow[R\to 0]{} 0$

Functions for which $k^2_{v'j'} \leqslant 0$ are termed closed channels, and those for which $k^2_{v'j'} > 0$, open channels. Equation II.2.14 defines the S-matrix which is diagonal in total angular momentum J (since J is conserved). By using the asymptotic forms of the Spherical Hankel functions it can be re-written.

$$U^{Jj\ell v}_{j'\ell'v'} \xrightarrow[R\to\infty]{} \exp\left[-i\left(k_{v'j'}R - \frac{\ell'\pi}{2}\right)\right]\delta_{j\ell v,\, j'\ell'v'} - \left(\frac{k_{vj}}{k_{v'j'}}\right)^{1/2} S^J(j\ell v\,;\, j'\ell'v')\exp\left[i\left(k_{v'j'}R - \frac{\ell'\pi}{2}\right)\right] \qquad \text{II.2.14b}$$

This shows more clearly why such a condition is used, since it demonstrates the decomposition of $U^J$ into an outgoing incident wave and outgoing scattered waves. We now require a linear combination of $\Psi^{JM}_{j\ell v}$ which satisfies the boundary conditions II.2.3a,b. By using the expansion of a plane wave into Spherical Bessel functions (Abramowitz and Stegun).

$$e^{ik_{vj}z} = \sum_{\ell} (2\ell+1)\, i^\ell\, j_\ell(k_{vj}R)\left(\frac{4\pi}{2\ell+1}\right)^{1/2} Y_{\ell 0}(\hat{\underset{\sim}{R}}) \qquad \text{II.2.15}$$

and the expression for a product of two spherical harmonics, we obtain

$$e^{ik_{vj}z}\chi_{vj}(r)\,Y_{jm_j}(\hat{\underset{\sim}{r}}) = \sum_{JM\ell} (4\pi(2\ell+1))^{1/2}\, i^\ell\, j_\ell(k_{vj}R) \times \langle j\ell m_j 0 | j\ell JM\rangle\, \mathcal{Y}^{JM}_{j\ell}(\hat{\underset{\sim}{R}}, \hat{\underset{\sim}{r}})\,\chi_{vj}(r) \qquad \text{II.2.16}$$

In order for the first term in the total wavefunction to go over to this asymptotically, the expansion used is

$$\Psi_{v_j m_j} = \frac{i(\pi)^{1/2}}{k_{v_j}} \sum_{JM\ell} \langle j\ell m_j 0 | j\ell JM\rangle\, i^{\ell} (2\ell+1)^{1/2}\, \Psi^{JM}_{j\ell v}(\hat{R},\hat{r}) \qquad \text{II.2.17}$$

Substitution of II.2.14, II.2.8 and II.2.7 in II.2.17 gives the asymptotic form

$$\begin{aligned}\Psi_{v_j m_j} \xrightarrow{R\to\infty}\ & e^{ik_{v_j}z}\, Y_{jm_j}(\hat{r})\,\chi_{v_j}(r) \\ & + \frac{i(\pi)^{1/2}}{k_{v_j}} \sum_{JM\ell} \langle j\ell m_j 0 | j\ell JM\rangle\, i^{\ell}(2\ell+1)^{1/2} \\ & \times \sum_{j'\ell'v'} R^{-1} i^{-\ell'} \left(\frac{k_{v'j'}}{k_{v_j}}\right)^{1/2} \left[\delta_{j\ell v, j'\ell'v'} - S^{J}(j\ell v, j'\ell'v')\right] \\ & \times e^{ik_{v'j'}R} \sum_{m_{\ell'} m_{j'}} \langle j'\ell' m_{j'} m_{\ell'} | j'\ell' JM\rangle\, Y_{\ell' m_{\ell'}}(\hat{R})\, Y_{j' m_{j'}}(\hat{r})\, \chi_{v'j'}(r)\end{aligned} \qquad \text{II.2.18}$$

Where use has been made of the asymptotic form

$$h^{(1)}_{\ell'}(k_{v'j'}R) \xrightarrow[R\to\infty]{} -\frac{i}{k_{v'j'}} \exp\left[i\left(k_{v'j'}R - \frac{\ell'\pi}{2}\right)\right]$$

Comparison of II.2.18 with II.2.3b gives the following expression for the scattering amplitude

$$\begin{aligned}f_{v_j m_j \to v'j' m_{j'}}(\hat{R}) = {} & i\left(\frac{\pi}{k_{v_j} k_{v'j'}}\right)^{1/2} \sum_{JM\ell\ell' m_{\ell'}} i^{\ell-\ell'} (2\ell+1)^{1/2} \langle j\ell m_j 0 | j\ell JM\rangle \\ & \times \langle j'\ell' m_{j'} m_{\ell'} | j'\ell' JM\rangle\, T^{J}(j\ell v, j'\ell'v')\, Y_{\ell' m_{\ell'}}(\hat{R})\end{aligned} \qquad \text{II.2.19}$$

Where $T^J$ is the transition T-matrix, related to the S-matrix by

$$T^J(j\ell v, j'\ell'v') = \delta_{j\ell v, j'\ell'v'} - S^J(j\ell v, j'\ell'v')$$

Other asymptotic boundary conditions for open channels can be imposed using the Spherical Bessel and Hankel functions. Other forms used are:-

$$U^{J}_{j'\ell'v'}{}^{j\ell v} \xrightarrow[R\to\infty]{} -2i\, k_{vj}R\, j_{\ell'}(k_{vj}R)\,\delta_{j\ell v, j'\ell'v'} + \left(\frac{k_{vj}}{k_{v'j'}}\right)^{1/2} T^J(j\ell v, j'\ell'v')\left(i k_{v'j'}R\, h^{(1)}_{\ell'}(k_{v'j'}R)\right) \qquad \text{II.2.20a}$$

$$U^{J}_{j'\ell'v'}{}^{j\ell v} \xrightarrow[R\to\infty]{} -2i\left\{ k_{v'j'}R\, j_{\ell'}(k_{v'j'}R)\,\delta_{j\ell v, j'\ell'v'} + \left(\frac{k_{vj}}{k_{v'j'}}\right)^{1/2} K^J(j\ell v, j'\ell'v')\left(-k_{v'j'}R\, n_{\ell'}(k_{v'j'}R)\right)\right\} \qquad \text{II.2.20b}$$

II.2.20a obtains the T-matrix directly, however II.2.20b has the computational advantage that all the functions appearing are real (apart from the -2i factor) and it is therefore the usual practise to obtain $K^J(j\ell v, j'\ell' v')$, the reactance matrix, and calculate $S^J$ and $T^J$ from it. The K,S and T-matrices are related by (in matrix notation)

$$\underset{\sim}{S} = (\underset{\sim}{I} + i\underset{\sim}{K})(\underset{\sim}{I} - i\underset{\sim}{K})^{-1} = \underset{\sim}{I} - \underset{\sim}{T} \qquad \text{II.2.21}$$

where $\underset{\sim}{I}$ denotes the unit matrix. The symmetry of the coupling matrix $V^J$ ensures the symmetry of the S,K and T-matrices and reflects the invarience of the dynamics under time reversal. The S-matrix is also unitary as required by the conservation of total flux.

The most commonly used cross-section is the degeneracy averaged total cross-section for a transition vj→v'j'. This is obtained by using equation II.2.6, averaging over initial $m_j$, summing over final $m_j'$, and integrating over angle $d\hat{\underline{R}}$ (see, e.g. Arthurs and Dalgarno (1960)).

$$\sigma(v_j \to v'j') = \frac{1}{(2j+1)} \frac{k_{v'j'}}{k_{vj}} \sum_{m_j m_{j'}} \int \left| f_{vjm_j \to v'j'm_{j'}}(\hat{\underline{R}}) \right|^2 d\hat{\underline{R}} \qquad \text{II.2.22}$$

$$= \frac{\pi}{k_{vj}^2 (2j+1)} \sum_{J} (2J+1) \sum_{\ell \ell'} \left| T^J(j\ell v, j'\ell' v') \right|^2$$

The symmetry of the T-matrix ensures that the cross-sections satisfy the detailed balance condition,

$$k_{vj}^2 (2j+1)\, \sigma(v_j \to v'j') = k_{v'j'}^2 (2j'+1)\, \sigma(v'j' \to v_j) \qquad \text{II.2.23}$$

The solution of the coupled differential equations (II.2.10) to obtain a T-matrix and hence cross-sections, is generally referred to as the close-coupling (CC) method.

The summation over j'', $\ell$'', v'' is, in theory, infinite for each value of J. However, in practice the summation must be truncated. If one is interested in transitions up to a given state vj, successive basis states (with their $\ell$ values) are added until the results of interest are converged.

Frequently, at low energies, energetically inaccessible states (closed channels) are included. These are required in order to accurately describe the target molecule when perturbed by the atom during the collision. The difficulty with the CC method is the (2j+1) degeneracy of the rotor levels. Therefore the number of channels increases extremely rapidly with

increasing j. This problem is slightly alleviated by the conservation of parity $(-1)^{j+\ell}$, which uncouples solutions of even and odd parity, which can then be solved separately. Also, if the molecule is homonuclear, only Legendre polynomials of even order $\lambda$ are present in II.2.11, which uncouples solutions with even and odd j. However, except for $H_2$ and the hydrides, CC calculationsof rovibrational cross-sections are impracticable even on modern fast computers, since, at energies sufficiently high for vibrational excitation, a large number of rotational levels are energetically accessible. For example,in $N_2$ there are more than thirty rotational levels below the first excited vibrational level. If only even j is considered, since $N_2$ is homonuclear, there are 265 coupled channels for one parity and 240 for the other. This is only considering rotational levels in the ground vibrational state. Rotational levels in excited vibrational levels would also be required. On modern computers only around 70 channels are practicable. In the case of $H_2$, however, the rotational levels are relatively widely spaced since it is such a light molecule. There are only up to j = 8 levels below the first excited vibrational level. This gives sets of 25 and 20 coupled equations for even j transitions. If a similar number of rotational levels are retained in the first excited vibrational state the numbers increase to 50 and 40; the solution of which is comfortably within the limitations of modern computers.

## 3. Approximate Methods

The computer time required to solve a system of N coupled, second order differential equations, such as II.2.10, varies approximately as $N^2$ to $N^3$, depending on the numerical algorithm employed. Therefore, for all but the simplest systems, to treat rovibrational excitation quantum mechanically, an approximation must be introduced to obtain some decoupling of these equations. All the approximations discussed in this section are based on a simplified treatment of one or more terms in the full CC equations and, therefore, their validity will be determined by the relative importance of these terms in the collision. For example, in the coupled states approximation, the centrifugal term is approximated and therefore it is expected to be accurate for collisions where the effect of the centrifugal potential is relatively minor. In practice, however, the range of validity of a given approximation is frequently determined by numerical comparisons with CC calculations.

### (a) The Energy Sudden Approximation

The energy sudden approximation is valid for collisions where the transition time for rotation of the target molecule is much larger than the collision time, i.e. the molecule rotates only slightly during the time the atom spends in the interaction region. This is the case for relatively high energy collisions involving heavy molecules. It is the comparison of times, not energies, which is important. Although very few atom-molecule calculations have been performed using this approximation alone (Khare (1978), Chu and Dalgarno

(1975a)), it is frequently used in conjunction with further approximations, most notably the infinite order sudden discussed in(c). It has also been widely used in electron-molecule collisions, where it is known as the adiabatic nuclei approximation (for example Collins and Norcross (1978)), since the small mass of the electron is ideally suited.

The target molecule is assumed to be at rest during the collision. The scattering problem can thus be solved for all stationary rotor states, and then state to state amplitudes can be obtained from this. The latter problem is the simpler. Use is made of the relationship II.3.1, derived by Chase (1956).

$$f_{vjm_j \to v'j'm_{j'}}(\hat{R}) = \int Y^{*}_{j'm_{j'}}(\hat{r})\, f_{v\to v'}(\hat{r},\hat{R})\, Y_{jm_j}(\hat{r})\, d\hat{r} \qquad \text{II.3.1}$$

where $f_{v\to v'}(\hat{r},\hat{R})$ is the scattering amplitude using a fixed rotor orientation $\hat{r}$. This requires that $f_{v\to v'}(r,R)$ must be calculated at sufficient orientations to enable the integral to be solved. However, since the scattering problem is independent of the orientation of the whole system in space, this can be considered as allowing the atom to approach from all directions instead. We are free to chose $\hat{r}$ as our polar z-axis. In this new co-ordinate system the interaction potential, V, is axially symmetric, and hence $\ell_z$ is conserved although $\ell$ is not (figure 2).

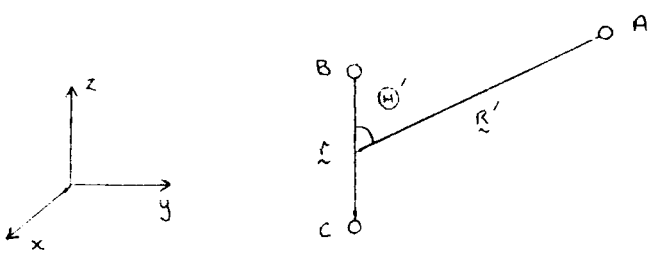


Figure 2.

This is why this approximation is sometimes referred to as the "$\ell_z$ conserving approximation". In this new co-ordinate system $\underline{R}$ is replaced by $\underline{R}' = (R, \Theta', \Phi')$ where $\Theta' \equiv \gamma$ in the original space fixed co-ordinates (figure 1).

Since we are considering the target at rest the rotor states are degenerate, all taken to be j=0. Hence $\mathcal{E}_{vj}$, and thus $k_{vj}$ are independent of j, so the index j is dropped in the following equations; $k_v = k_{vO}$. Analogously to II.2.8, the total wavefunction is expanded as

$$\Psi_{\ell_v}(\underset{\sim}{R}', \underset{\sim}{r}) = R^{-1} \sum_{\ell' v' m_{\ell'}} U^{\ell_v}_{\ell' v' m_{\ell'}}(R)\, Y_{\ell' m_{\ell'}}(\hat{\underset{\sim}{R}})\, \chi_{v'}(r) \qquad \text{II.3.2}$$

(Where the summation over $m_{\ell'}$ was previously incorporated in $\mathcal{Y}^{JM}_{j'\ell'}(\underline{R}, \underline{r})$, and the summations over j' and $m_{j'}$ collapse).

Substitution into the Schrodinger equation II.2.1 with $k_{vj} = k_v$ we obtain the coupled equations for the radial functions

$$\left[\frac{d^2}{dR^2} + k^2_{v'} - \frac{\ell'(\ell'+1)}{R^2}\right] U^{\ell_v}_{\ell' v' m_{\ell'}}(R) = \sum_{v''\ell''} V^{m_{\ell'}}_{v'\ell', v''\ell''}(R)\, U^{\ell_v}_{\ell'' v'' m_{\ell'}} \qquad \text{II.3.3}$$

Where

$$V^{m_{\ell'}}_{v'\ell', v''\ell''}(R) = \frac{2\mu}{\hbar^2}(2\pi) \iint_{*} \chi_{v'}(r)\, Y_{\ell' m_{\ell'}}(\Theta', 0)\, V(R, \Theta', r) \times Y_{\ell'' m_{\ell'}}(\Theta', 0)\, \chi^{*}_{v''}(r)\, d(\cos\Theta')\, dr \qquad \text{II.3.4a}$$

Using the usual single centre expansion II.2.11, this reduces to

$$V^{m_{\ell'}}_{v'\ell', v''\ell''}(R) = \frac{2\mu}{\hbar^2}(2\pi) \sum_{\lambda} (-1)^{m_{\ell'}} (2\ell'+1)^{1/2} (2\ell''+1)^{1/2} \times \begin{pmatrix} \ell' & \lambda & \ell'' \\ 0 & 0 & 0 \end{pmatrix} \begin{pmatrix} \ell' & \lambda & \ell'' \\ m_{\ell'} & 0 & -m_{\ell'} \end{pmatrix} \int \chi_{v'}(r)\, v_\lambda(R, r)\, \chi^{*}_{v''}\, dr \qquad \text{II.3.4b}$$

Since $\ell_z$ is conserved, the equations are diagonal in $m_\ell$ Therefore, instead of coupled equations indexed by j, $\ell$ and v, we now have sets of equations coupled by $\ell$ and v only, which have to be solved for all allowed values of $m_\ell$. The boundary conditions satisfied by II.3.3 are

$$U^{\ell_v}_{\ell'_v m_{\ell'}} \xrightarrow[R\to 0]{} 0$$

$$U^{\ell_v}_{\ell'_v m_{\ell'}} \xrightarrow[R\to\infty]{} 0 \qquad (k_v^2 \leq 0)$$

$$U^{\ell_v}_{\ell'_v m_{\ell'}} \xrightarrow[R\to\infty]{} (-ik_{v'} R h^{(2)}_{\ell'}(k_{v'}R))\,\delta_{\ell_v,\ell'_{v'}} - \left(\frac{k_v}{k_{v'}}\right)^{1/2} S^{m_{\ell'}}(\ell_v,\ell'_{v'})\,(ik_{v'} R h^{(1)}_{\ell'}(k_{v'}R)) \qquad (k_v^2 > 0) \qquad \text{II.3.5}$$

An approximate space-fixed S-matrix can now be obtained from the sudden S-matrix defined by II.3.5.

$$S^J(j\ell_v, j'\ell'_{v'}) = \sum_{m_{\ell'}} (2j+1)^{1/2}(2j'+1)^{1/2} \begin{pmatrix} j' & \ell' & J \\ 0 & m_{\ell'} & -m_{\ell'} \end{pmatrix} \begin{pmatrix} j & \ell & J \\ 0 & m_{\ell'} & -m_{\ell'} \end{pmatrix} S^{m_{\ell'}}(\ell_v,\ell'_{v'}) \qquad \text{II.3.6}$$

This comes basically from equation II.3.1; the integral being performed analytically by rotation to a new co-ordinate system and using the properties of the rotation matrices involved (Khare (1978), Secrest (1975)). The coupled equations still have to be solved for all values of $m_\ell$ which is highly impractical for large $\ell$. However, from physical arguments, Khare (1978) has shown that only the first few terms contribute significantly; roughly $m_\ell \leq (j_{max} + 1)$ values, where $j_{max}$ is the largest j accessible from the j = 0 state. Also since $V^{m_{\ell'}} = V^{-m_{\ell'}}$ only $m_\ell \geq 0$ need be considered.

Once this approximate space-fixed S-matrix is obtained it can be used in the full CC equations, II.2.19 and II.2.22, to obtain all the necessary scattering information.

An important simplification can be obtained by using the Clebsh-Gordon series for spherical harmonics (Rose 1957) in II.3.1 giving

$$f_{vjm_j \to v'j'm_{j'}}(\hat{R}) = (-1)^{m_{j'}}(2j+1)^{1/2}(2j'+1)^{1/2}\sum_{j''}(2j''+1)^{1/2} \times \begin{pmatrix} j' & j & j'' \\ -m_{j'} & m_j & \Delta m_j \end{pmatrix}\begin{pmatrix} j' & j & j'' \\ 0 & 0 & 0 \end{pmatrix} f_{v00 \to v'j''\Delta m_j} \; ; \; \Delta m_j = m_{j'} - m_j \qquad \text{II.3.7a}$$

which in turn leads to:-

$$\sigma(vj \to v'j') = (2j'+1)\left(\frac{k_{v0}}{k_{vj}}\right)^2 \sum_{j''}\begin{pmatrix} j' & j & j'' \\ 0 & 0 & 0 \end{pmatrix}^2 \sigma(v0 \to vj'') \qquad \text{II.3.7b}$$

Hence we only need calculate $\sigma(v0 \to v'j'')$ and all other cross-sections can be trivially derived from them. This property is present whenever the energy sudden approximation is used, and is of great use in the infinite order sudden (IOS) approximation.

This approximation has been applied by Khare (1978) to the purely rotational excitation of $N_2$ and TlF by Ar. Generally reasonable agreement with the CC results of Tsien et al. (1973) is obtained for Ar - $N_2$, and good agreement for Ar - TlF, consistent with using a heavier molecule. However, at small total angular momentum J, equation II.3.6 gives a $S(0\ell v, j'\ell'v')$ which is very sensitive to $S^{m_{\ell'}}(\ell v, \ell'v')$ and the results become unreliable. At low J, the electrostatic potential is dominant and therefore an approximation can be made on the centrifugal term also, ie the IOS can be used successfully. This is demonstrated by Khare (1978), where the IOS is satisfactory for low J, but not for high J where the coupled-states component of the IOS fails.

(b) The Coupled States Approximation

This approximation was independently and simultaneously developed by McGuire and Kouri (1974) and by Pack (1974). It is also

known by the more informative names of "$J_z$ conserving" and "centrifugal sudden" approximation. The derivation can be obtained in several ways (Khare (1977), Secrest (1975), Kouri (1979) and others). In order to emphasise the similarities with the energy sudden approximation, the brief derivation presented here uses a body-fixed reference frame, which rotates such that the z-axis always lies along $\hat{\underline{R}}$, i.e. it always points towards the atom (figure 3). In this frame the potential is axially symmetric giving conservation of $J_z$.

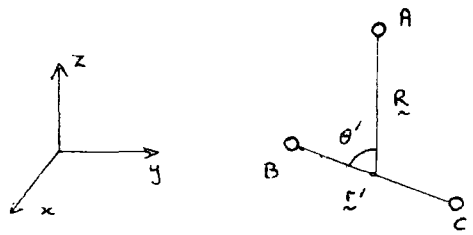


figure 3

In this new body-fixed, rotating frame $\hat{\underline{r}}' = (\theta', \phi')$ and the Schrodinger equation is

$$\left[-\frac{\hbar^2}{2\mu R}\left(\frac{\partial^2}{\partial R^2}\right)R + \frac{\hat{l}^2}{2\mu R^2} + H_{BC}(\underline{r}') + V(\underline{r}', \underline{R}) - E\right]\Psi(\underline{R}, \underline{r}') = 0 \qquad \text{II.3.8}$$

Where $\Psi(\underline{R}, \underline{r}')$ is the wavefunction within this frame. The approximation consists of ignoring the off-diagonal elements of the orbital angular momentum operator $\hat{l}^2$, which are the Coriolis terms associated with the non-inertial frame, and setting the diagonal elements to $L(L+1)\hbar^2$ where L is now simply a parameter. This can be thought of as approximating the centrifugal potential by an effective orbital angular momentum eigenvalue. Physically, it is assuming that the collision is such that the precise value of the centrifugal potential is relatively unimportant. The wavefunction is expanded as

$$\Psi_{Jv}(\underline{R}, \underline{r}) = R^{-1}\sum_{j'v'm_{j'}} U^{Jv}_{j'v'm_{j'}}(R)\, Y_{j'm_{j'}}(\hat{\underline{r}}')\, \chi_{v'j'}(r) \qquad \text{II.3.9}$$

where the subscripts j,v specify the initial state. Substitution in II.3.8 gives the coupled equations

$$\left[\frac{d^2}{dR^2} + k^2_{v'j'} - \frac{L(L+1)}{R^2}\right] U^{Ljv}_{j'v'm_{j'}}(R) = \sum_{j''v''} V^{m_{j'}}_{v'j',v''j''}(R)\, U^{Ljv}_{j''v''m_{j'}}(R) \qquad \text{II.3.10}$$

The additional superscript L has been added to specify the orbital angular momentum parameter, and

$$\begin{aligned} V^{m_{j'}}_{v'j',v''j''}(R) &= \frac{2\mu}{\hbar^2}(2\pi)\iint \chi_{v'j'}(r)\, Y_{j'm_{j'}}(\theta',0)\, V(R,\theta',r) \\ &\qquad \times Y^{*}_{j''m_{j'}}(\theta',0)\, \chi^{*}_{v''j''}(r)\, d(\cos\theta')\, dr \\ &= \frac{2\mu}{\hbar^2}\sum_{\lambda}(-1)^{m_{j'}}(2j'+1)^{1/2}(2j''+1)^{1/2}\begin{pmatrix} j' & \lambda & j'' \\ 0 & 0 & 0\end{pmatrix}\begin{pmatrix} j' & \lambda & j'' \\ -m_{j'} & 0 & m_{j'}\end{pmatrix} \\ &\qquad \times \int \chi_{v'j'}(r)\, v_\lambda(R,r)\, \chi^{*}_{v''j''}(r)\, dr \end{aligned} \qquad \text{II.3.11}$$

In the CS approximation we have used a rotating, body-fixed frame to conserve $j_z$ and introduced the approximation of ignoring the Coriolis terms in order to uncouple the equations in $\ell$. In the energy sudden approximation a co-ordinate system is used so as to conserve $\ell_z$ and the approximation of degenerate rotor states introduced in order to uncouple the equations in j.

The similarity in approach is reflected in the similarity of the equations developed.

Equation II.3.10 is subject to the boundary conditions:-

$$U^{Ljv}_{j'v'm_{j'}} \xrightarrow{R\to 0}$$

$$U^{Ljv}_{j'v'm_{j'}} \xrightarrow{R\to\infty} 0 \qquad k^2_{v'j'} \le 0 \qquad \text{II.3.12}$$

$$U^{Ljv}_{j'v'm_{j'}} \xrightarrow{R\to\infty} (-i k_{v'j'} R\, h^{(2)}_L(k_{v'j'}R))\,\delta_{jv,j'v'} \qquad k^2_{v'j'} > 0$$

$$-\left(\frac{k_{vj}}{k_{v'j'}}\right)^{1/2} S^{m_{j'}}_L(jv,j'v')\,(i k_{v'j'} R\, h^{(1)}_L(k_{v'j'}R))$$

An approximate space-fixed S-matrix can be obtained from the approximate body fixed $S_L^{m_j'}(jv,j'v')$ defined by II.3.12 by (Khare 1977)).

$$S^J(jlv,j'l'v') = i^{l+l'-2L}(2l+1)^{1/2}(2l'+1)^{1/2} \times \sum_{m_j} \begin{pmatrix} j & l & J \\ m_j & 0 & -m_j \end{pmatrix} \begin{pmatrix} j' & l' & J \\ m_j & 0 & -m_j \end{pmatrix} S_L^{m_j}(jv,j'v') \qquad \text{II.3.13}$$

Cross-sections, etc. can then be obtained as in CC calculations. Since $V^{m_j'} = V^{-m_j'}$ only $m_j' \geq 0$ need be considered. We therefore now have equations coupled in j,v which have to be solved for available $m_j \leq \min(j,j')$. The only point remaining is the choice of the parameter L. It has to be representative of an orbital angular momentum and only for $L = l$ or $l'$ can any real simplification be made in the equations. The choice of L has been fully discussed by McGuire and Kouri (1974) , Kouri (1979) and others. Hunter (1975) notes that neither choice give a fully symmetric S-matrix. In fact, the scattering amplitude for the choices $l$ and $l'$ are related by a unitary transformation (Khare (1977)).

$$f^{L=l}_{v_j m_j \to v'j' m_{j'}}(\hat{R}) = \sum_{\bar{m}} D^{j}_{m_{j'}\bar{m}}(\Phi,\Theta,0)\, f^{L=l'}_{v_j \bar{m} \to v'j'\bar{m}}(\hat{R})\, D^{j}_{m_j \bar{m}}(\Phi,\Theta,0) \qquad \text{II.3.14}$$

Where the D functions are those of Rose (1957). However the degeneracy averaged cross-sections are identical, due to the properties of the rotation matrices. The main difference is that for $L = l'$ it follows $\Delta m_j = 0$, i.e. no magnetic transitions are allowed, yet $\Delta m_j \neq 0$ transitions are allowed with $L = l$ .

The CS approximation has been widely and successfully employed both for atom-rigid-rotor and atom-vibrating rotor collisions. The CS is a kind of sudden approximation in that it assumes that the relative kinetic energy is sufficiently large that the precise value of the centrifugal potential is not important. Whether this assumption is justified depends on how the different classical turning points vary with $\ell$. If the electrostatic interaction potential is purely repulsive, then the rate of change of turning points with $\ell$ is not large and the CS is expected to be valid. If attractive wells are present, however, there may be three turning points, all rapidly changing with $\ell$, and the assumption of an effective orbital angular momentum eigenvalue will not be valid. The accuracy of the CS approximation in given physical situations has been mainly deduced by the comparison of CC and CS calculations. Kouri et al. (1976) found that the impact parameter should be smaller than the classical turning point, and that the energy should be well above threshold for the transition being considered in order for CS results to be reliable. The former condition restricts the CS to short-range potentials. This is demonstrated in the results of Kouri and McGuire (1974) for $Li^+ - H_2$ where the CS was found to be unreliable due to the long range interaction. By retaining some of the Coriolis terms, however, Kinnersley (1979) has obtained satisfactory results for the same system. Alexander and McGuire (1976) employ the CS approximation in the vibrational excitation of $H_2$ by He where the interaction potential used is short ranged and purely repulsive. These results are in excellent

agreement with the CC calculations presented in Chapter IV. From theoretical criteria and from the comparison of numerical tests, the CS approximation is expected to give reliable results for electrostatic potentials with no long range anisotropies and at reasonably high energies. The latter condition is to eliminate the situation of three turning points when an attractive well is present in the interaction potential. Therefore "reasonably high" should be interpreted in this context, i.e. the kinetic energy should be at least comparable to the well depth.

(c) The Infinite Order Sudden Approximation

This is a combination of the two approximations previously discussed, i.e. the $\ell_z$-conserving, energy sudden and the $j_z$-conserving coupled states. It was first introduced by Tsien and Pack (1970) and later generalised independently by Secrest (1975) and Hunter (1975). There are several derivations in the literature using both a space-fixed reference frame (Secrest (1975), Tsien and Pack (1970)) and a body-fixed formalism (Pack (1974), Bowman and Leasure (1977)). The brief derivation presented here uses a body-fixed frame, as in section (b). The rotor states are assumed degenerate with $k_{vj} = k_{vO} = k_v$, and the orbital angular momentum operator is replaced by a representative L(L + 1) term, corresponding to the neglect of the Coriolis terms. The resulting coupled equations are therefore only coupled in the vibrational quantum number (cf. II.3.3 and II.3.8).

$$\left[\frac{d^2}{dR^2} + k_{v'}^2 - \frac{L(L+1)}{R^2}\right] U_{v'}^{Lv}(R,Y) = \sum_{v''} V_{v'v''}(R,Y)\, U_{v''}^{Lv}(R,Y) \qquad \text{II.3.15}$$

$$V_{v'v''}(R,\gamma) = \frac{2\mu}{\hbar^2}\int \chi_{v'}(r)V(R,r,\gamma)\chi_{v''}(r)\,dr \qquad \text{II.3.16}$$

$\gamma$ is the angle between the rotor axis and the line joining the atom to the centre of mass of the molecule and is now simply a parameter. These equations are subject to the boundary conditions

$$U^{Lv}_{v'}(R,\gamma) \xrightarrow[R\to 0]{} 0$$

$$U^{Lv}_{v'}(R,\gamma) \xrightarrow[R\to\infty]{} 0 \qquad (k^2_{v'} \leq 0)$$

$$U^{Lv}_{v'}(R,\gamma) \xrightarrow[R\to\infty]{} (-ik_{v'}Rh^{(2)}_L(k_{v'}R))\,\delta_{vv'} \qquad (k^2_{v'} > 0)$$

$$-\left(\frac{k_v}{k_{v'}}\right)^{1/2} S^L_{vv'}(\gamma)(ik_{v'}Rh^{(1)}_L(k_{v'}R)) \qquad \text{II.3.17}$$

Using the Chase result (II.3.1) we can obtain a body-fixed S-matrix corresponding to that defined by II.3.12 (see e.g. Secrest (1975) , Schinke and McGuire (1978)a).

$$S^{m_j}_L(jv,j'v') = (2\pi)\int_0^{\pi} Y^*_{j'm_j}(\gamma,0)\,S^L_{vv'}(\gamma)\,Y_{jm_j}(\gamma,0)\sin\gamma\,d\gamma \qquad \text{II.3.18}$$

which can in turn be used in II.3.13 to obtain an approximate space-fixed S-matrix $S^J(j\ell v,\ j'\ell' v')$ from which final cross-sections can be calculated. Since the energy sudden approximation has been employed, only cross-sections out of the ground rotational states need be calculated and II.3.7b can be used to trivially calculate the others. Setting $j = 0$ in II.3.18.

$$S_L^{m_j}(ov, j'v') = \delta_{m_j,0}\sqrt{4\pi}\int_0^{\pi} Y_{j'0}(\gamma,0)\, S^L_{vv'}(\gamma)\sin\gamma\, d\gamma \qquad \text{II.3.19}$$

Hence the sumation in II.3.13 over $m_j$ collapses. If we take the orbital angular momentum parameter L equal to the initial value $L = \ell = J$ (since $j = 0$), II.3.13 reduces to

$$S^J(oJv, j'\ell'v') = i^{\ell'-J}(-1)^J(2\ell'+1)^{1/2}\begin{pmatrix} j' & \ell' & J \\ 0 & 0 & 0 \end{pmatrix} \times \sqrt{4\pi}\int_0^{\pi} Y_{j'0}(\gamma,0)\, S^J_{vv'}(\gamma)\sin\gamma\, d\gamma \qquad \text{II.3.20}$$

The coupled equations II.3.15 must be solved at sufficient values of $\gamma$ in order to solve the integral in II.3.20. The values of $\gamma$ can be chosen to be the points a Gauss-Legendre quadrature. Another method is to expand

$$S^L_{vv'}(\gamma) = \sum_n a_n^{Lvv'} P_n(\cos\gamma) \qquad \text{II.3.21}$$

This allows analytic evaluation of the integral. The number of terms in the series is determined by the number of values of $\gamma$ considered. This approach has two advantages over a quadrature scheme. Successive values of $\gamma$ can be calculated until the series converges, whereas in a quadrature, if the number of points is increased the $S^L_{vv'}(\gamma)$ calculated for a lower number of points are useless. Quadrature points are set, but by using II.3.21 the values of $\gamma$ chosen can be concentrated in the region where the integrand is varying most rapidly.

The cross-sections obtained using the S-matrix of II.3.20 obey

$$k_{v0}^2\,\sigma(v0 \to v'j') = k_{v'0}^2\,\sigma(v'0 \to vj') \qquad \text{II.3.22}$$

However, these are not reciprocal processes and this detailed balance type condition is imposed by the IOS. Only by virtue of II.3.21 do cross-section calculated from II.3.7b exhibit true detailed balance

$$(2j+1)k_{vj}^2\,\sigma(vj \rightarrow v'j') = (2j'+1)k_{v'j'}^2\,\sigma(v'j' \rightarrow vj) \qquad \text{II.3.23}$$

Although there is a large reduction in the number of coupled channels by using the IOS approximation, the equations must be solved at each orientation. If the S-matrix is strongly dependent on $\gamma$, calculations at many orientations may be required. A numerical technique designed to reduce the number of values of $\gamma$ required has been discussed by Secrest (1979). The approach is to interpolate the amplitude and phase of the S-matrix, which vary more slowly with $\gamma$ than the real and imaginary parts.

The IOS seems well suited to rovibrational calculations. The approximation will be reliable when both the energy sudden and the CS approximations are valid. Vibrational excitation requires high collision energies relative to the energies of the rotational states, which is required by the energy sudden approximation. Also, vibrational transitions are generally dominated by the short range region of the potential, which is ideally suited to a CS approach. In a collision where the molecule has a small rotational constant and there are many rotational levels a CC calculation becomes intractible. However, the more closely packed the rotational levels become, the greater the validity of the IOS (and the energy sudden).

Another advantage of the IOS is that the single centre expansion of the potential (II.2.11) has no advantage. In CC or the other approximate methods where the interaction potential is integrated over spherical harmonics, the expansion into Legendre polynomials allows the angular integrals to be performed analytically. However, in the IOS, no such integrals are required.

Green (1978) has tested the IOS for pure rotational transitions in HC$\ell$ + Ar, HC$\ell$ + He, CO + He and HCN + He against CC or CS results. Except for HC$\ell$ + Ar, the sudden condition is valid for a relative kinetic energy of 100 $cm^{-1}$. The failure of HC$\ell$ + Ar is consistent with Ar being heavier than He and, therefore, for a given kinetic energy, having a lower velocity. For the much lighter system, $H_2 + H^+$, Schinke and McGuire (1978)a have compared IOS and CC results for rotational excitation. At a total energy of 3.7eV the results are in generally good agreement, except for $\Delta j = 2$ transitions. This exception is due to the long range charge quadrupole interaction. Although the CS approximation is not suited to long range anisotropies, the CS results are in good agreement with the CC results of $\sigma(0 \rightarrow 2)$ of McGuire (1976). The IOS fails for $\Delta j = 2$ transitions because the $H^+$ spends a relatively long time in the region of the interaction potential involved (since it is long range). The increasing failure of the IOS with increasing total angular momentum is consistent with this. The results improve with increasing energy, as expected. Shinke and McGuire (1978)b have also performed IOS calculations of rovibrational excitation in $H_2 + H^+$, where the vibration is treated in a CC framework.

Their comparison with the experimental results of Hermann et al. (1978) is rather poor. This discrepancy is attributed to inaccuracies in the potential surface employed, however their basis functions have been shown to be incorrect (see Chapter V).

(d) Other Quantum Mechanical Approximations

In this section we discuss briefly some alternative quantum mechanical approximations in general use, which appear to have a more restricted range of validity than those discussed in (a) - (c).

(i) The Effective Potential Methods

The approximations discussed in (a) - (c) are essentially based on a simplified treatment of the orbital angular momentum operator or the wavenumbers. The main coupling is therefore transferred to the matrix elements of the electrostatic potential which are treated correctly. Other quantum mechanical approaches which reduce the dimensions of the CC equations are based on averaging the interaction potential over orientation, to obtain an effective potential, prior to performing the dynamical calculations.

The effective potential (EP) approximation of Rabitz (1972) was the first of the decoupling schemes for rotational excitation. This method has been reviewed by Rabitz (1976). In this approximation, the coupling potential matrix elements (II.2.12a) are preaveraged over the degenerate $m_j$ states to obtain an EP of the form

$$V^{J}_{v_j l, v'_j l'}(R) \equiv V^{J}_{v_j, v'_j}(R) = \sum_{\lambda} f_{\lambda}^{eff}(j,j') \int \chi_{v_j}(r)\, v_{\lambda}(R,r)\, \chi^{*}_{v'_j}(r)\, dr \qquad \text{II.3.24}$$

where $$f_\lambda^{eff}(j,j') = (-1)^\eta \left[(2j+1)(2j'+1)\right]^{1/4} (2\lambda+1)^{-1/2} \begin{pmatrix} j' & \lambda & j \\ 0 & 0 & 0 \end{pmatrix} \qquad \text{II.3.25}$$

$$\eta = \tfrac{1}{2}(|j-j'|+\lambda+j')$$

The resulting equations are coupled only in j and v, and the number of channels is reduced to the number of rovibrational basis states. Consequently the EP approximation requires less calculation than the CS approximation, where the equations must be solved for each value of $m_j$. The angular part of the interaction potential does not act during the collision but simply gives rise to the weighting coefficients in II.3.24, before the dynamical calculations are performed. Because of this preaveraging, no $m_j$ dependent cross sections can be calculated and the EP cross sections satisfy

$$k_{vj}^2 \sigma(vj \to v'j') = k_{v'j'}^2 \sigma(v'j' \to vj) \qquad \text{II.3.26}$$

instead of the correct detailed balance condition (II.3.23) which has to be enforced by a correction factor of (2j' + 1)/(2j + 1) on the right hand side of II.3.26. This is because each rotational state, which is 2j + 1 degenerate, is represented by a single effective rotational state (Zarur and Rabitz (1974)).

Comparison with CC calculations of rotational excitation in a model $N_2$ + He system (Chu and Dalgarno (1975b)) suggests that the EP approximation fails for systems with large anisotropies and at energies close to threshold. Green (1975) reaches a similar conclusion in studies of CO + He.

The interpretation of bulk data, obtained by experiment, frequently requires detailed knowledge of only degeneracy-averaged, rotationally summed cross sections for transitions between different vibrational levels. Therefore, there exists the possibility of not only preaveraging the potential

over the degenerate $m_j$ states, but also over the rotational states, leaving the equations coupled only in vibration. Such a scheme has been presented by Gianturco and Lamanna (1977). An effective potential is defined which depends on the collision energy and which contains a statistical average of the anisotropic potential terms ( $v_{\lambda \neq 0}$ of II.3.24). This weighted average of the full potential modifies the strength of the potential according to the magnitude of the $v_{\lambda \neq 0}$ contributions, and to the collision energy.

(ii) The L-Dominant and Decoupled L-Dominant Approximations

In the case of short-range interactions the corresponding cross sections are dominated by collisions which occur at small impact parameters, i.e. at low values of orbital angular momentum. The corresponding centrifugal barriers are therefore small and relatively unimportant relative to the electrostatic interaction potential terms. Hence the approximations discussed in (a) - (c) are expected to be most valid. The opposite situation can arise where the interaction is dominated by the centrifugal terms, where long range electrostatic interactions still act at large values of the orbital angular momentum, although the latter are controlling the dynamics. Schemes, designed to take advantage of such a situation, are the L-dominant (LD) and the decoupled L-dominant (DLD) approximations of Depristo and Alexander (1975 and 1976 respectively).

The LD approximation is based on the observation that in pure rotational problems at large J, the largest elements of the standard CC S-matrix, $S^J(j\ell, j'\ell')$ are those for which

$\ell, \ell' < J$. Equivalently indexing the channels by j and $\lambda = \ell + j - J$ (hence $0 \leq \lambda \leq 2j$), the most important channels are those with $\lambda \leq j$. Accordingly in the LD approximation one solves the CC equations retaining only channels with $\lambda \leq j$. This requires a calculation intermediate in size between CC and coupled states (CS). In the DLD approximation the coupling between channels $j\lambda$ and $j\lambda'$ is also ignored, since the Percival Seaton coefficients in the potential matrix elements (II.2.12b) for large J and small $\lambda$ are dominated by terms with $\Delta\lambda = 0$. This is equivalent to the value of $(j + \ell)$ being conserved.

As expected, the DLD approximation gives good results for systems with long range interactions, such as $Li^+ + H_2$ (Depristo and Alexander (1976)) but fails for systems with short range potentials, such as He - HD (Green (1976)). However, vibrational excitation generally occurs through hard short-range collisions, and therefore the LD and DLD approximations would be expected to fail for vibrationally inelastic cross sections.

(iii) The Adiabatic Distorted Wave IOS Approximation

As discussed in (c), the IOS approximation is well suited to rovibrational excitation, since vibrational transitions require high collision energies, relative to the rotational energy level spacing, and are dominated by the short range region of the potential. Although there is a large reduction in the number of coupled channels, the equations must be solved at sufficient orientations in order to solve the integral in II.3.20. If the S-matrix is strongly dependent

on orientation, the equations may have to be solved many times, resulting in considerable expense in computing time. However, cross sections for vibrationally inelastic transitions are, in general, very small. Usually several orders of magnitude smaller than for purely rotationally inelastic transitions. Such small transition probabilities are ideally suited to the use of perturbation techniques, such as the distorted wave approximation (see e.g. Balint-Kurti (1975)).

The adiabatic distorted wave (ADW) IOS approximation of Eno and Balint-Kurti (1979) treats the rotational motion within the IOS approximation, and treats the vibrational excitation by ADW techniques. The use of adiabatic wavefunctions is based on the observation that a CC treatment of the vibration, in $H_2$ + He calculations, requires four diabatic vibrational basis states to achieve convergence for v = 0 to v = 1 transitions (Bowman and Leasure (1977), Eno and Balint-Kurti (1979)). This suggests that a distorted wave approximation based on diabatic wavefunctions would give poor results. The advantages of adiabatic over diabatic wavefunctions has been discussed by Eno and Balint-Kurti (1981).

To make the ADWIOS approximation computationally efficient, Eno and Balint-Kurti (1979) have employed approximate analytic methods for evaluating the distorted wave integrals (Eno, Balint-Kurti and Saktreger (1978)). Also, by a suitable choice of basis functions, the adiabatic coupling terms can be expressed as analytic functions of the potential. Hence the evaluation of the angle-fixed S-matrices is reduced to analytic formulae and completely avoids the solution of differential equations.

Eno and Balint-Kurti (1979) and Bieniek (1980) have compared ADWIOS results with the CC results of Lin and Secrest (1979) for $H_2$ + He. However, both these comparisons are rendered invalid due to errors in the CC calculations (Lin (1981)). A comparison of the values of cross sections for the rovibrational excitation of $H_2$ by He from CC, ADWIOS and IOS (with a CC treatment of the vibration) calculations is presented in Chapter IV.4.

# CHAPTER III

## NUMERICAL SOLUTION OF THE COUPLED EQUATIONS

### 1. Introduction

The coupled equations which have to be solved are of a form frequently encountered in atomic and molecular physics and can be written in the general form:

$$\frac{d^2}{dR^2} G_n(R) = \sum_{n'=1}^{N} W_{nn'}(R)\, G_{n'}(R) \qquad \text{III.1.1}$$

Where the coupling matrix $W_{nn'}$ contains no differential operators. There exists many numerical methods of solution, however, no one can be considered best. The efficiency of a given method will depend on the particular problem, the degree of accuracy required, etc. Some algorithms may give a reasonable answer with little effort but require much more effort to produce greater accuracy. If the solution is required at many energies some methods will take a lot of time to obtain the first solution, but be able to generate solutions at subsequent energies with much less effort.

Basically, there are two methods of approach. The more traditional is to use the exact coupling matrix $W_{nn'}$ and to obtain an approximate numerical solution to the equations; referred to as the approximate solution (AS) approach (cf. Secrest (1979)). The other is to substitute an approximate form of the coupling matrix, which allows analytic solution of the equations, referred to as the approximate potential (AP) approach.

These two approaches can be further categorised by the manner in which the solution is obtained. The solution can be initialised well into the classically forbidden region,

where its form is known, since the potential is very large, and step by step integrated out into the asymptotic region, where it can be matched to the appropriate boundary conditions to obtain all the relevant scattering information. This is referred to as the solution-following (SF) method, used in many of the more traditional algorithms. The methods of de Vogelaere (1955) (see e.g. Lester (1976)) and that of Sams and Kouri (1969) use the SF method in the AS approach. The SF method in the AP approach is employed by the algorithms of Grodon (1969), Light (1971) and Wilson (1969).

The second category is referred to as invariant imbedding (II). In II the scattering problem is solved for a section of the potential, to obtain an R-matrix. Using connection formulae, this R-matrix is combined with other sector R-matrices to obtain a solution for larger sections of the potential until the problem is solved for the entire potential. Using the AS approach, the only II technique still in general use is the log-derivative method of Johnston (1973). Although the amplitude-density method (Johnston and Secrest (1966)) was the first to employ an AS/II technique, it is only used in exceptional circumstances. However the connection formulae derived are still of great value. The only method to date employing an AP/II approach is the R-matrix propagator method of Light and Walker (1976). It was originally introduced in the context of reactive scattering and later adapted to inelastic problems (Stechel, Walker and Light (1978)). Although it stands alone in its category it is becoming one of the most widely used in inelastic scattering.

## 2. Relative Merits of Approaches

The AS methods follow the solution explicitly and therefore the step size used in the integration algorithm is dependent on the energy of the collision. In order to accurately trace out the solution, its value must be known at a reasonable number of points per wavelength. Hence as the energy increases, the wavelength of the solution decreases and more steps must be taken over the integration range. However, the step size in the AP method is almost independent of the collision energy, since such algorithms are based on the potential. For the same reason, AP methods can take larger steps than AS methods. The AP methods require much more numerical effort per step than AS, however much of this effort is independent of the energy. Therefore by employing an AP method much of the information calculated at the first energy can be saved and used to generate solutions at subsequent energies very cheaply. Sometimes this attractive feature of an AP approach cannot be implemented for practical reasons. In large calculations involving many channels and steps, the storage requirements can become excessively large.

In order to be able to describe the target accurately during the collision, usually several energetically inaccessible (closed) channels have to be included in the basis. Such channels cause problems in the SF approach since computers, obviously, use finite arithmetic. Closed channels grow extremely rapidly, much more so than the others, leading to loss of linear independence of the solutions and hence

instabilities. In order to overcome this, numerous stabilisations must be performed as the solution is integrated out. This is performed by using unitary transformations to transform the solution vectors to new linear combinations to suppress such fast growing channels. The II methods do not suffer from this handicap. They are inherently stable due to the manner in which the scattering information is propagated across the integration range.

If few solutions of high accuracy are required, it is more efficient to use an AS approach. Although AP methods can produce highly accurate results, in general this requires small integration steps and therefore the advantage of AP methods is lost if only a few solutions are required. The numerical effort required to improve accuracy grows much faster in the AP approach than in the AS.

## 3. Choice of Algorithm for IOS calculations

The coupling matrix corresponding to the IOS equations coupled in vibration at a given rotor orientation $\gamma$ is given by (c.f. Chapter II eq. II.3.15).

$$W_{nn'}(R) = V_{nn'}(R) + \delta_{nn'}\left(\frac{L(L+1)}{R^2} - k_n^2\right) \qquad \text{III.3.1}$$

There are two important properties of III.3.1. concerning the choice of an appropriate algorithm. Firstly the equations are coupled in vibration only, and secondly that the orbital angular momentum term has the same value in each channel and is only present in the diagonal elements.

In general the vibrational energy level spacing is relatively large and therefore for reasonably small collision energies only a few vibrational channels need be retained in the basis set. The dimension of the matrix $W_{nn'}$ is therefore reasonably small. With such a small number of channels the numerical effort per step required by an AP method will not be largely in excess of that required by an AS method. However, the advantage of an AP approach is the use of much larger step lengths. Since few channels are involved an AP method will therefore be the most suitable.

The second property of III.3.1 noted is concerned with the solution of the equations at many values of L. The orbital angular momentum parameter term comes into the equations in a similar manner to the total energy - i.e. the equations are diagonal in L and it has the same value in each channel. The properties of AP methods, which allow the generation of solutions at different energies, can also be used to generate results for different values of L. To obtain an integral cross section the IOS equations must be solved at many values of L. By use of an AP method, information calculated in the solution for an initial value of L can be stored and used to generate the solutions for subsequent values of L with much less effort. However, there is one important difference in the manner in which L and the total energy, E, enter into the equations. The energy term, E, is independent of the integration co-ordinate R, but the L term is not. Therefore, in theory, the step size will be dependent on L. For the systems studied however, it turns out that the step size is not very strongly dependent on L, therefore the

generation of solutions for large numbers of values of L with little numerical effort is possible. There may be situations where the R dependence of the L term is important in the choice of step sizes. In such cases, the approximate potential used can be modified to deal with this dependence analytically. The step size will then be virtually independent of L, and the generation of large numbers of solutions for different values of L possible, whatever the system. Details of such a procedure and explicit expressions are derived in Section 4(c).

We note that the orbital angular momentum term is similarly treated in the coupled equations of the coupled states approximation and the effective potential method of Rabitz (1972), and hence similar savings in computer time are possible. Alexander (1974) has made use of this property in calculations employing Gordon's algorithm to solve the equations of the effective potential method. However, he makes no mention of the dependence of the step length on L.

The IOS approximation is exactly that - an approximation. Therefore, extremely high accuracy in the solution of the coupled equations involved is not warrented. The solution of the equations to three or four figures is sufficient, and this is easily within range of an AP method without requiring excessively small step sizes.

All the properties of the IOS coupled equations (the accuracy required, their mathematical form and the number of solutions required) suggest the use of an AP method. Of the AP methods, the R-matrix propagator method of Stechel,

Walker and Light (1978) was chosen. In contrast to, for example, Gordon's Algorithm it is relatively simple to program and, being an II method, inherently stable.

## 4. The R-Matrix Propagation Method

### (a) General Theory

Although originally presented as a method for solving the coupled second order differential equations for reactive scattering (Light and Walker (1976)), the description below is for equations appropriate to inelastic scattering, following Stechel, Walker and Light (1978) (hereafter referred to as SWL). In this context, the R-matrix referred to is the matrix relating functions to their derivatives at a given value of the integration co-ordinate.

The main advantage of this algorithm is its stability. It is an invarient imbedding method and hence completely insensitive to the numerical problems associated with closed channels. It has additional attractive features, other than those usually associated with an approximate potential method. It is based on basic matrix operations (diagonalisation, inversion, etc.) and by use of standard routines the code is simple to write and easily understandable. It is also reported to be fast and accurate.

The method is derived from the Magnus exponentiation method (see e.g. Light (1971)), but, basically, there is a re-arrangement in the manner in which the scattering information is propagated.

The general form of the coupled equations (III.1.1) can be written in matrix notation

$$\frac{d^2}{dR^2}\,\underset{\sim}{G}(R) = \underset{\sim}{W}(R)\,\underset{\sim}{G}(R) \qquad \text{III.4.1}$$

This set of N coupled second order differential equations can be re-written as 2N coupled first order equations

$$\frac{d}{dR}\begin{bmatrix}\underset{\sim}{G}(R)\\ \underset{\sim}{G}'(R)\end{bmatrix} = \begin{bmatrix}\underset{\sim}{O} & \underset{\sim}{I}\\ \underset{\sim}{W}(R) & \underset{\sim}{O}\end{bmatrix}\begin{bmatrix}\underset{\sim}{G}(R)\\ \underset{\sim}{G}'(R)\end{bmatrix} = \underset{\sim}{A}\begin{bmatrix}\underset{\sim}{G}(R)\\ \underset{\sim}{G}'(R)\end{bmatrix} \qquad \text{III.4.2}$$

where $\underset{\sim}{I}$ and $\underset{\sim}{O}$ are the unit and zero matrix respectively and $\underset{\sim}{A}$ is the 2N x 2N matrix as defined.

In the Magnus method, a 2N x 2N propagator $\underset{\sim}{U}$ is formed to relate $\underset{\sim}{G}(R)$ and $\underset{\sim}{G}'(R)$ to $\underset{\sim}{G}(R + \Delta R)$ and $\underset{\sim}{G}'(R + \Delta R)$ across the interval $\Delta R$ by

$$\begin{bmatrix}\underset{\sim}{G}(R+\Delta R)\\ \underset{\sim}{G}'(R+\Delta R)\end{bmatrix} = \underset{\sim}{U}\begin{bmatrix}\underset{\sim}{G}(R)\\ \underset{\sim}{G}'(R)\end{bmatrix} \qquad \text{III.4.3}$$

where U is given by the Magnus exponentiation

$$\underset{\sim}{U} = \exp\left\{(\Delta R)\,\underset{\sim}{A} - \frac{(\Delta R)^3}{12}\begin{bmatrix}\underset{\sim}{W}' & \underset{\sim}{O}\\ \underset{\sim}{O} & -\underset{\sim}{W}'\end{bmatrix} + \cdots\right\} \qquad \text{III.4.4}$$

where $\underset{\sim}{W}'$ is the matrix of derivatives of $\underset{\sim}{W}$. Usually $\Delta R$ is taken sufficiently small that by diagonalising $\underset{\sim}{W}$ at the centre of the sector, $\underset{\sim}{W}'$ is negligible across the sector, i.e. $\underset{\sim}{W}$ is approximated as a constant reference potential. Higher terms are ignored and only the first term in the exponentiation is used. In theory these propagators can be multiplied together to get a matrix to propagate G and G' across the entire integration range. However, the problem of stability

arises, and frequent time consuming stabilisation transformations are required.

In contrast to this, the R-matrix in general satisfies:-

$$\begin{bmatrix} \underset{\sim}{G}_A \\ \underset{\sim}{G}_B \\ \underset{\sim}{G}_C \\ \vdots \end{bmatrix} = \begin{bmatrix} \underset{\sim}{R}_{AA}\underset{\sim}{R}_{AB}\ \underset{\sim}{R}_{AC} \cdots \\ \underset{\sim}{R}_{BA}\ \underset{\sim}{R}_{BB} \\ \underset{\sim}{R}_{CA} \\ \vdots \end{bmatrix} \begin{bmatrix} \underset{\sim}{G}'_A \\ \underset{\sim}{G}'_B \\ \underset{\sim}{G}'_C \\ \vdots \end{bmatrix} \qquad \text{III.4.5}$$

Where A, B, C etc. are surfaces in configuration space on which the relationship between the translational wavefunctions G and their derivatives $G'$ is required in order to solve the equations. In 3 dimensional reactive scattering of an atom and a diatomic molecule there are 3 asymptotic arrangement channels, hence the R-matrix is blocked 3 x 3. However, for inelastic scattering, there is sufficient information on one surface located in asymptotic configuration space to enable an S-matrix, and hence cross-sections etc., to be calculated. By convention the direction of the derivatives is outwardly normal to the surface. In order to propagate the solution it is necessary to carry information from one surface at R to another at $R + \Delta R$. Since two surfaces are involved the "sector" R-matrices, which are solutions of the scattering problem within the sector, are blocked 2 x 2, i.e. they are 2N x 2N matrices.

The general procedure is to divide the integration range into sectors. At an integration co-ordinate R we have a "global" R-matrix relating G(R) and $G'(R)$ which is N x N. Within the sector $\Delta R$ we have a sector R-matrix relating $G(R + \Delta R)$, $G'(R + \Delta R)$, G(R) and $G'(R)$ which is 2N x 2N. We then construct a new global R-matrix at $R + \Delta R$, from the old

global R-matrix at R and the sector R-matrix across $\Delta R$.

Consider two adjacent sector ( $i-1$ ) and ( $i$ ) with mid-points $R_{i-1}$ and $R_i$ as in Figure 1.

$\underset{\sim}{R}^{(i-1)}$ and $\underset{\sim}{R}^{(i)}$ are global R-matrices on the surfaces shown, $\underset{\sim}{r}^{(i)}$ is the sector R-matrix relating the two surfaces and $h_i$ is the width of sector ( $i$ ).

At the centre of the $i^{th}$ sector, $R_i$, diagonalise the coupling matrix $\underset{\sim}{W}$. This is equivalent to transforming from the original target basis functions $\chi_n$ to new basis functions $\phi_n$ , say, which are linear combinations of the old, i.e.

$$\phi_n = \sum_{n'} T_{n'n}^{(i)} \chi_n \qquad \text{III.4.6}$$

such that $$\underset{\sim}{T}^{(i)^{-1}} \underset{\sim}{W}(R_i) \underset{\sim}{T}^{(i)} = \underset{\sim}{\lambda}^2(i) \qquad \text{III.4.7}$$

Note that due to the symmetry of $\underset{\sim}{W}$, $\underset{\sim}{T}$ is orthogonal i.e. $\underset{\sim}{T}^{(i)^{-1}} = \underset{\sim}{T}^{(i)^{T}}$ . We therefore have new equations in translational wavefunctions $\underset{\sim}{F}$ given by

$$F_n^{(i)}(R) = \sum_{n'} T_{n'n}^{(i)} G_{n'}(R) \qquad \text{III.4.8}$$

If we assume that this diagonilisation is exact across the entire sector, the equations are now completely decoupled within the sector, i.e.

$$\frac{d^2}{dR^2} F_n^{(i)}(R) = \left(\lambda_n^{(i)}(R)\right)^2 F_n^{(i)}(R) \qquad \text{III.4.9}$$

Adopting the notation:-

$$\underset{\sim}{F}_L(i) = \underset{\sim}{F}^{(i)}\left(R_i - \tfrac{1}{2}h_i\right)$$

$$\underset{\sim}{F}_R(i) = \underset{\sim}{F}^{(i)}\left(R_i + \tfrac{1}{2}h_i\right) \qquad \text{III.4.10}$$

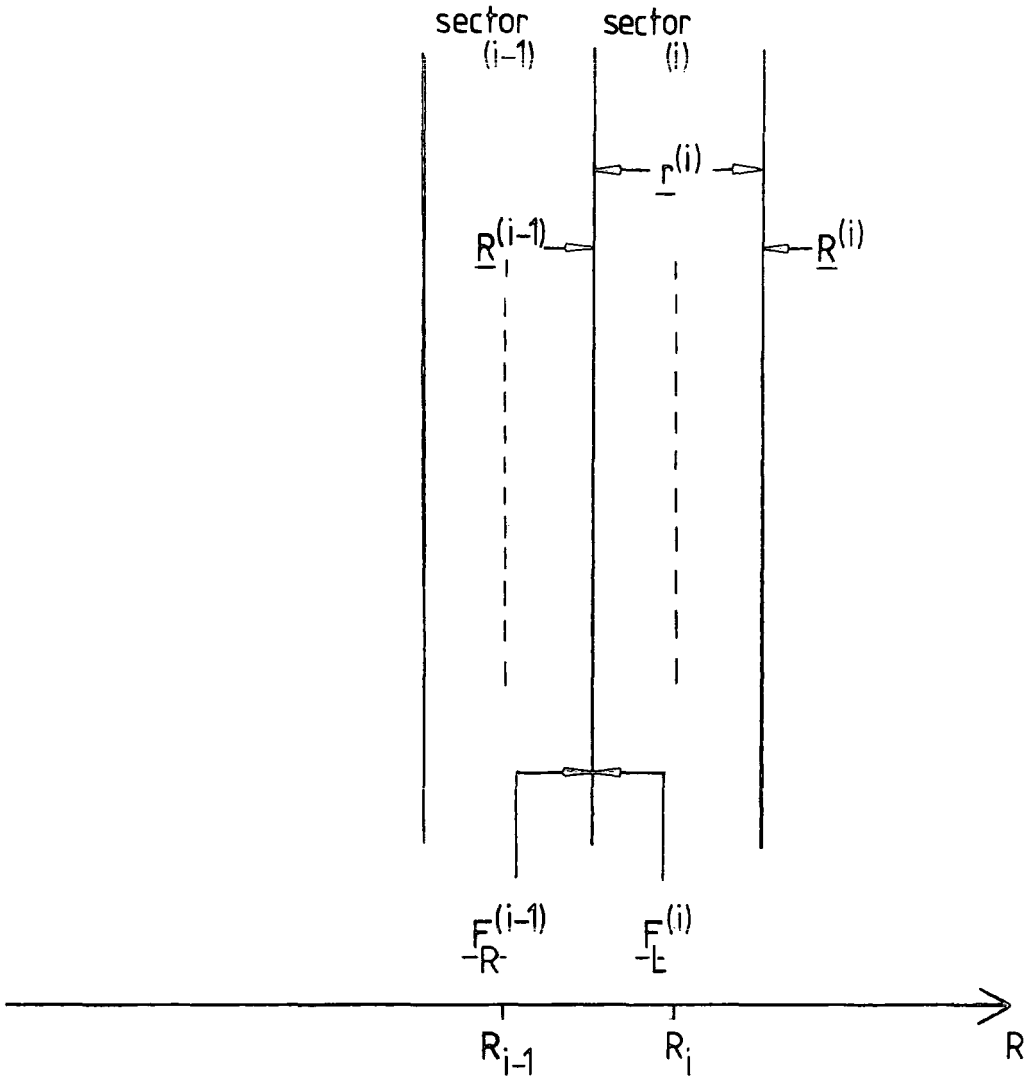


Figure 1 Schematic diagram showing the sectorisation of configuration space and the assembly of sector R-matrices to form the global R-matrix.

In this locally diagonal representation, the sector R-matrix $\underset{\sim}{r}^{(i)}$ is given by

$$\begin{bmatrix} \underset{\sim}{F}_L(i) \\ \underset{\sim}{F}_R(i) \end{bmatrix} = \begin{bmatrix} \underset{\sim}{r}_1^{(i)} & \underset{\sim}{r}_2^{(i)} \\ \underset{\sim}{r}_3^{(i)} & \underset{\sim}{r}_4^{(i)} \end{bmatrix} \begin{bmatrix} -\underset{\sim}{F}_L'(i) \\ \underset{\sim}{F}_R'(i) \end{bmatrix} \qquad \text{III.4.11}$$

where the negative sign on the right hand side is due to the convention of taking outwardly normal derivatives. The similarity with Magnus propagations (III.4.3) is now evident, but the information has been re-arranged. The precise form of the elements of $\underset{\sim}{r}^{(i)}$ depends on the form of $\lambda_n^{(i)}(R)$, and is discussed later in Section 4(c).

In order to cross into the next sector, one must transform from the representation in the $(i-1)^{th}$ sector to that in the $(i)^{th}$ sector, to maintain continuity of the total wave-function and its derivative. Although $\underset{\sim}{F}_R(i-1)$ and $\underset{\sim}{F}_L(i)$ refer to the same integration co-ordinate they are expressed in different representations. To do this, a return is made from the $\underset{\sim}{F}(i-1)$ representation back into the original $\underset{\sim}{G}$, and then into $\underset{\sim}{F}(i)$.

$$\underset{\sim}{F}_R(i-1) = \left[\underset{\sim}{T}^{(i-1)}\right]^T \underset{\sim}{G} = \left[\underset{\sim}{T}^{(i-1)}\right]^T \underset{\sim}{T}^{(i)} \underset{\sim}{F}_L(i) \qquad \text{III.4.12}$$

i.e.
$$\underset{\sim}{F}_R(i-1) = \underset{\sim}{Q}(i-1,i)\,\underset{\sim}{F}_L(i)$$

$$\underset{\sim}{F}_R'(i-1) = \underset{\sim}{Q}(i-1,i)\,\underset{\sim}{F}_L'(i)$$

where
$$\underset{\sim}{Q}(i-1,i) = \left[\underset{\sim}{T}^{(i-1)}\right]^T \underset{\sim}{T}^{(i)}$$

We now want to construct the new global R-matrix such that

$$\underset{\sim}{F}_R(i) = \underset{\sim}{R}^{(i)}\,\underset{\sim}{F}_R'(i) \qquad \text{III.4.13}$$

By using III.4.12 and the definition of the R-matrix III.4.13

$$\underset{\sim}{F}_L(i) = \underset{\sim}{Q}^{T}(i-1,i)\,\underset{\sim}{R}^{(i-1)}\,\underset{\sim}{Q}(i-1,i)\,\underset{\sim}{F}_L'(i) \qquad \text{III.4.14}$$

The definition of the sector R-matrix III.4.11 gives

$$\begin{aligned}\underset{\sim}{F}_L(i) &= -\underset{\sim}{r}_1^{(i)}\,\underset{\sim}{F}_L'(i) + \underset{\sim}{r}_2^{(i)}\,\underset{\sim}{F}_R'(i)\\ \underset{\sim}{F}_R(i) &= -\underset{\sim}{r}_3^{(i)}\,\underset{\sim}{F}_L'(i) + \underset{\sim}{r}_4^{(i)}\,\underset{\sim}{F}_R'(i)\end{aligned} \qquad \text{III.4.15}$$

Substituting of III.4.14 into III.4.15, eliminating $\underset{\sim}{F}_L(i)$ and $\underset{\sim}{F}_L'(i)$, gives

$$\begin{aligned}\underset{\sim}{F}_R(i) &= \left[\underset{\sim}{r}_4^{(i)} - \underset{\sim}{r}_3^{(i)}\,\underset{\sim}{Z}^{(i)}\,\underset{\sim}{r}_2^{(i)}\right]\underset{\sim}{F}_R'(i)\\ \underset{\sim}{Z}^{(i)} &= \left[\underset{\sim}{r}_1^{(i)} + \underset{\sim}{Q}^{T}(i-1,i)\,\underset{\sim}{R}^{(i-1)}\,\underset{\sim}{Q}(i-1,i)\right]^{-1}\end{aligned} \qquad \text{III.4.16}$$

This gives the new global R-matrix assembled from the old gobal R-matrix and the sector R-matrix. It is a subset of the equations first given by Zvijac and Light (1976).

$$\underset{\sim}{R}^{(i)} = \underset{\sim}{r}_4^{(i)} - \underset{\sim}{r}_3^{(i)}\,\underset{\sim}{Z}^{(i)}\,\underset{\sim}{r}_2^{(i)} \qquad \text{III.4.17}$$

$\underset{\sim}{Q}(i-1,i)$ and $\underset{\sim}{T}^{(i)}$ are orthogonal. Also, if $\underset{\sim}{R}^{(i-1)}$ and $\underset{\sim}{r}^{(i)}$ are symmetric, this recursion relation preserves the symmetry of the global R-matrix, which in turn ensures a unitary S-matrix.

The equations II.4.17 are the basis of the propagation. Calculating $\underset{\sim}{r}^{(i)}$ and $\underset{\sim}{T}^{(i)}$ in each sector, they are repeatedly used to propagate the R-matrix from near the

origin out to the asymptotic region, where boundary conditions are imposed.

(b) Specifying Boundary Conditions

Near the origin, R = 0, in the first sector, $i = 1$, the R-matrix has to be initialised such that the regular solutions satisfy

$$\underset{\sim}{F}_R(1) = \underset{\sim}{R}^{(1)} \underset{\sim}{F}_R'(1) \qquad \text{III.4.18}$$

For regular boundary conditions with a large repulsive potential near the origin the solutions are exponentials. We therefore have

$$\left( R^{(1)} \right)_{ij} = \delta_{ij} \left| \lambda_j \right|^{-1} \qquad \text{III.4.19}$$

This is the starting point. Using the recursion described in Section 4(a), the R-matrix is propagated outwards from the origin across the integration range until its value is known on a surface in the asymptotic region, at sector M, say. The global R-matrix $\underset{\sim}{R}^{(M)}$ is expressed in the locally diagonal representation appropriate to the $M^{th}$ sector. In order to match the solution to asymptotic boundary conditions, a final transformation is required to return to the original basis representation $\chi_n$, to obtain a solution for the original radial wavefunctions $\underset{\sim}{G}$ (rather than the $\underset{\sim}{F}_R(M)$) using:-

$$\underset{\sim}{G}_R(M) = \underset{\sim}{T}^{(M)} \underset{\sim}{F}_R(M) \qquad \text{III.4.20}$$

$$\underset{\sim}{G}_R'(M) = \underset{\sim}{T}^{(M)} \underset{\sim}{F}_R'(M)$$

Hence

$$\underset{\sim}{R}^{final} = \underset{\sim}{T}^{(M)} \underset{\sim}{R}^{(M)} \left[ \underset{\sim}{T}^{(M)} \right]^T \qquad \text{III.4.21}$$

$$\underset{\sim}{G}_R(M) = \underset{\sim}{R}^{final} \underset{\sim}{G}_R'(M)$$

$R^{final}$ is the asymptotic R-matrix expressed in the original primitive basis on the right hand side of the $M^{th}$ sector. The symptotic form of $\underset{\sim}{G}$ can be written as

$$\underset{\sim}{G} = \underset{\sim}{A} - \underset{\sim}{B}\,\underset{\sim}{S}^{\circ}$$
$$\underset{\sim}{G}' = \underset{\sim}{A}' - \underset{\sim}{B}'\,\underset{\sim}{S}^{\circ} \qquad \text{III.4.22}$$

Where $\underset{\sim}{A}$ is a diagonal matrix of incoming open channel asymptotic wavefunctions and $\underset{\sim}{B}$ a diagonal matrix of outgoing asymptotic wavefunctions. $\underset{\sim}{S}^{\circ}$ is basically the S-matrix.

From III.4.22 and III.4.21 we obtain directly

$$\underset{\sim}{S}^{\circ} = \left(\underset{\sim}{R}^{final}\,\underset{\sim}{B}' - \underset{\sim}{B}\right)^{-1}\left(\underset{\sim}{R}^{final}\,\underset{\sim}{A}' - \underset{\sim}{A}\right) \qquad \text{III.4.23}$$

In the case of the IOS equations coupled in vibration at a given rotor orientation $\gamma$ (cf. II.3.17).

$$\left(\underset{\sim}{G}(R)\right)_{vv'} \equiv U^{Lv}_{v'} \xrightarrow[R\to\infty]{} \left(-ik_{v'}R\,h^{(2)}_{L}(k_{v'}R)\right)\delta_{vv'} - \left(\frac{k_v}{k_{v'}}\right)^{1/2} S^{L}_{vv'}(\gamma)\left(ik_{v'}R\,h^{(1)}_{L}(k_{v'}R)\right) \qquad \text{III.4.24}$$

hence
$$\left(\underset{\sim}{A}\right)_{vv'} = \delta_{vv'}\left(-ik_{v'}R\,h^{(2)}_{L}(k_{v'}R)\right) \qquad \text{III.4.25a}$$

$$\left(\underset{\sim}{B}\right)_{vv'} = \delta_{vv'}\left(ik_{v'}R\,h^{(1)}_{L}(k_{v'}R)\right) \qquad \text{III.4.25b}$$

$$\left(S^{\circ}\right)_{vv'} = \left(\frac{k_v}{k_{v'}}\right)^{1/2} S^{L}_{vv'}(\gamma) \qquad \text{III.4.25c}$$

Computationally, it is simpler to work in terms of the K-matrix since all the functions appearing are real. The appropriate definitions are then (cf. II.2.20b)

$$\left(\underset{\sim}{A}\right)_{vv'} = \delta_{vv'}\left(k_{v'}R\,j_{L}(k_{v'}R)\right) \qquad \text{III.4.26a}$$

$$\left(\underset{\sim}{B}\right)_{vv'} = \delta_{vv'}\left(k_{v'}R\,n_{L}(k_{v'}R)\right) \qquad \text{III.4.26b}$$

$$\left(S^{\circ}\right)_{vv'} = \left(\frac{k_v}{k_{v'}}\right)^{1/2} K^{L}_{vv'}(\gamma) \qquad \text{III.4.26c}$$

We can therefore obtain an S-matrix from III.4.23 by using the definitions of III.4.25 or III.4.26 and hence all the scattering information.

(c) Form of Propagators

Within the sector the equations are completely uncoupled. Therefore, the elements of the sector R-matrix, $\underset{\sim}{r}_1$, $\underset{\sim}{r}_2$, $\underset{\sim}{r}_3$ and $\underset{\sim}{r}_4$, must be diagonal to prevent mixing of the solutions. Dropping the sector index $i$ from III.4.9, each solution satisfies

$$\frac{d^2}{dR^2} F_n(R) = \left(\lambda_n(R)\right)^2 F_n(R) \qquad \text{III.4.27}$$

We therefore have a one-channel problem for each solution within the sector. Considering only those elements of the sector R-matrix concerned with $F_n$ we also have (cf. III.4.11)

$$\begin{bmatrix} F_n(a) \\ F_n(b) \end{bmatrix} = \begin{bmatrix} (r_1)_{nn} & (r_2)_{nn} \\ (r_3)_{nn} & (r_4)_{nn} \end{bmatrix} \begin{bmatrix} -F_n'(a) \\ F_n'(b) \end{bmatrix} \qquad \text{III.4.28}$$

where a is the value of R at the left hand side of the sector and b is the value at the right hand side (ie. $a = R_i - \frac{1}{2}h_i$, $b = R_i + \frac{1}{2}h_i$)

Equation III.4.27 is an ordinary second order differential equation and let its solutions be A(R) and B(R). The general solution and its derivative are therefore

$$\begin{aligned} F_n(R) &= \alpha A(R) + \beta B(R) \\ F_n'(R) &= \alpha A'(R) + \beta B'(R) \end{aligned} \qquad \text{III.4.29}$$

where $\alpha$ and $\beta$ are arbitrary constants. The Wronskian of A(R) and B(R) is a constant, denoted by W

$$W = A(R)B'(R) - B(R)A'(R) \qquad \text{III.4.30}$$

Equation III.4.28 must hold for any solution of III.4.27 and therefore the sector R-matrix must be independent of $\alpha$ and $\beta$. We can therefore chose any two solutions, $F_1$ and $F_2$ say, with convenient $\alpha$ and $\beta$ to determine the R-matrix. The solutions are taken to be such that they satisfy the boundary conditions.

$$F_1(a) = 1 \qquad F_1'(a) = 0$$
$$F_2(b) = 1 \qquad F_2'(b) = 0 \qquad \text{III.4.31}$$

Substitution of III.4.31 in III.4.28 gives the elements of the sector R-matrix in terms of $F_1$ and $F_2$.

$$(r_1)_{nn} = -\frac{F_2(a)}{F_2'(a)} \qquad (r_2)_{nn} = 1/F_1'(b)$$
$$(r_3)_{nn} = -1/F_2'(a) \qquad (r_4)_{nn} = \frac{F_1(b)}{F_1'(b)} \qquad \text{III.4.32}$$

The solutions $F_1$ and $F_2$ satisfying the boundary conditions III.4.31 are given by

$$F_1(R) = W^{-1}\left[B'(a)A(R) - A'(a)B(R)\right] \qquad \text{III.4.33a}$$

$$F_2(R) = W^{-1}\left[B'(b)A(R) - A'(b)B(R)\right] \qquad \text{III.4.33b}$$

which can be easily verified. Substitution of III.4.33a, b into III.4.32 gives the explicit form of the sector R-matrix in terms of solutions A(R) and B(R).

$$(r_1)_{nn} = \frac{B'(b)A(a) - A'(b)B(a)}{A'(b)B'(a) - B'(b)A'(a)}$$

$$(r_2)_{nn} = W\left[B'(a)A'(b) - A'(a)B'(b)\right]^{-1} \qquad \text{III.4.34}$$

$$(r_3)_{nn} = W\left[A'(b)B'(a) - B'(b)A'(a)\right]^{-1}$$

$$(r_4)_{nn} = \frac{B'(a)A(b) - A'(a)B(b)}{B'(a)A'(b) - A'(a)B'(b)}$$

Note that $(r_2)_{nn} = (r_3)_{nn}$, hence the sector R-matrix is symmetric, ensuring that the recurrence relation III.4.17 maintains the symmetry of the global R-matrix and hence the unitarity of the S-matrix.

The simplest form of the sector R-matrix is obtained by approximating $\lambda_n(R)$ as constant within the sector, $\lambda_n$ say. The solutions of III.4.27 are therefore given by

$$A(R) = e^{-|\lambda_n|R}, \quad B(R) = e^{|\lambda_n|R} \qquad \lambda_n^2 > 0 \qquad \text{III.4.35}$$

$$A(R) = \cos(|\lambda_n|R), \quad B(R) = \sin(|\lambda_n|R) \qquad \lambda_n^2 \leq 0$$

Substitution into III.4.34 using $b = a + h_i$ gives

$$(r_1)_{nn'} = (r_4)_{nn'} = \delta_{nn'} \begin{cases} |\lambda_n|^{-1} \coth|h_i\lambda_n| & \lambda_n^2 > 0 \\ -|\lambda_n|^{-1} \cot|h_i\lambda_n| & \lambda_n^2 \leq 0 \end{cases} \qquad \text{III.4.36}$$

$$(r_2)_{nn'} = (r_3)_{nn'} = \delta_{nn'} \begin{cases} |\lambda_n|^{-1} \operatorname{csech}|h_i\lambda_n| & \lambda_n^2 > 0 \\ -|\lambda_n|^{-1} \operatorname{csec}|h_i\lambda_n| & \lambda_n^2 \leq 0 \end{cases}$$

Any form of $\lambda_n(R)$ can be used which gives known solutions, A(R) and B(R), to III.4.27. The diagonalising transformation must be constant within the sector to maintain decoupling of the equations. However, there may be situations where this transformation is slowly varying but the potential, and hence $\lambda_n(R)$, is rapidly varying with R. Employing a sector R-matrix appropriate to the varying $\lambda_n(R)$ would permit larger step lengths. Such a situation can arise in the coupled equations of the IOS approximation. The coupling matrix in the IOS can be written (cf. III.3.1)

$$W_{nn'}(R) = W^1_{nn'}(R) + \delta_{nn'}\left(\frac{L(L+1)}{R^2}\right) \qquad \text{III.4.37a}$$

where

$$W^1_{nn'}(R) = V_{nn'}(R) - \delta_{nn'} k_n^2 \qquad \text{III.4.37b}$$

In matrix notation we have

$$\underset{\sim}{W}(R) = \underset{\sim}{W}^1(R) + \underset{\sim}{I}\left(\frac{L(L+1)}{R^2}\right) \qquad \text{III.4.37c}$$

The transformation which diagonalises $\underset{\sim}{W}^1(R)$ will also diagonalise $\underset{\sim}{W}(R)$, i.e. it is independent of L.

$$\underset{\sim}{T}^T \underset{\sim}{W}^1 \underset{\sim}{T} = \underset{\sim}{q}^2 \qquad \text{III.4.38a}$$

$$\underset{\sim}{T}^T \underset{\sim}{W} \underset{\sim}{T} = \underset{\sim}{q}^2 + \underset{\sim}{I}\left(\frac{L(L+1)}{R^2}\right) \qquad \text{III.4.38b}$$

The sector must be sufficiently small that the transformation is constant across it. The off-diagonal elements of $\underset{\sim}{W}$ are all contained in $\underset{\sim}{W}^1$, therefore it is reasonable to approximate $\underset{\sim}{q}^2$ as constant within the sector. The form of the eigenvalues of $\underset{\sim}{W}$ can be approximated by

$$(\lambda_n(R))^2 = q_n^2 + \frac{L(L+1)}{R^2} \qquad \text{III.4.39}$$

where $q_n^2$ is a constant. The solutions of III.4.27 with $(\lambda_n(R))^2$ as defined by III.4.39 are expressed in terms of Spherical Bessel functions for $q_n^2 < 0$ or Modified Spherical Bessel functions for $q_n^2 \geq 0$ of the 1st and 2nd kind (Abramowitz and Stegun 1965).

$$A(R) = \begin{cases} |q_n| R\, j_L(|q_n| R) & q_n^2 < 0 \\ |q_n| R \sqrt{\dfrac{\pi}{2|q_n| R}}\, I_{L+\frac{1}{2}}(|q_n| R) & q_n^2 \geq 0 \end{cases} \qquad \text{III.4.40}$$

$$B(R) = \begin{cases} |q_n|R\, n_L(|q_n|R) & q_n^2 < 0 \\ |q_n|R \sqrt{\frac{\pi}{2|q_n|R}}\, I_{-L-\frac{1}{2}}(|q_n|R) & q_n^2 \geq 0 \end{cases} \qquad \text{III.4.40}$$

Substitution of these solutions into III.4.34 yields the appropriate sector R-matrix. Such propagators are much more cumbersome than those derived by use of a constant $\lambda_n$. However, their evaluation can be made extremely efficient by using the recursion relations which exist between Bessel functions. Consider the case $q_n^2 < 0$.

Let $\quad C_L(|q_n|R) \equiv |q_n|R\, j_L(|q_n|R)$ or $|q_n|R\, n_L(|q_n|R)$

Then it can be easily shown (Abramowitz and Stegun)

$$C_{L+1}(|q_n|R) = \frac{(L+1)}{|q_n|R} C_L(|q_n|R) - \frac{1}{|q_n|} C'_L(|q_n|R) \qquad \text{III.4.41}$$

$$C'_{L+1}(|q_n|R) = \frac{1}{|q_n|}\left[ C_L(|q_n|R) - \frac{(L+1)}{|q_n|R} C_{L+1}(|q_n|R)\right]$$

Similar expressions can be derived for the case $q_n^2 \geq 0$. Therefore the solutions required for the propagators, A(a), A'(a), B(a) etc. can easily be generated from the corresponding values used in the previous partial wave. This approach requires a considerable amount of storage, since at each sector boundary the values of A(R), A'(R), B(R) and B'(R) must be known for each eigenvalue $q_n$. We also require the value of R at the sector boundary and the values of $q_n$, at the mid-point of the sector, for the recursion relations. In total, for an N-channel calculation each step requires the storage of 5N + 1 numbers in addition to the transformation matrix of dimension $N^2$. For the small number of channels normally required, this storage presents no problem.

Indeed, the reduction in the total number of steps required will offset this storage.

The use of sector R-matrices assembled from the functions defined by III.4.40 has two very important advantages. It will not only allow larger step lengths, but also make such step lengths virtually independent of L. As the diagonal terms of the matrix $\underset{\sim}{W}$ increase, the relative importance of the off-diagonal terms is reduced. Because of this, the step lengths are dependent on L (and similarly the total energy E), but this dependence will be weak. The computer program can therefore generate results for large numbers of partial waves, using the same step lengths for each, extremely efficiently.

(d) The Step Length Algorithm

Whichever form of sector R-matrix is employed, the diagonalising transformation must be constant, to within a given tolerance, across the sector. Use of propagators defined by III.4.36 demands the additional condition that $W_{nn'}(R)$ is constant also, whereas use of propagators defined by III.4.40 demands only that $W_{nn'}{}^{1}(R)$ is constant. In the discussion below it is convenient to denote $\lambda_n \equiv q_n$ in the latter case. The derivative of the coupling matrix is related to that of the interaction potential, and the sector width controlling this advised by SWL is given by

$$VSTEP = h_{i+1} = BETA \times \left[\left(\frac{2\mu}{\hbar^2} V'(R)\right)^2\right]^{-1/6} \qquad \text{III.4.42}$$

where BETA is a tolerance and $V'(R)$ is a measure of the rate of change of the potential, given as the rate of change of the average eigenvalue.

$$\frac{2\mu}{\hbar^2} V'(R) = \frac{1}{N} \sum_{n=1}^{N} \left( \frac{\lambda_n^2(i) - \lambda_n^2(i-1)}{R_i - R_{i-1}} \right) \qquad \text{III.4.43}$$

The problem with this approach is that local minima or maxima, where $V'(R) \rightarrow 0$, can cause gross overestimation. This can be overcome by not allowing too large an increment, relative to the last sector.

$$GSTEP = h_{i+1} = h_i \times FACT \qquad \text{III.4.44}$$

A method of directly estimating the rate of change of the diagonalising transformation, $\underset{\sim}{T}^{(i)}$ is to examine $\underset{\sim}{Q}(i-1, i)$. If $\underset{\sim}{T}^{(i)} = \underset{\sim}{T}^{(i-1)}$ then

$$\underset{\sim}{Q}(i-1,i) = \left[\underset{\sim}{T}^{(i-1)}\right]^T \left[\underset{\sim}{T}^{(i)}\right] = \underset{\sim}{I} \qquad \text{III.4.45}$$

The deviation of $\underset{\sim}{Q}$ from a unit matrix can be used to control the step length via,

$$CSTEP = h_{i+1} = CUPMAX \times \left( \frac{N-1}{2 \times CUPLR} \right)^{1/2}$$

$$CUPLR = \frac{Tr\,(\underset{\sim}{I} - \underset{\sim}{Q})}{N\,(R_i - R_{i-1})^2}$$

Final control over the step length can be implemented by specifying a minimum and maximum step length, STMIN and STMAX. The final predicted step length being

$$STEP = \min\,(STMAX, VSTEP, CSTEP, GSTEP)$$

$$h_{i+1} = \max\,(STEP, STMIN)$$

BETA, CUPMAX, FACT, STMIN and STMAX are all input tolerances which must be specified to obtain the best results for the problem considered.

Use of the two propagators discussed earlier will only differ in the value of VSTEP. Employing propagators appropriate to a constant eigenvalue within the sector (III.4.36) PR1 say, restricts VSTEP more severely than use of those defined by III.4.40, PR2. The eigenvalues of PR1 contain the term $L(L + 1)/R^2$ whereas those of PR2 do not.

PR1 $\quad \lambda_n^2 \equiv q_n^2 + L(L+1)/R^2$

PR2 $\quad \lambda_n^2 \equiv q_n^2$

The approximation of $q_n^2$ constant within the sector will be closely related to T being constant also, since both are based on the rate of change of the interaction potential. Therefore PR2 comprises basically only one condition on the step length, that it is sufficiently small that diagonalisation is accurate over the entire sector. PR1 has the additional condition that $L(L + 1)/R^2$ must also be approximately constant. The step length algorithm presented is completely independent of the total energy E both for PR1 and PR2, however PR2 has the additional, extremely powerful, advantage that it is also independent of L. Storage of the transformation matrices and the eigenvalues $q_n^2$ can therefore be used to generate solutions for a large range of L values. The same procedure can be followed in PR1, however care must be taken that the step sizes used for the initial L value are sufficiently small to obtain accurate results for subsequent values. This may necessitate calculating solutions for only a small range of L values using given step sizes, then changing the step sizes to facilitate the calculation of another range of values, etc.

Although the step length algorithm is completely independent of E (and also L for PR2), in theory the step sizes

are not. If the diagonal elements of the coupling matrix are increased in magnitude by a change in E or L, the relative importance of the off-diagonal elements is reduced and larger step lengths are possible. However this dependence is weak, and the failure of the step length algorithm to take account of it is not important.

(e) Propagating Variable Numbers of Channels

In order to obtain convergence of the scattering information it is frequently necessary to carry a large number of locally closed (negative kinetic energy) channels. These are required in the expansion of the total wavefunction in order to accurately describe the target when it is perturbed. The corresponding translational functions frequently carry no useful scattering information since they gain no appreciable amplitude. The possibility therefore exists of carrying just a sufficient number of channels depending on the degree of perturbation in the sector. The procedure is to drop channels when they are no longer required to accurately describe the target and pick them up when they are.

The contraction of the basis set is simply performed by truncation of the global R-matrix - the row and column corresponding to the dropped channel is cut out. The R-matrix remains symmetric and hence preserves the unitarity of the S-matrix. The addition of channels in sector $i$, say, is performed by taking the global R-matrix on the outer surface $\underset{\sim}{R}^{(i)}$ and bringing it up to the larger dimension by adding elements appropriate to the initial conditions III.4.19.

SWL suggest two criteria for the inclusion or exclusion of closed channels. The first is the obvious procedure of

specifying a tolerance parameter based upon the extent to which a channel is closed. If the negative kinetic energy of a channel is larger than the tolerance then the channel is dropped from the calculation. However, such a channel may be strongly coupled to those retained, and therefore important, and should not be omitted. The off-diagonal elements of $\underset{\sim}{Q}$ determine how strong the coupling between channels is. The quantity recommended to estimate the extent to which channel j is coupled to 1, 2 ... (j-1) is given by

$$\gamma_j = \frac{1}{(2_j - 2)(R_\lambda - R_{\lambda-1})} \left[ \sum_{k=1}^{j-1} \left( Q_{jk}^2 + Q_{kj}^2 \right) \right]^{1/2}$$

In propagating across a given sector we retain all locally open channels, a minimum number of locally closed, and, in addition, any closed channels which cannot be dropped by the criteria above.

## 5. The Algorithm of de Vogelaere

The method of de Vogelaere (1955) is a solution following algorithm in the approximate solution approach. The algorithm is based on the following matrix equations, which construct the solution matrix, $\underset{\sim}{G}$, and its derivative $\underset{\sim}{G}'$ at the integration co-ordinate (R + h) from their previous values (see e.g. Lester (1976)).

$$\underset{\sim}{G}(R+\tfrac{1}{2}h) = \underset{\sim}{G}(R) + \tfrac{1}{2}h\,\underset{\sim}{G}'(R) - \frac{h^2}{24}\left(4\,\underset{\sim}{W}(R)\,\underset{\sim}{G}(R) - \underset{\sim}{W}(R-\tfrac{1}{2}h)\,\underset{\sim}{G}(R-\tfrac{1}{2}h)\right) \qquad \text{III.5.1}$$

$$\underset{\sim}{G}(R+h) = \underset{\sim}{G}(R) + h\,\underset{\sim}{G}'(R) - \frac{h^2}{6}\left(\underset{\sim}{W}(R)\,\underset{\sim}{G}(R) + 2\,\underset{\sim}{W}(R+\tfrac{1}{2}h)\,\underset{\sim}{G}(R+\tfrac{1}{2}h)\right) \qquad \text{III.5.2}$$

$$\underset{\sim}{G}'(R+h) = \underset{\sim}{G}'(R) - \frac{h}{6}\left(\underset{\sim}{W}(R)\,\underset{\sim}{G}(R) + 4\,\underset{\sim}{W}(R+\tfrac{1}{2}h)\,\underset{\sim}{G}(R+\tfrac{1}{2}h) + \underset{\sim}{W}(R+h)\,\underset{\sim}{G}(R+h)\right) \qquad \text{III.5.3}$$

The terms neglected in III.5.1, 2 and 3 are of order $h^4$, $h^5$ and $h^5$ respectively. The algorithm is initialised at some point, sufficiently deep within the classically forbidden region, and, by repeated use of III.5.1, 2, 3, the solution matrix and its derivative can be propagated into the asymptotic region. It is not possible to know, in advance, which initial conditions will lead to the correct asymptotic boundary conditions (III.4.22). Therefore, it is necessary to find a complete set of solutions and, at the end of the calculation, take the appropriate linear combinations which satisfy the desired boundary conditions. Since we do not know how to pick the initial wavefunction, we chose an arbitrary linear combination of all solutions such that $\underset{\sim}{G} = \underset{\sim}{0}$. The algorithm is initialised at $R_0$, say, by

$$\underset{\sim}{G}(R_0 - \tfrac{1}{2}h) = -\tfrac{1}{2}h\,\underset{\sim}{G}'(R_0) \quad ; \quad \underset{\sim}{G}(R_0) = 0 \qquad \text{III.5.4}$$

where $\underset{\sim}{G}'(R_0)$ is an arbitrary non-singular matrix (frequently chosen to be the unit matrix, $\underset{\sim}{I}$). When the solution is propagated into the asymptotic region it will not satisfy the correct boundary condition, but will be of the form

$$\underset{\sim}{G} = \underset{\sim}{A}\underset{\sim}{X} - \underset{\sim}{B}\underset{\sim}{Y} \qquad \text{III.5.5}$$

$$\underset{\sim}{G}' = \underset{\sim}{A}'\underset{\sim}{X} - \underset{\sim}{B}'\underset{\sim}{Y} \qquad \text{III.5.6}$$

Where A and B are as defined in Section 4b and $\underset{\sim}{X}$ and $\underset{\sim}{Y}$ are constant. A and B are diagonal matrices and satisfy a Wronskian relation

$$\underset{\sim}{M} = \underset{\sim}{A}\underset{\sim}{B}' - \underset{\sim}{A}'\underset{\sim}{B} \qquad \text{III.5.7}$$

(For A and B defined in order to calculate the S matrix (III.4.25a,b) $\underset{\sim}{M} = -2i\underset{\sim}{I}$. For the definitions used to calculate the K-matrix (III.4.26a, b) $\underset{\sim}{M} = \underset{\sim}{I}$).

Using III.5.5, 6 and 7 it is easily shown that

$$\underset{\sim}{X} = \underset{\sim}{M}^{-1}\left(\underset{\sim}{A}'\underset{\sim}{G} - \underset{\sim}{A}\underset{\sim}{G}'\right) \qquad \text{III.5.8}$$

$$\underset{\sim}{Y} = \underset{\sim}{M}^{-1}\left(\underset{\sim}{B}'\underset{\sim}{G} - \underset{\sim}{B}\underset{\sim}{G}'\right) \qquad \text{III.5.9}$$

The linear combinations which satisfy the correct asymptotic boundary conditions are given by

$$\underset{\sim}{G}^{A}(R) = \underset{\sim}{G}\,\underset{\sim}{X}^{-1} = \underset{\sim}{A} - \underset{\sim}{B}\left(\underset{\sim}{Y}\underset{\sim}{X}^{-1}\right) \qquad \text{III.5.10}$$

Comparing III.5.10 with III.4.22 gives

$$\underset{\sim}{S}^{o} = \underset{\sim}{Y}\underset{\sim}{X}^{-1} \qquad \text{III.5.11}$$

and hence all the scattering information can be obtained.

The problem of stability, caused by the growth of the closed channel solutions, is common to all solution following algorithms. During the solution of the equations some of the weakly growing solutions may be many orders of magnitude smaller than the fast growing, closed channel solutions and, since we are carrying only a finite number of digits, significance is lost and the solutions lose their linear independence. This results in the solution matrix becoming singular. To overcome this, stabilisation must be performed periodically, by taking linear combinations of the solutions. These new linear combination are chosen such that they are, numerically, more linearly independent than the original solutions. This can be achieved by multiplying III.5.1, 2 and 3 by the inverse of the solution matrix (Wagner and

McKoy (1973)). This transformation, therefore, replaces $\underset{\sim}{G}$ by $\underset{\sim}{I}$, and $\underset{\sim}{G}'$ by $\underset{\sim}{G}'\underset{\sim}{G}^{-1}$. It is not necessary to perform this stabilisation at every step in the integration and the frequency of stabilisation will depend on the particular calculation.

# CHAPTER IV

# ROVIBRATIONAL EXCITATION OF $H_2$ BY He

## 1. Introduction

For several reasons, an important test case for the study of rovibrational excitation of diatomic molecules by atoms is the $H_2$ + He system. First, there exist several ab initio potential surfaces for this sytem. Secondly, experimental results are available and, thirdly, the $H_2$ + He system is the simplest closed-shell neutral-atom-molecule pair suitable for such purposes.

Krauss and Mies (1965) studied the $H_2$ + He system employing a self consistent field (SCF), molecular orbital method, for a limited range of orientations. These calculations were extended by Gordon and Secrest (1970). The Krauss-Mies and Gordon-Secrest potentials are analytic fits to limited-basis set, SCF calculations which do not contain the correlation effects responsible for the long range behaviour of the surface. In contrast, the series of configuration interaction points computed by Tsapline and Kutzelnigg (1973) do incorporate some correlation effects. These points have been extended and fitted to an analytic form by Raczkowski and Lester (1977). The incorporation of correlation effects gives the Tsapline-Kutzelnigg potential a shallow Van der Waal's minimum, whereas the Krauss-Mies and Gordon-Secrest potentials are purely repulsive.

The experimental results are in the form of vibrational relaxation rate coefficients for $H_2$ dilute in He. Audibert et al. (1973, 1974, 1976) have used a stimulated Raman

technique to obtain values of these rates for the temperature range 50-450K, and, by varying the relative concentrations of ortho and para $H_2$, have obtained values for each of these species individually. Values for the temperature range 1350-3000K have been obtained by Dove and Teitelbaum (1974) by employing a shock tube method.

Of all atom-molecule systems, $H_2$ + He is the most manageable computationally. Not only because it is the simplest neutral-atom diatom system, but also because the rotational levels of $H_2$ are widely separated and there are relatively few rotational levels between the vibrational levels. This feature makes feasible a rigorous close-coupling (CC) calculation for this system. Heavier diatomic molecules have a large number of rotational levels which must be considered in scattering calculations, and, because of the 2j + 1 rotational degeneracy, the number of coupled equations becomes excessively large. This relatively large rotational energy level spacing in the $H_2$ molecule also provides a stringent test of approximate treatments of the rotational motion of the molecule, particularly the energy sudden and the infinite order sudden approximations (see Chapter II.3a and 3c respectively).

Due to the computational difficulties, the early CC calculations carried out by Eastes and Secrest (1972) and McGuire and Micha (1972) were largely exploratory in nature, involving small channel bases. Eastes and Secrest employed the Gordon-Secrest potential in calculations for para $H_2$ + He and were interested principally in the energy range below

the first vibrational threshold. These calculations were extended to higher collision energies by Lin and Secrest (1979). Lin (1979, 1980) has also performed detailed calculations at energies close to the first and second vibrational thresholds. Raczkowski et al. (1978) have performed CC calculations for para $H_2$ + He employing both the Gordon-Secrest and the Tsapline-Kutzelnigg potentials. Their aim was to produce a set of benchmark calculations and to investigate the effect of the different potential surfaces on the rovibrational cross sections and vibrational relaxation rates. More recent CC calculations by Orlikowski (1981), also employing the Tsapline-Kutzelnigg potential, extend to energies much closer to the first vibrational threshold to obtain a more accurate determination of the vibrational relaxation rates.

McGuire and Toennies (1975) employed several potential surfaces in their coupled states (CS) calculations. However, these results were later shown to be unreliable (Alexander and McGuire (1976)) due to the neglect of closed channels, i.e. from the insufficiency of the basis set. Alexander and McGuire (1976) performed CS calculations for para $H_2$ + He employing a total of five different potential surfaces. These surfaces are all based on the Gordon-Secrest potential, but with various modifications designed to investigate the sensitivity of rovibrational cross sections and the vibrational relaxation rate to the presence of long range interactions and potential minima. Alexander (1976) has performed similar CS calculations for ortho $H_2$ + He, employing one of these modified Gordon-Secrest potential surfaces.

Bowman and Leasure (1977) have performed IOS calculations of rovibrational excitation of $H_2$ by He, treating the vibrational coupling by CC techniques. Similar studies have been undertaken by Eno and Balint-Kurti (1979) and Bieniek (1980) within the framework of the adiabatic distorted wave (ADW) IOS approximation, where the vibrational coupling is treated by ADW techniques. Eno and Balint-Kurti (1981) have also explicitly investigated the efficiency of employing ADW techniques, compared to a CC treatment, for the calculation of fixed-angle S-matrices for the $H_2$ + He system. Rabitz and Zarur (1974) and Alexander (1974) applied the effective potential approximation of Rabitz (1972) in studies of rovibrational excitation of $H_2$ by He. The semiclassical strong-coupling correspondence principle of Percival and Richards (1970) has been applied by Clark (1977).

## 2. Description of the System

The model system employed is that used by Eastes and Secrest (1972) and subsequently by Lin and Secrest (1979) and Lin (1979, 1980). The He-$H_2$ interaction potential is that of Gordon and Secrest (1970) which takes the form

$$V(R,r) = C \exp\left(-\alpha_0 R + \alpha_1 R \Delta r\right)\left[\left(1+\gamma_0 \Delta r\right) + \beta\left(1+\gamma_2 \Delta r\right) P_2\left(\hat{R}\cdot\hat{r}\right)\right] \qquad \text{IV.2.1}$$

where $\Delta r = r - r_0$, with $r_0$, the equilibrium separation of the $H_2$ molecule. The basis functions of the $H_2$ molecule are approximated by rotating harmonic oscillator wavefunctions, which satisfy

$$\left[-\frac{d^2}{dr^2} + \frac{j(j+1)}{\langle r^2\rangle_{v_j}} + \Delta r^2 - \mathcal{E}_{v_j}\right] \chi_{v_j}(r) = 0 \qquad \text{IV.2.2}$$

where $\langle r^2 \rangle_{vj}$ is the expectation value of $r^2$ in the vj state given by

$$\langle r^2 \rangle_{vj} = \int_{-\infty}^{\infty} \chi_{vj}(r)\, r^2\, \chi_{vj}(r)\, dr = r_o^2 + v + 1/2 \qquad \text{IV.2.3}$$

The units assumed in IV.2.2 in order to write the Schrodinger equation in this form are:-

Unit of energy $\varepsilon$, the zero point energy of $H_2$ = 0.26881eV

Unit of R, $\sqrt{\frac{\hbar}{2m\varepsilon}}$ = 0.076153 Å

Unit of r, $\sqrt{\frac{\hbar}{2M\varepsilon}}$ = 0.124206 Å  IV.2.4

where m is the reduced mass of He with $H_2$ = 0.22261 x $10^{-23}$g., and M is the reduced mass of the $H_2$ molecule = 0.83684 x $10^{-24}$g. Expressed in these units, the constants in IV.2.1 are given by

| | |
|---|---|
| C = 1127.9 | $\gamma_o$ = -0.07417 |
| $\alpha_o$ = 0.2792 | $\gamma_2$ = 0.2298 |
| $\alpha_1$ = 0.008445 | $r_o$ = 6.0514 |
| $\beta$ = 0.251 | IV.2.5 |

The solutions of IV.2.2 are given by

$$\chi_{vj}(r) = (\pi^{1/2} 2^v v!)^{-1/2} H_v(\Delta r) \exp(-\Delta r^2/2) \qquad \text{IV.2.6}$$

with eigenvalues

$$\varepsilon_{vj} = 2v + 1 + \frac{j(j+1)}{r_o^2 + v + 1/2} \qquad \text{IV.2.7}$$

where $H_v(\Delta r)$ is a Hermite polynomial. The evaluation of the coupling matrix elements both for close-coupled and IOS calculations requires (cf. II.2.12a and II.3.16)

$$V_{vv'}(R,\gamma) = \int_0^\infty \chi_{vj}(r)\, V(R,r)\, \chi_{v'j'}(r)\, dr \qquad \text{II.2.8}$$

which can be expressed as a series of integrals of the form

$$I_n = \int_0^\infty (\Delta r)^n e^{\alpha_1 R \Delta r - \Delta r^2}\, dr \qquad \text{IV.2.9}$$

Since the magnitude of the basis wavefunction is extremely small for $r < 0$ when $v \lesssim 10$ the range of integration can safely be extended to $-\infty$ to $\infty$ . This allows analytic evaluation of IV.2.9 (Gradshteyn and Ryzhik (1980))

$$I_n = \int_{-\infty}^\infty (\Delta r)^n e^{\alpha_1 R \Delta r - \Delta r^2} dr = \frac{\sqrt{\pi}}{2^{n-1}} \frac{d^{n-1}}{dq^{n-1}} \left( q e^{q^2} \right) \qquad \text{IV.2,10}$$

where $q = \left(\frac{\alpha_1 R}{2}\right)$

The analytic evaluation of the matrix elements becomes cumbersome for large v, since each matrix element is expressed as a series of $I_n$, which is itself a polynomial. The extension of the integration ranges makes $I_n$ ideally suited to evaluation by Gauss-Hermite quadrature which employs the weight function $e^{-\Delta r^2}$. It turns out that the numerical approach is much simpler than the analytic (see Section 3a).

## 3. Numerical Details

### (a) Matrix Elements

Consider the analytic evaluation of the matrix element with v = v' = 2. The required expression is

$$V_{22}(R,\gamma) = C e^{-\alpha_0 R + q^2} \left[ v_0^{22}(R) + \beta v_2^{22}(R) P_2(\hat{R}\cdot\hat{r}) \right] \qquad \text{IV.3.1}$$

where

$$v_\lambda^{22}(R) = 1 + 5\gamma_\lambda q + 4q^2 + 8\gamma_\lambda q^3 + 2q^4 + 2\gamma_\lambda q^5 \qquad \lambda = 0,2$$

and $q = \left(\frac{\alpha_1 R}{2}\right)$ as before. Each $v_\lambda(R)$ is a fifth order polynomial, the coefficients of which have to be worked out by hand, from the required coefficients of $I_n$ and those of the powers of q within $I_n$. Such a task is not difficult, although care must be taken to ensure no simple algebraic error is made. For larger v, the expressions become more cumbersome. For example, $v = v' = 3$ contains $I_n$ for $n = 0$ to $n = 7$, and each $I_n$ is an nth order polynomial resulting in $v_\lambda(R)$ being a seventh order polynomial. As v increases, the possibility of an algebraic or programming error increases, as does the computer time required to evaluate the expression.

In comparison, the numerical evaluation of the integrals IV.2.8 can be achieved simply and efficiently by Gauss-Hermite quadrature. The integrand can be written (cf. IV.2.1 and IV.2.6).

$$\chi_{vj}(r)\, V(R,r)\, \chi_{v'j'}(r) = B(r) \exp\left(D(r)R\right)\left[A_0(r) + \beta A_2(r) P_2(\hat{R}\cdot\hat{r})\right] e^{-\Delta r^2}$$

where
$$B(r) = C\left(\pi 2^{v+v'} v!\, v'!\right) H_v(\Delta r)\, H_{v'}(\Delta r) \qquad \text{IV.3.2}$$
$$A_\lambda(r) = (1 + \gamma_\lambda \Delta r)$$
$$D(r) = (-\alpha_0 + \alpha_1 \Delta r)$$

The weight function $e^{-\Delta r^2}$ need not be calculated. The quantities B(r), D(r) and $A_\lambda(r)$ are independent of R and can be calculated at all the required quadrature points on initialisation of the potential routine and used repeatedly for all values of R. The only expensive task, computationally, is the exponentiation. This can be avoided by employing a fixed step length, $\Delta R$, in the integration algorithm by noting that

$$\exp\left(D(r)(R+\Delta R)\right) = \exp\left(D(r)R\right)\exp\left(D(r)\Delta R\right) \qquad \text{IV.3.3}$$

With $\Delta R$ constant, exp $(D(r)\Delta R)$ can also be set in the initialisation. The exponential factor can then be calculated at each step by multiplication of the previous factor by exp $(D(r)\Delta R)$.

It is much simpler to evaluate the matrix elements numerically. Only if analytic evaluation offered a significant reduction in the computer time required for the complete calculation of cross sections, would such a course be pursued. However, to test the efficiency and accuracy of numerical evaluation, matrix elements for $v(v') \leqslant 2$ were calculated analytically. Table 1 contains a comparison between $V_{vv'}(R,\gamma)$ evaluated analytically for $v(v') \leqslant 2$ and the corresponding values calculated using a 16 and 8 point Gauss Hermite quadrature for $v(v') \leqslant 3$. The values calculated using a 16 point quadrature agree with the analytic results for $v \leqslant 2$ to 11 significant figures at all values of R. The discrepancies between values obtained using 8 and 16 points only appear at large values of R (where the potential is extremely small) for $v \geqslant 2$. As can be seen, these discrepancies are extremely small ($< 0.3 \times 10^{-4}\%$). Also, we are interested in the calculation of cross sections at total energies between the $v = 1$ and $v = 2$ vibrational states, i.e. $v = 2$ and $v = 3$ are closed channels in our calculation. This tiny loss of accuracy introduced by using an 8 point rather than a 16 point quadrature will therefore have no significant effect on the final cross sections. If the numerical routine takes advantage of a fixed step length in the integration algorithm, as discussed previously, it takes much less time to produce virtually identical results, than one which does not. Compared

TABLE 1 Comparison of potential matrix elements evaluated analytically (a), numerically by 16-point Gauss-Hermite quadrature (b) and by 8 point quadrature (c).

| R(au) | | $V_{vv'}(R,\gamma)$ (a.u.) at $\cos\gamma=1$ | | | |
|---|---|---|---|---|---|
| | | $V_{02}$ | $V_{12}$ | $V_{22}$ | |
| 10.4 | a) | 3.3138393277-9 | 1.7103630963-8 | 3.6094608412-8 | |
| | b) | 3.3138393277-9 | 1.7103630963-8 | 3.6094608412-8 | |
| | c) | 3.3138393276-9 | 1.7103630961-8 | 3.6094608379-8 | |
| | | $V_{03}$ | $V_{13}$ | $V_{23}$ | $V_{33}$ |
| 6.4 | b) | 3.9897144664-7 | 4.7860434216-6 | 2.7599752602-5 | 7.0185445383-5 |
| | c) | 3.9897144664-7 | 4.7860434215-6 | 2.7599752597-5 | 7.0185445261-5 |
| 10.4 | b) | 8.0694613692-10 | 6.0798988442-9 | 2.2760710711-8 | 4.1638936158-8 |
| | c) | 8.0694613604-10 | 6.0798988168-9 | 2.2760710152-8 | 4.1638927602-8 |

TABLE 2 Comparison of approximate computer time required to evaluate $V_{vv'}(R,\gamma)$ for $v(v') \leq 2$ at 500 values of R on the IBM 370/168 at NUMAC

| | Analytic | Numerical | | |
|---|---|---|---|---|
| | | 16 point quadrature | 8 point quadrature | a) 8 point quadrature and fixed step. |
| Time(s) | 0.09 | 3.50 | 1.75 | 0.1 |

a) With routine adapted to take advantage of fixed step lengths.

in Table 2 are the approximate computer times required for the evaluation of $V_{vv'}(R,\gamma)$ at 500 values of R for $v(v') \leq 2$ (i.e. 6 elements allowing for the symmetry $V_{vv'}(R,\gamma) = V_{v'v}(R,\gamma)$) on the IBM 370/168 at NUMAC. As can be seen, analytic evaluation is most efficient. However as v increases the computational effort involved in calculating $V_{vv'}(R,\gamma)$ will increase rapidly. This is not true for numerical evaluation, where the time taken for the evaluation of each element is independent of v, if the same number of quadrature points is sufficient for larger v.

(b) Close-Coupling calculations - MOLSCAT

To perform CC calculations we obtained a version of S. Green's MOLSCAT heavy particle scattering program from Daresbury Laboratory and installed it on the IBM 370/168 of the local system, NUMAC, at Newcastle University. To verify that the prgram was working correctly, attempts were made to reproduce the results of Eastes and Secrest (1972) - hereafter referred to as ES. ES report individual S-matrix elements for rovibrationally inelastic transitions using an exactly defined basis set and model system, described in Section 2. These results provide a stringent test of the algorithm, tolerances, etc. of MOLSCAT and of the accuracy of the potential routines.

MOLSCAT has the capability of solving the coupled equations by the method of either de Vogelaere or Gordon (see Chapter III). Since we wanted to solve the equations for several energies the obvious choice is Gordons method, which is an approximate potential algorithm. However, there were

two severe problems in using Gordons method. In order to generate solutions for several energies efficiently a large amount of information, calculated in the solution at the initial energy, must be stored. With the large number of channels involved, and a sufficiently large number of steps to maintain accuracy, the storage required exceeded that available. This storage requirement could have been eliminated, but the advantage of employing Gordon's method, i.e. the efficient generation of solutions at many energies, would also be lost. The second problem was the presence of a small bug in the code relevant to Grodon's method. If closed channels are included in the calculation at the initial energy, the algorithm "chokes on itself" (S. Green-private correspondence). In some regions of the integration range the step length predictor fails and predicts smaller and smaller step lengths. To overcome this, S. Green advised choosing an initial energy sufficiently large that all the channels are open and then subsequently lowering the energy to the desired value. However, the choice of step length is energy dependent (although weakly) as discussed in Chapter III.4(c). There is therefore the possibility that the step length employed at the high initial energy may not be sufficiently small to maintain accuracy at the lower energies. The initial energy would have to be much larger than the subsequent energies and the discrepancy in the step lengths required possibly significant, with no way of checking.

In comparison to Gordon's algorithm, that of de Vogelaere always ran smoothly, producing extremely consistent results with changing step lengths and tolerances, etc. All the

CC calculations were therefore performed by MOLSCAT employing the de Vogelaere algorithm to solve the coupled equations. The matrix elements were calculated numerically as described in Section 3a.

Table 3 contains a comparison between values of $|S^J(j\ell v,OOO)|^2$ calculated using MOLSCAT and the corresponding results of ES at a total energy $E = 3\varepsilon$, relative to the ground state $v = j = O$, for partial waves $J = O$ and $J = 1O$. The table also contains results obtained by MOLSCAT using different step lengths and integration ranges. These results are obtained using the version of MOSCAT on NUMAC employing 16 and 32 steps per smallest de Broglie wavelength in the de Vogelaere algorithm (N16 and N32 respectively) and a version made available on the CRAY-1 computer at Daresbury Laboratory employing 16 steps per wavelength (C16). An integration range of 5.2 to 75.2 units was used for N16, N32 and C16. To demonstrate that this is sufficient the table also includes a N32 run using an extended range of 5.2 to 100.0 units (EXN32). The results clearly demonstrate that 16 steps per wavelength and the shorter integration range are sufficient and also the accuracy and stability of both the versions of MOLSCAT employed. The agreement with the results of ES is excellent, even when $|S^J(j\ell v,OOO)|^2$ is as small as $10^{-7}$. The level of agreement is all the more striking if it is noted that ES used a completely different numerical method, adapted from that of Sams and Kouri (1969) a,b. The small discrepancy in the comparison between the smallest results is certainly not attributable to round-off error in MOLSCAT. However, such quantities are extremely

TABLE 3 Comparison of the results of Eastes and Secrest (1972) with calculations using MOLSCAT for total angular momentum J = 0 and J = 10 and a total energy E = 3$\epsilon$. The $H_2$ states are specified by the values of (v,j). ES, results of Eastes and Secrest; N16, results with version of MOLSCAT on NUMAC using 16 steps per wavelength in de Vogelaere; N32, NUMAC version with 32 steps per wavelength; C16, results using version of MOLSCAT on the CRAY-1 with 16 steps per wavelength; EXN32, as N32 but using an extended integration range.

| $H_2$ states included in basis set | | $J = 0$, $\lvert S^0(jjv;000)\rvert^2$ for various (v,j) | | | | |
|---|---|---|---|---|---|---|
| | (v,j) = | (0,0) | (0,2) | (0,4) | (1,0) | (1,2) |
| (0,0) to (0,6), (1,0) to (1,6), | ES | 2.7775-1 | 5.9864-1 | 1.2145-1 | 1.6279-6 | 7.6856-7 |
| (2,0), (2,2), | N16 | 2.7826-1 | 5.9851-1 | 1.2109-1 | 1.6205-6 | 7.7318-7 |
| (3,0), (3,2). | N32 | 2.7827-1 | 5.9850-1 | 1.2109-1 | 1.6209-6 | 7.7338-7 |

| | | $J = 10$, $\lvert S^{10}(j,10-j,v;000)\rvert^2$ | | | | |
|---|---|---|---|---|---|---|
| | (v,j) = | (0,0) | (0,2) | (0,4) | (1,0) | (1,2) |
| (0,0) to (0,6), (1,0) to (1,4), | ES | 3.1000-1 | 2.1471-1 | 3.2178-2 | 8.5295-7 | 8.9507-8 |
| (2,0). | C16 | 3.1048-1 | 2.1472-1 | 3.2121-2 | 8.5481-7 | 9.1340-8 |
| | N16 | 3.1048-1 | 2.1472-1 | 3.2121-2 | 8.5488-7 | 9.1345-8 |
| | N32 | 3.1046-1 | 2.1474-1 | 3.2125-2 | 8.5502-7 | 9.1373-8 |
| | EXN32 | 3.1046-1 | 2.1474-1 | 3.2125-2 | 8.5504-7 | 9.1350-8 |
| (0,0) to (0,6), (1,0) to (1,4), | ES | 3.0994-1 | 2.1474-1 | 3.2164-2 | 7.7137-7 | 1.4014-7 |
| (2.0), (2,2). | N16 | 3.1042-1 | 2.1476-1 | 3.2107-2 | 7.7349-7 | 1.4232-7 |
| | N32 | 3.1040-1 | 2.1477-1 | 3.2111-2 | 7.7363-7 | 1.4236-7 |
| | EXN32 | 3.1040-1 | 2.1477-1 | 3.2112-2 | 7.7364-7 | 1.4233-7 |

sensitive to the precise description of the system (matrix elements, reduced mass, etc.). MOLSCAT was working units of mass in atomic mass units and energy in inverse centimetres, yet the model system is defined in terms of other units. The small discrepancies ( $\lesssim 2\%$) could easily be attributed to the conversion factors employed. Overall the results show MOLSCAT to be stable and accurate, and the excellence of the agreement with the results of ES would appear to prove conclusively that the model system has been accurately described also.

The paper of ES concentrated mainly on vibrationally elastic transitions, with only one of the eight energies investigated being above the first vibrational threshold. Lin and Secrest (1979) (hereafter referred to as LS) extended these calculations to higher energies, up to $5\varepsilon$ above the ground state of the $H_2$ molecule, $\varepsilon$. In this paper, LS publish partial cross sections $\sigma^J(vj \rightarrow v'j')$ for J = 3 at the same energy used by ES for the results in Table 3, E = $3\varepsilon$, for various $H_2$ basis sets. Comparison of these vibrationally inelastic cross-sections with those calculated using MOLSCAT is shown in Table 4. The basis set used is $\{6,6\}$ in the notation of LS i.e. j = 0, 2, 4, 6 for each of v = 0,1. As can be seen, the discrepancies are large, attaining a factor of twenty for the smaller partial cross sections. As a final check the cross sections in Table 4 were calculated manually from the appropriate S-matrix elements and MOLSCAT found to be accurate. In view of the agreement with ES and the numerical checks detailed in Table 3, it appears that the results of LS are seriously in error. In private

TABLE 4 A comparison of inelastic partial wave cross sections, $\sigma^J$, for J = 3 and E = 3ε; column (a) contain the results obtained using MOLSCAT, column (b) the results of LS for basis set $\{6,6\}$. 3.919-8 denotes $3.919 \times 10^{-8}$

| | $\sigma^3(vj \rightarrow v'j')$ | |
|---|---|---|
| $(v,j) \rightarrow (v',j')$ | (a) | (b) |
| $(0,0) \rightarrow (1,0)$ | 3.919-8 | 5.915-8 |
| $\rightarrow (1,2)$ | 1.464-8 | 2.621-8 |
| $\rightarrow (1,4)$ | 2.108-10 | 3.710-9 |
| $(0,2) \rightarrow (1,0)$ | 1.091-8 | 6.936-9 |
| $\rightarrow (1,2)$ | 2.734-8 | 4.567-8 |
| $\rightarrow (1,4)$ | 5.266-10 | 1.056-8 |
| $(0,4) \rightarrow (1,0)$ | 1.911-8 | 2.188-8 |
| $\rightarrow (1,2)$ | 8.652-8 | 7.168-8 |
| $\rightarrow (1,4)$ | 3.046-9 | 4.236-8 |

correspondence with Lin, he admitted to an error in his potential routine which had been used in the calculation of the partial cross sections in Table 4. However, he maintained that the fault had been rectified before the calculation of the total cross sections, converged with respect to total angular momentum J, had been performed and therefore that these main results were correct.

The paper of LS also contains graphs which display the variation with energy of the total cross section for various transitions. The lower energy points are taken from ES and the higher energy points are their own calculations. At the point where these two sets of results meet, a pronounced structure is present. This is attributed by LS to the opening of the first vibrational threshold. Therefore, it is not only the magnitude of the cross sections which may be in error, but also their physical interpretation. Since such structure is an obvious characteristic for calculations using approximate methods to attempt to reproduce, it is of great importance that its presence or absence be determined.

In order to obtain sufficient computer time to calculate total cross sections, the version of MOLSCAT made available on the CRAY-1 computer at Daresbury Laboratory was used. A comparison between the results obtained using this version and the version on the IBM 370/168 at NUMAC has already been presented in Table 3. The CRAY-1 version maintained accuracy and stability, with changes in step length and integration range, to the same degree as that on NUMAC.

Calculations were performed for para $H_2$ at five energies, ranging from just above the first vibrational threshold ($E = 2\varepsilon$)

to midway between the first and second thresholds (E = 3$\varepsilon$). An additional calculation at 1.5eV above the first threshold was performed in order to compare with the results of Raczkowski et al. (1978). For all the para-$H_2$ calculations, the basis set employed was that used by LS; {6,6,6,4} i.e. j = 0, 2,4,6 for v = 0,1,2 and j = 0,2,4 for v = 3. The integration range used by LS was found to be sufficient for all the lower energy calculations, as demonstrated in Table 3. However for the high energy, E = 2$\varepsilon$ + 1.5eV, an integration range of 2.0 - 70.0 was required. For high values of J both the lower and upper limits of the integration range should be increased. The upper limit is automatically extended by MOLSCAT until the S-matrix has converged to within a given tolerance, set at 0.1%. The lower limit required will only increase slightly as J increases (e.g. 5.2 at J = 0 can be increased to 6.5 at J = 60). Therefore, no significant gain is obtained by raising the lower limit as J increases, and the same lower limit was used at all J.

Fully converged calculations were performed for three energies. For the other three only one parity block, $(-1)^J$, was calculated i.e. only cross-sections for transitions involving states with j = 0 are complete. Also, for two of these energies sufficient partial waves were calculated to converge only the vibrationally inelastic cross sections. The various details of the number of partial waves, time per partial wave, etc. for the different total energies are contained in Table 5. The integration range specified will be increased by MOLSCAT as required. For example, at

TABLE 5 Details of CC calculations performed using MOLSCAT on the CRAY-1 Computer.
(* 44 + 96 = 140 is Time for first parity + Time for second parity = Total time).

Para $H_2$ + He calculations

| Energy | Integration Range | Time/partial wave(s) | Max J value | Basis set size | |
|---|---|---|---|---|---|
| 2.02$\varepsilon$ | 5.2 - 75.2 | 86 | 12 | {6,6,6,4} | $(-1)^J$ Parity only, only vibrationally inelastic $\Delta v \neq 0$ cross sections converged with respect to J. |
| 2.1$\varepsilon$ | 5.2 - 75.2 | 87 | 60 | {6,6,6,4} | $(-1)^J$ Parity only, all cross sections converged. |
| 2.15$\varepsilon$ | 5.2 - 75.2 | 89 | 20 | {6,6,6,4} | $(-1)^J$ Parity only, only $\Delta v \neq 0$ converged. |
| 2.5$\varepsilon$ | 5.2 - 75.2 | *44 + 96 = 140 | 60 | {6,6,6,4} | Full calculation , i.e. Both parities, and all cross-sections converged |
| 3.0$\varepsilon$ | 5.2 - 75.2 | 49 + 105 = 154 | 80 | {6,6,6,4} | Full calculation |
| 2$\varepsilon$+1.5eV | 2.0 - 70.0 | 77 + 163 = 240 | 90 | {6,6,6,4} | Full calculation |

Ortho $H_2$ + He calculations

| Energy | Integration Range | Time/partial wave(s) | Max J value | Basis set size | |
|---|---|---|---|---|---|
| 3.0$\varepsilon$ | 5.2 - 85.0 | 58 + 106 = 164 | 80 | {7,7,5,1} | Full calculation |

$E = 2\varepsilon + 1.5eV$ for $J = 90$, the integration range employed was 2.0 - 90.0 and the calculation required 108 + 234 = 342 s (Time for one parity block + Time for other block = total time). Also the times specified are for partial waves $J \geq 6$. For $J < 6$ the number of channels is reduced and consequently so is the time required.

Calculations were performed for ortho $H_2$ at only one energy, $E = 3\varepsilon$. Table 6 shows the convergence of results with basis set size for $J = 10$. As can be seen, a basis set of $\{7,7,5,1\}$ (i.e. $j = 1,3,5,7$ for $v = 0,1$, $j = 1,3,5$ for $v = 2$ and $j = 1$, $v = 3$) is sufficient for most transitions. As expected, convergence deteriorates as the limit of the basis set is approached, but remains within a few per cent even for the $v = 0$, $j = 7$ to $v = 1$, $j = 5$ transition. As the larger basis $\{7,7,7,5\}$ required more than twice the computer time, the basis $\{7,7,5,1\}$ was used in the full calculation. Theintegration range used was 5.2 to 85.0. These details are summarised in Table 5.

In all calculations for para and ortho $H_2$, 16 steps per smallest de Broglie wavelength was employed in the de Vogelaere algorithm.

(c) IOS Calculations

(i) Solution of the coupled equations for fixed orientation

The calculation of cross sections using the IOS approximation consists of two operations. The equations, coupled in vibration at given rotor orientations, are solved to obtain appropriate S-matrices, which are then used in the calculation of the cross sections. The computer time required for these

| (i) | → (f) | Basis set {7,5,3,1} | {7,5,5,1} | {7,7,3,1} | {7,7,5,1} | {7,7,7,5} |
|---|---|---|---|---|---|---|
| 0,1 | → 0,1 | 1.726-1 | 1.726-1 | 1.726-1 | 1.726-1 | 1.726-1 |
| | 0,3 | 4.869-2 | 4.869-2 | 4.870-2 | 4.870-2 | 4.870-2 |
| | 0,5 | 3.916-3 | 3.916-3 | 3.916-3 | 3.916-3 | 3.916-3 |
| | 0,7 | 2.182-5 | 2.182-5 | 2.232-5 | 2.231-5 | 2.231-5 |
| 0,3 | → 0,3 | 2.228-1 | 2.228-1 | 2.228-1 | 2.228-1 | 2.228-1 |
| | 0,5 | 1.899-2 | 1.899-2 | 1.898-2 | 1.898-2 | 1.898-2 |
| | 0,7 | 1.919-4 | 1.919-4 | 1.979-4 | 1.978-4 | 1.978-4 |
| 0,5 | → 0,5 | 3.334-1 | 3.334-1 | 3.333-1 | 3.333-1 | 3.333-1 |
| | 0,7 | 3.282-3 | 3.282-3 | 3.385-3 | 3.384-3 | 3.384-3 |
| 0,7 | → 0,7 | 5.489-1 | 5.489.1 | 5.488-1 | 5.488-1 | 5.488-1 |
| 1,1 | → 1,1 | 6.601-1 | 6.601-1 | 6.601-1 | 6.601-1 | 6.601-1 |
| | 1,3 | 3.145-2 | 3.147-2 | 3.146-2 | 3.147-2 | 3.147-2 |
| | 1,5 | 1.182-5 | 1.173-5 | 1.207-5 | 1.198-5 | 1.199-5 |
| 1,3 | → 1,3 | 1.238+0 | 1.238+0 | 1.238+0 | 1.238+0 | 1.238+0 |
| | 1,5 | 3.572-4 | 3.538-4 | 3.652-4 | 3.617-4 | 3.620-4 |
| 1,5 | → 1,5 | 4.246+0 | 4.246+0 | 4.246+0 | 4.246+0 | 4.246+0 |
| 0,1 | → 1,1 | 1.045-7 | 1.046-7 | 1.046-7 | 1.048-7 | 1.048-7 |
| | 1,3 | 1.076-8 | 1.083-8 | 1.052-8 | 1.059-8 | 1.059-8 |
| | 1,5 | 5.354-12 | 5.798-12 | 4.731-12 | 5.218-12 | 5.233-12 |
| 0,3 | → 1,1 | 1.393-7 | 1.390-7 | 1.405-7 | 1.402-7 | 1.402-7 |
| | 1,3 | 3.061-8 | 3.095-8 | 2.912-8 | 2.945-8 | 2.945-8 |
| | 1,5 | 2.595-11 | 2.903-11 | 1.792-11 | 2.123-11 | 2.135-11 |
| 0,5 | → 1,1 | 4.514-8 | 4.717-8 | 4.220-8 | 4.415-8 | 4.415-8 |
| | 1,3 | 1.730-7 | 1.767-7 | 1.627-7 | 1.663-7 | 1.663-8 |
| | 1,5 | 3.554-10 | 4.029-10 | 1.443-10 | 1.841-10 | 1.866-10 |
| 0,7 | → 1,1 | 1.815-8 | 1.786-8 | 2.066-9 | 1.862-9 | 1.903-9 |
| | 1,3 | 2.214-7 | 2.160-7 | 3.465-8 | 3.156-8 | 3.217-8 |
| | 1,5 | 2.355-8 | 2.570-8 | 5.234-9 | 6.284-9 | 6.463-9 |

Table 6 Convergence of cross-sections $\sigma(i \rightarrow f)$ (in units of $\mathring{A}^2$) with basis set size for total angular momentum $J = 10$, and total energy $E = 3\varepsilon$ ($\varepsilon = 0.26881$ eV). The $H_2$ states are specified by the values (n,j). 1.726-1 denotes $1.726 \times 10^{-1}$.

two steps is very different, with the integration of the coupled equations accounting for by far the majority of the total running time. In the calculations considered here, retaining 4 vibrational channels and using 8 orientations, the integration takes up over 95% of the total time. The efficiency of the complete computer code is therefore almost entirely dependent on the efficiency of the integration algorithm and hence most effort was aimed at improving this part of this code.

Computer programmes were written in FORTRAN IV and developed on the IBM 370/168 at NUMAC to calculate IOS cross sections using the R-matrix propagator method to solve the coupled equations involved. The integration routine incorporated the step length algorithm and a capability to propagate variable numbers of channels as discussed in Chapter III.4. The program was also equipped for the efficient generation of results for many energies and partial waves. The form of the sector R-matrices was chosen to be that appropriate to a constant potential within the sector (i.e. III.4.36).

To check the integration algorithm, it was used to reproduce the results of SWL obtained for the model atom-forced harmonic oscillator system described by Secrest and Johnston (1966). In the units of Secrest and Johnston, the Schrodinger equation is

$$\left[-(2M)^{-1}\frac{\partial^2}{\partial R^2} - \tfrac{1}{2}\frac{\partial^2}{\partial r^2} + \tfrac{1}{2}r^2 + V(R-r)\right]\Psi = \tfrac{1}{2}E\Psi \qquad \text{IV.3.3}$$

with

$$V(R-r) = A\exp\left[-\alpha(R-r)\right]$$

where R is the integration co-ordinate and r is the oscillator coordinate. As can be seen, the basis functions are harmonic oscillators, defined by

$$\left[ -\tfrac{1}{2}\frac{\partial^2}{\partial r^2} + \tfrac{1}{2} r^2 \right] \psi_v(r) = \varepsilon_v \psi_v(r) \qquad \text{IV.3.4}$$

$$\psi_v(r) = C_v e^{-r^2/2} H_v(r)$$
$$\varepsilon_v = v + 1/2 \qquad \text{IV.3.5}$$

where $C_v$ is a normalisation coefficient and $H_v(r)$ is a Hermite polynomial. The scattering problem is completely specified by M,E,$\alpha$ and A. The values of these parameters are

$$M = 0.6667 \quad A = 41000 \quad \alpha = 0.30 \quad E = 8.0$$

Initially the integration algorithm was used with a fixed step length. Table 7 contains a comparison of the results obtaind using several step lengths with the highly accurate results of SWL. All calculations retained 6 basis states. As can be seen the agreement is excellent, as would be expected. Indeed, identical agreement with SWL is obtained if the number of steps is increased to 2000. The table also demonstrates that the results converge monotonically to the correct answer as the number of sectors is increased. This monotonic convergence is an extremely useful feature, however if a variable step length is used, the results tend to oscillate. As noted previously (Chapter III.2), approximate potential algorithms require a lot of numerical effort to obtain highly accurate results, although they can obtain reasonable accuracy with much less effort. This is reflected in the results of Table 7 where the use of 70 steps gives good results.

TABLE 7 Comparison of $|S(v,v')|^2$ obtained using different numbers of steps over the integration range with the results of Stechel et al. (1978).

a) 70 steps, b) 100 steps, c) 150 steps, d) 200 steps, e) Result of Stechel et al.

| v | v' = 0 | 1 | 2 | 3 |
|---|---|---|---|---|
| 0 | a) 0.8918486+0 | | | |
| | b) 0.8913110+0 | | | |
| | c) 0.8911631+0 | | | |
| | d) 0.8911379+0 | | | |
| | e) 0.8911111+0 | | | |
| 1 | 0.1069453+0 | 0.8515397+0 | | |
| | 0.1074700+0 | 0.8507947+0 | | |
| | 0.1076144+0 | 0.8505921+0 | | |
| | 0.1076390+0 | 0.8505576+0 | | |
| | 0.1076651+0 | 0.8505194+0 | | |
| 2 | 0.1205915-2 | 0.4150071-1 | 0.9559706+0 | |
| | 0.1218835-2 | 0.4172081-1 | 0.9557300+0 | |
| | 0.1222325-2 | 0.4177891-1 | 0.9556663+0 | |
| | 0.1222920-2 | 0.4178882-1 | 0.9556555+0 | |
| | 0.122359 -2 | 0.418008 -1 | 0.9556422+0 | |
| 3 | 0.1828761-6 | 0.1435146-4 | 0.1322752-2 | 0.9986627+0 |
| | 0.1859456-6 | 0.1451468-4 | 0.1330399-2 | 0.9986549+0 |
| | 0.1867725-6 | 0.1455806-4 | 0.1332432-2 | 0.9986528+0 |
| | 0.1869138-6 | 0.1456549-4 | 0.1332781-2 | 0.9986525+0 |
| | 0.18707 -6 | 0.14576 -4 | 0.133335 -2 | 0.9986519+0 |

The results of SWL were obtained using a variable step length as discussed in Chapter III.4d. To test the numerical method thoroughly, the integration range used was R = 0 to 100 units and a total of 5300 sectors employed. However, 4500 of these sectors are in the range R = 0 - 20, although there are no locally open channels until near R = 30. SWL also report that a 125 variable-step calculation employing an integration range R = 20 - 60 gives results within 5% of those of the highly accurate calculation. The results in Table 7 using a fixed step length and 100 sectors gives results which agree with SWL to within $\lesssim$ 0.2%. This suggests that the step lengths used are not appropriate. However, this may be peculiar to the model system, and the efficiency of the step length algorithm must be studied with reference to the IOS $H_2$ + He calculation.

The solution of the coupled equations at a fixed rotor orientation in the IOS is equivalent to a full CC calculation where only j = 0 states are retained, employing an isotropic potential equal to the full potential calculated at the appropriate angle. Therefore, MOLSCAT can be used to verify the R-matrix integration algorithm for the $H_2$ + He IOS calculation. A comparison between $|T(v,v')|^2$ obtained by MOLSCAT and from the R-matrix algorithm at a fixed orientation $\cos\gamma = 0$ for L = 4 and total energy E = 3$\varepsilon$ is contained in Table 8. The calculation using MOLSCAT employed 16 steps per smallest de Broglie wavelength in the de Vogelaere algorithm and that using the R-matrix algorithm a total of 1000 sectors. The excellence of agreement reflects the stability and accuracy of both the computer codes.

Table 8 Squares of angle fixed T-matrix elements, $|T^{L}(v,v')|^2$ for $\cos\gamma = 0$, $L = 4$ and $E = 3\varepsilon$ ($\varepsilon = 0.26881$ eV). Upper entries, MOLSCAT : lower entries, R-Matrix propagator method.

| $(v,v')$ = | (0,0) | (0,1) | (1,1) |
|---|---|---|---|
| | 3.99823 + 0 | 1.01533 - 9 | 3.94277 + 0 |
| | 3.99829 + 0 | 1.01507 - 9 | 3.94278 + 0 |

The results of table 8 were used as benchwork results with which to test the step length algorithm. After considerable experimentation with the tolerances, it became clear that the step length algorithm described in Chapter III.4d is excessively dependent on the rate of change of the potential. Although the algorithm allows large step sizes near the asymptotic region it also forces the step size in the classically forbidden region to be far smaller than required. If the tolerances are relaxed, allowing larger steps near R = 0, the larger step sizes further out become too great to maintain accuracy. This behaviour is reflected in the distribution of sectors in the calculation of SWL where 85% of the sectors are well within the classically forbiddden region. The results of Table 7 suggest that this concentration of effort is unnecessary and wasteful. Attempts were made to remedy this by explicitly relaxing the dependence of the step size on the rate of change of the potential, rather than allowing STMIN and STMAX to come into operation. None of these attempts were particularly successful. With this system, where the potential is a smoothly decaying exponential, the step length algorithm does not present a large reduction in computer time. Maintaining accuracy to 4 figures, a variable step length gave approximately a 20% reduction in computer time over a fixed step calculation. However, with a variable step length there is always the possibility of failure, in that the algorithm may waste time by employing an excessively small step length at some points, or lose accuracy by employing an excessively large step at others. For solution of the coupled equations at one

orientation, retaining 4 vibrational channel and using approximately 300 steps of fixed length, the computer time required is $\lesssim$ 2s. This is assuming that a numerical routine which takes advantage of the fixed step length is employed to calculate the matrix elements. Therefore for an IOS calculation involving 8 orientations the total time per partial wave is $\lesssim$ 16s. This is only for the first partial wave. The calculation of results for subsequent values of L will only require $\lesssim$ 6s. The IOS calculations, therefore, do not require a large amount of computer time and the modest saving of 20% by employing a variable step length is not warrented, considering the possible dangers involved.

In these preliminary calculations the sector R-matrices used were appropriate to approximating the elements of the locally diagonal matrix as constant (III.4.36). As discussed in Chapter III.4.c and d there are advantages in using more cumbersome sector R-matrices which are appropriate to approximating the elements of the locally diagonal matrix as $[\text{constant} + L(L+1)/R^2]$. Both these schemes, however, require that the step length must be sufficiently small that the diagonalisation, performed at the centre of the sector, is accurate over the entire sector. For the purely repulsive interaction potential employed here, the step size required to maintain diagonalisation was sufficiently small that the coupling matrix (including the $L(L+1)/R^2$ term) could be accurately approximated as constant within the sector. Therefore for this system the step size is limited by the off-diagonal terms and hence almost independent of L. This is demonstrated by the fact that the number of sectors

required to maintain accuracy did not vary significantly with L. The rate of change of the term $L(L + 1)/R^2$ increases with L and therefore a step length which is sufficiently small to accurately calculate results for the highest L value will also be sufficient for the lower values.

SWL investigated the efficiency of propagating variable numbers of channels (as described in Chapter III.4.e) with reference to the model system of Johnston and Secrest (1966). They concluded that in such a weak coupling system propagating variable numbers of channels gave no substantial increase in the efficiency of the algorithm. This was due to the rapid convergence of the results with basis set size and therefore few closed channels are required. As would be expected, this also proved to be true for the $H_2$ + He system. A typical calculation at a given orientation involves retaining 4 vibrational channels (two of which are closed) and employing 300 steps. In such a calculation, only in the last 20 sectors could channels be dropped while still maintaining accuracy of the results to 3 figures. Indeed the extra time required to check how many channels to propagate exceeded the time saved by propagating fewer.

Once the equations have been integrated out to the upper limit of the integration range, the code continues outwards until the largest relative change in the S-matrix elements is less than a given tolerance. This ensures that the integration range employed is sufficient.

(ii) Quadrature over orientation

Once the S-matrices at given orientations have been calculated they must be integrated over orientation to obtain a body-fixed S-matrix (II.3.18). The values of the

angle of orientation were chosen to be the points of a Gauss-Legendre quadrature. In examing the efficiency of the quadrature and the number of points required, we need only discuss integrals appropriate to $\sigma(v0 \rightarrow v'j'')$ since all other cross-sections can be derived trivially from II.3.7b, i.e.

$$\sigma(v_j \rightarrow v'j') = (2j'+1)\left(\frac{k_{v0}}{k_{vj}}\right)^2 \sum_{j''} \begin{pmatrix} j' & j & j'' \\ 0 & 0 & 0 \end{pmatrix}^2 \sigma(v0 \rightarrow v'j'') \qquad \text{IV.3.6}$$

Therefore, if all cross-sections involving states up to $j_{max}$ are required we need all $\sigma(v0 \rightarrow v'j'')$ up to $j'' = 2j_{max}$, due to the properties of the 3-j coefficients, for a complete summation. In considering the number of quadrature points, the accuracy of results up to $\sigma(v0 \rightarrow v'2j_{max})$ must be considered. The evaluation of $\sigma(v0 \rightarrow v'j'')$ involves solution of the integral

$$\int_0^{\pi} Y^*_{j''0}(\gamma,0)\, S^L_{vv'}(\gamma) \sin\gamma\, d\gamma = 2\int_0^{\pi/2} Y^*_{j''0}(\gamma,0)\, S^L_{vv'}(\gamma) \sin\gamma\, d\gamma \quad , j'' \text{ even}$$

$$= 0 \quad , j'' \text{ odd} \qquad \text{IV.3.7}$$

since we are dealing with a homonuclear species and therefore the S-matrix is symmetric about $\pi/2$. The number of quadrature points required to maintain accuracy will increase with $j''$ as the oscillatory behaviour of $Y^*_{j''0}(\gamma,0)$ increases.

Gauss-Legendre is the obvious quadrature scheme to use, however there are two methods of implementation. The standard limits of a Gauss-Legendre quadrature integral are $\cos\gamma = -1$ to 1 i.e. $\gamma = 0$ to $\pi$. If an N-point quadrature is required over the range 0 to $\pi/2$, one can either choose points from a standard 2N-point quadrature and only use half of them, or alternatively adjust the points and weights of a standard

N-point quadrature in order to half the integration range according to (Abramowitz and Stegun 1965).

$$\text{if} \qquad \int_{-1}^{1} f(x)\,dx = \sum_{i} \omega_i f(x_i)$$

$$\text{then} \qquad \int_{0}^{1} f(x)\,dx = \sum_{i} \left(\frac{\omega_i}{2}\right) f\left(x_{i/2} + 1/2\right) \qquad \text{IV.3.8}$$

MOLSCAT can not only perform close-coupling calculations for a variety of systems (atom-rigid rotor, atom-vibrating rotor, etc.) but can also perform calculations within the framework of various approximate methods. One of the available approximations is the IOS. A comparison between $\sigma(v0 \rightarrow v'j')$ calculated with our own IOS code and MOLSCAT, both using adjusted points and weights is presented in Table 9. The calculation retained 4 vibrational channels and employed an 8-point quadrature at an energy of $E = 3\varepsilon$ with $L = 4$. As can be seen the agreement is excellent and demonstrates the accuracy of both codes. For the cross-sections $\sigma(vj \rightarrow v'j')$, MOLSCAT does not include the factor $(k_{v0}/k_{vj})^2$ in IV.3.6, however this is unimportant.

Our own IOS code was used to compare the efficiency of the two quadrature schemes. The results are shown in Table 10 for $L = 5$ and $E = 3\varepsilon$. As can be seen it is much more efficient to use half the points of a 2N quadrature. The values employed in each scheme are shown in Figure 1. It seems surprising that the adjusted points do not give the better results. They are concentrated more at high values of $\gamma$ and, due to the $\sin\gamma$ weighting, this is the region where the major contribution to the integral comes from. The S-matrix elements themselves are smoothly varying

Table 9 Comparison of IOS cross sections $\sigma^{L}(v0 \rightarrow v'j)$ (in units of $\mathring{A}^2$) for L = 4 and E = 3$\varepsilon$ . Upper entries, R-matrix propagator code: lower entries, MOLSCAT.

| (v,v') = | (0,0) | (0,1) | (1,1) |
|---|---|---|---|
| j = 0 | 7.5095-2 | 2.0050-8 | 4.1528-1 |
| | 7.5110-2 | 2.0050-8 | 4.1538-1 |
| j = 2 | 3.0783-2 | 3.4265-8 | 7.5117-2 |
| | 3.0783-2 | 3.4268-8 | 7.5117-2 |
| j = 4 | 1.4220-2 | 2.0298-8 | 1.0921-2 |
| | 1.4220-2 | 2.0298-8 | 1.0921-2 |
| j = 6 | 2.3774-3 | 4.6195-9 | 6.7559-4 |
| | 2.3774-3 | 4.6193-9 | 6.7560-4 |
| j = 8 | 2.1183-4 | 5.0882-10 | 2.4665-5 |
| | 2.1182-4 | 5.0879-10 | 2.4665-5 |
| j = 10 | 1.2021-5 | 3.3814-11 | 6.1697-7 |
| | 1.2021-5 | 3.3812-11 | 6.1699-7 |
| j = 12 | 1.1543-6 | 3.1965-12 | 4.1731-8 |
| | 1.1543-6 | 3.1964-12 | 4.1732-8 |

TABLE 10 Comparison of IOS cross sections calculated using different Gauss Legendre quadrature points: (a) 16 points adjusted for $0 \leqslant \gamma \leqslant \pi/2$; (b) 8 points taken directly from 16 point formula; (c) 8 points adjusted for $0 \leqslant \gamma \leqslant \pi/2$.

| | | $\sigma(00 \rightarrow 0j)$ | $\sigma(00 \rightarrow 1j)$ | $\sigma(10 \rightarrow 1j)$ |
|---|---|---|---|---|
| j = 0 | a) | 0.75951944-1 | 0.23152382-7 | 0.18753232+0 |
| | b) | " | " | " |
| | c) | 0.75951942-1 | 0.23152380-7 | " |
| j = 2 | | 0.37715011-1 | 0.39084723-7 | 0.90754042-1 |
| | | " | " | " |
| | | 0.37715022-1 | 0.39084739-7 | 0.90754043-1 |
| j = 4 | | 0.17178331-1 | 0.22922790-7 | 0.12891963-1 |
| | | " | " | " |
| | | 0.17178256-1 | 0.22922680-7 | 0.12891960-1 |
| j = 6 | | 0.28387590-2 | 0.51453693-8 | 0.78099093-3 |
| | | " | 0.51453698-8 | " |
| | | 0.28389475-2 | 0.51457810-8 | 0.78099807-3 |
| j = 8 | | 0.25047771-3 | 0.55968857-9 | 0.27967832-4 |
| | | 0.25047769-3 | 0.55968789-9 | 0.27967829-4 |
| | | 0.25030457-3 | 0.55910337-9 | 0.27966670-4 |
| j = 10 | | 0.14185059-4 | 0.36746041-10 | 0.70270571-6 |
| | | 0.14184689-4 | 0.36745529-10 | 0.70270657-6 |
| | | 0.14059642-4 | 0.36655230-10 | 0.68707793-6 |
| j = 12 | | 0.57539114-6 | 0.16759516-11 | 0.13764095-7 |
| | | 0.57588699-6 | 0.16782697-11 | 0.13769307-7 |
| | | 0.13477287-5 | 0.35617808-11 | 0.46012139-7 |

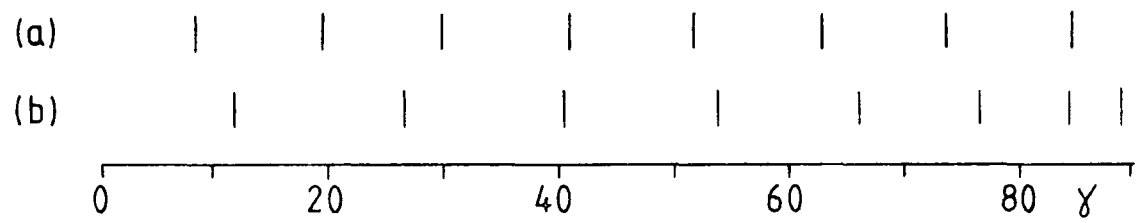


Figure 1 Distribution of values of $\gamma$ employed in 8 - point Gauss Legendre quadrature over the range $0 < \gamma < \pi/2$. (a) 8 points taken directly from 16 point formula : (b) 8 points adjusted for $0 < \gamma < \pi/2$

functions of $\gamma$ as shown in Figure 2.

Although $\sigma(v0 \rightarrow v'j'')$ must be calculated for large values of j'' to complete the summation in IV.3.6, the magnitude of such cross section decreases rapidly with increasing j''. Also the 3-j coefficients decrease as (j-j'') and (j'-j'') increase. Therefore, to maintain accuracy in the results of interest, it is not necessary to calculate cross-sections with large j'' to the same degree of precision. Hence, it may be possible to reduce the number of quadrature points and allow the accuracy of the high j'' cross sections to waver. However, if we employ the more efficient quadrature scheme with, for example, N = 6, we are dealing with the points of a standard 12-point Gauss Legendre quadrature. By definition such points are zeros of $Y_{12,0}(\gamma,0)$, therefore $\sigma(v0 \rightarrow v'j''=12) = 0$ , completely cancelling out any advantage.

In all of the IOS calculations, an 8-point Gauss Legendre quadrature was employed with the points and weights taken directly from a 16 point quadrature.

4. Results and Discussion

All the results of the close-coupling calculations, detailed in Table 5, and IOS calculations for $H_2$ + He are tabulated in the Appendix at the end of the thesis. At some energies not all the cross sections are converged with respect to total angular momentum and only one parity block was calculated. These results are also included in the appendix, since they may be of value in the future.

Table 11 contains a comparison between the present CC $\sigma(00 \rightarrow 0j)$ and the results of ES for j = 0,2,4 at an energy of E = 2.1$\epsilon$. The basis set used by ES was $\{4,2\}$, which is

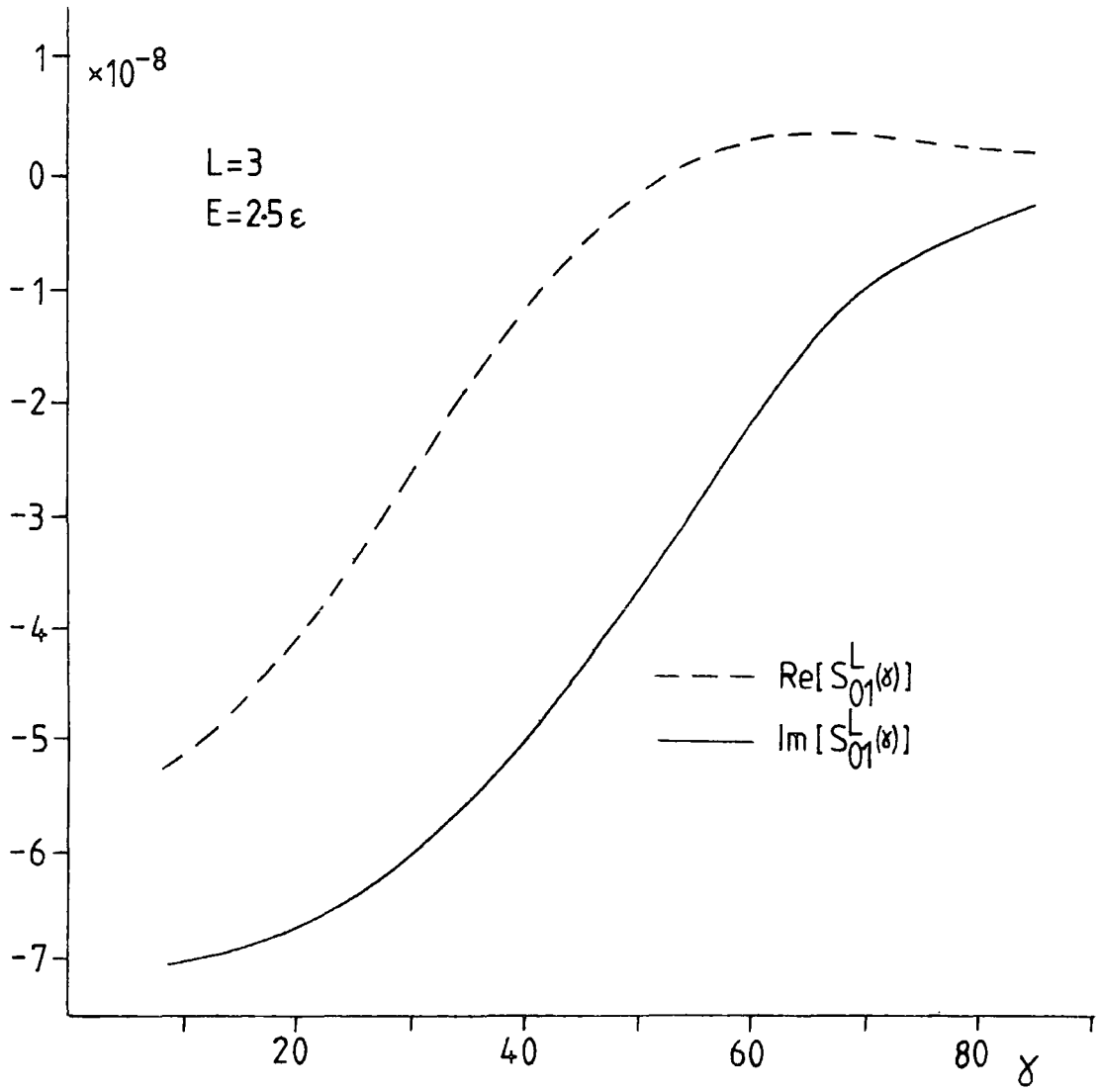


Figure 2 Fixed angle S-matrix $S^{3}_{01}(\gamma)$, as a function of $\gamma$ at $E = 2.5\varepsilon$ ($\varepsilon = 0.26881$eV). Real part- broken line : Imaginary part- full line.

Table 11 Vibrationally elastic integral cross sections $\sigma(00 \rightarrow 0j)$ ($\mathring{A}^2$) for E = 2.1$\varepsilon$ ($\varepsilon$ = 0.26881eV). Upper entries, present CC calculations : lower entries, CC results of Eastes and Secrest (1972).

| j = | 0 | 2 | 4 |
|---|---|---|---|
| | 4.161 + 1 | 3.551 + 0 | 1.578 - 1 |
| | 4.161 + 1 | 3.563 + 0 | 1.496 - 1 |

claimed to yield an accuracy of at least 0.5% in $\sigma(00 \rightarrow 0j)$ for j = 0,2 and at least 5% for j = 4. This is entirely consistent with the present CC results which employ a much larger basis set.

Table 12 contains a complete comparison of the converged integral cross sections of LS with the corresponding results of the present close coupling and IOS calculations at $E = 3\varepsilon$. Significant discrepancies are present in the inelastic cross sections attaining a factor of more than 20. In view of the consistency checks and the excellent agreement with the calculations of ES, the calculations of LS appear to be seriously in error. Lin (1981) concedes that a programming error led to incorrect results being presented in the papers of Lin and Secrest (1977, 1979) and Lin (1979, 1980a,b).

This error affects not only the magnitude of the numerical results but also their physical interpretation. Figure 3a shows the variation with energy of the cross section for the $j = 0 \rightarrow 2$ transition within the vibrational ground state v = 0. The lower energy points are taken from ES and the higher energy points from LS; also plotted are the present results at $E = 2.5\varepsilon$ and $E = 3.0\varepsilon$. The structure in the cross section apparent in the results of LS was attributed by them to the opening of the first excited vibrational level at $E = 2\varepsilon$. Figure 3a demonstrates that the present calculations indicate that such a structure is not present. A similar conclusion holds for the $j = 0 \rightarrow 4$ transition, whose cross section is plotted as a function of energy in Figure 3b.

Lin (1979, 1980a) also reports threshold structures in the vibrationally inelastic cross sections. In Figure 4

Table 12 Integral cross sections $\sigma(i \rightarrow f)$ ($\mathring{A}^2$) for $E = 3\varepsilon$ ($\varepsilon = 0.26881$eV). A, present CC calculations; B, results of Lin and Secrest (1979); C, present IOS calculations. The $H_2$ states are specified by (v,j).

| i \ f | (0,0) | (0,2) | (0,4) | (0,6) | (1,0) | (1,2) | (1,4) |
|---|---|---|---|---|---|---|---|
| | A)3.914+1 | 4.163+0 | 3.763-1 | 5.276-3 | 1.399-6 | 5.321-7 | 6.741-9 |
| (0,0) | B)3.827+1 | 4.768+0 | 5.990-1 | 1.153-2 | 2.423-6 | 8.904-7 | 1.263-7 |
| | C)3.766+1 | 4.953+0 | 9.411-1 | 1.006-1 | 3.973-7 | 6.031-7 | 3.171-7 |
| | 8.800-1 | 4.195+1 | 1.395+0 | 2.875-2 | 6.375-7 | 9.931-7 | 1.555-8 |
| (0,2) | 1.008+0 | 4.115+1 | 1.711+0 | 4.772-2 | 9.682-7 | 2.177-6 | 3.500-7 |
| | 1.047+0 | 4.159+1 | 2.984+0 | 4.815-1 | 1.275-7 | 6.978-7 | 4.361-7 |
| | 5.097-2 | 8.936-1 | 4.334+1 | 3.368-1 | 4.317-7 | 2.599-6 | 7.508-8 |
| (0,4) | 8.112-2 | 1.096+0 | 4.298+1 | 4.281-1 | 7.174-7 | 3.468-6 | 9.731-7 |
| | 1.275-1 | 1.912+0 | 4.769+1 | 2.996+0 | 4.295-8 | 2.794-7 | 7.502-7 |
| | 6.516-4 | 1.679-2 | 3.072-1 | 4.561+1 | 2.836-8 | 5.443-7 | 1.019-6 |
| (0,6) | 1.423-3 | 2.788-2 | 3.904-1 | 4.544+1 | 7.294-8 | 9.425-7 | 1.377-6 |
| | 1.242-2 | 2.813-1 | 2.732+0 | 6.275+1 | 7.871-9 | 1.003-7 | 3.876-7 |
| | 4.196-6 | 9.047-6 | 9.563-6 | 6.889-7 | 4.690+1 | 2.223+0 | 1.158-2 |
| (1,0) | 7.270-6 | 1.374-5 | 1.589-5 | 1.772-6 | 4.638+1 | 2.771+0 | 1.883-2 |
| | 1.192-6 | 1.809-6 | 9.513-7 | 1.912-7 | 4.501+1 | 3.840+0 | 3.004-1 |
| | 3.789-7 | 3.345-6 | 1.366-5 | 3.138-6 | 5.277-1 | 4.935+1 | 1.124-1 |
| (1,2) | 6.340-7 | 7.332-6 | 1.823-5 | 5.434-6 | 6.577-1 | 4.924+1 | 1.448-1 |
| | 4.294-7 | 2.351-6 | 1.469-6 | 5.784-7 | 9.115-1 | 5.482+1 | 2.441+0 |
| | 4.727-9 | 5.160-8 | 3.887-7 | 5.784-6 | 2.705-3 | 1.107-1 | 5.270+1 |
| (1,4) | 8.858-8 | 1.161-6 | 5.039-6 | 7.817-6 | 4.402-3 | 1.426-1 | 5.266+1 |
| | 2.224-7 | 1.447-6 | 3.884-6 | 2.201-6 | 7.023-2 | 2.404+0 | 9.689+1 |

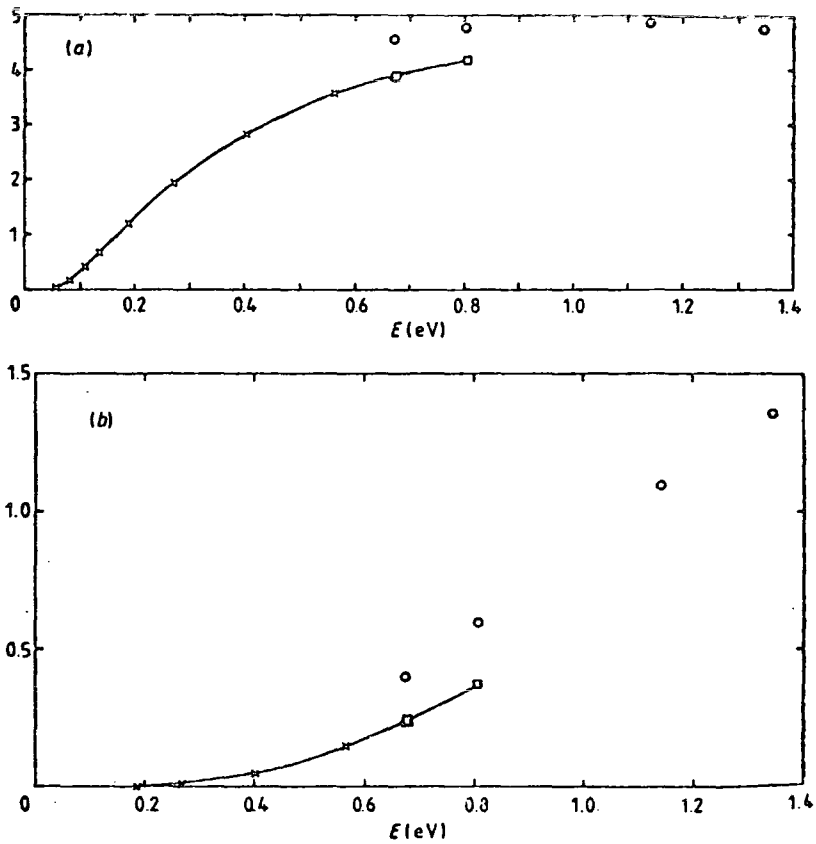


Figure 3 Vibrationally elastic cross sections $\sigma(00 \rightarrow 0j)$ ($\mathring{A}^2$) within the ground vibrational state. Crosses (x) denote the results of Eastes and Secrest (1972), circles (O) the results of Lin and Secrest (1977), and squares ( □ ) the present CC results. (a) The (0,0)→(0,2) transition and (b) the (0,0)→(0,4) transition. Energy in units of eV.

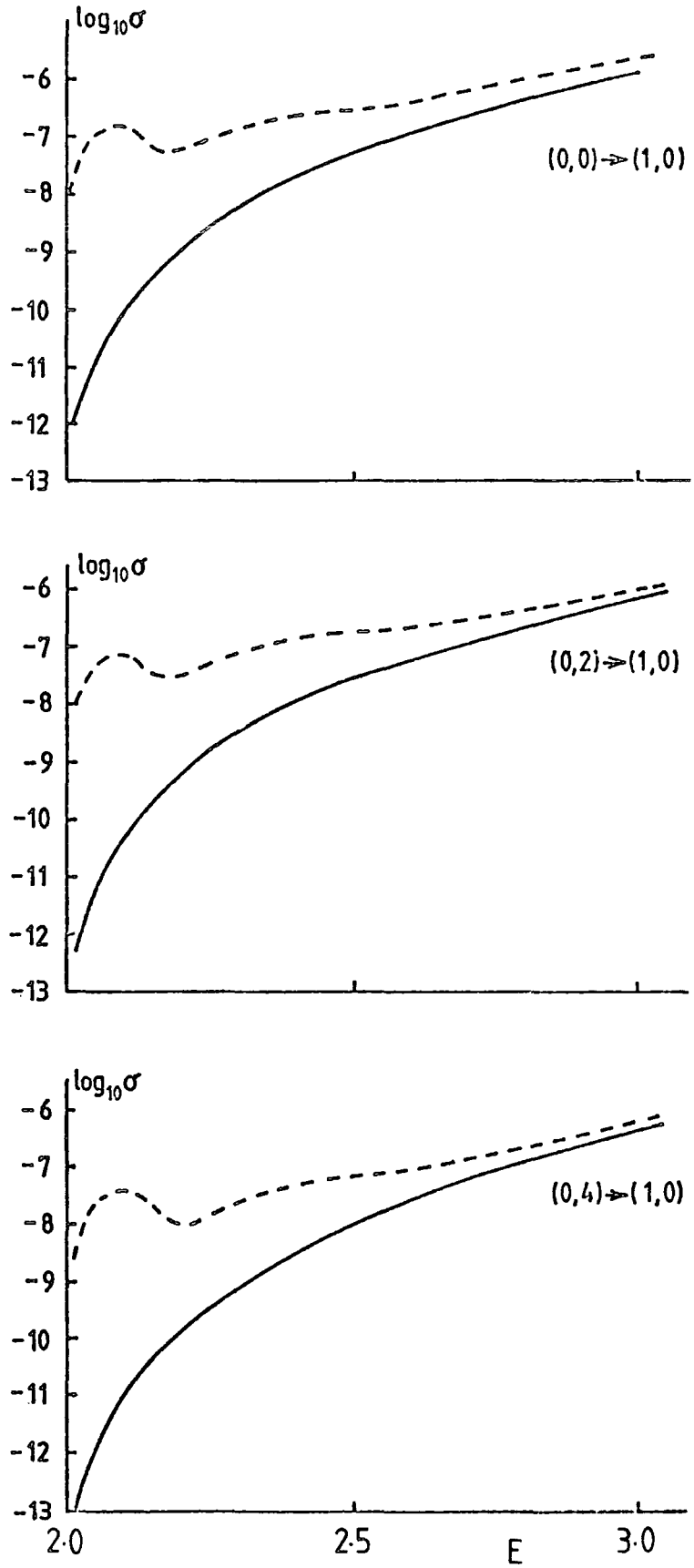


Figure 4 A comparison of the present CC calculations (continuous lines) with those of Lin (1979) (dashed lines) for various $(n,j)\rightarrow(n',j')$ transitions. Cross-sections, $\sigma$, in units of $Å^2$ and energies, relative to the (0,0) ground state, in units of $\varepsilon$ = 0.26881 eV.

is a comparison between the present CC results and those of Lin (1979). As the v = 1 threshold (E = 2ε) is approached the discrepancies with Lin's results increase, attaining four orders of magnitude at the lowest energies considered. The structures in the energy variation of the cross sections, apparent in the results of Lin, are absent in the results of the present calculations. Lin (1979) notes that the coupled states results of McGuire and Toennies (1975) for the $H_2$ + He system also exhibit such structures in the vibrationally inelastic cross sections near threshold. However this was later shown by Alexander and McGuire (1976) to be due to an insufficient basis set. The former calculation retained no closed channels, and as channels became open, as the collision energy increased, they were added to the basis set. This caused sharp dislocations in the energy variation of the cross sections as channels became open. The similar study by Alexander and McGuire (1976) retained closed channels at all energies, resulting in a smooth variation of the cross sections.

A comparison between the coupled states results of Alexander and McGuire (1976) and the present CC calculations of vibrational de-excitation cross sections is presented in Figure 5. Alexander and McGuire use exact $H_2$ rovibrational eigenvalues (Schaefer and Lester (1973)) as compared with the rotating harmonic oscillator energies employed in the present calculations. Therefore the comparison is made at energies above the respective v = 1, j = 0 energy and not total energy. Apart from the difference in basis state energy levels both calculations employ identical descriptions of the system

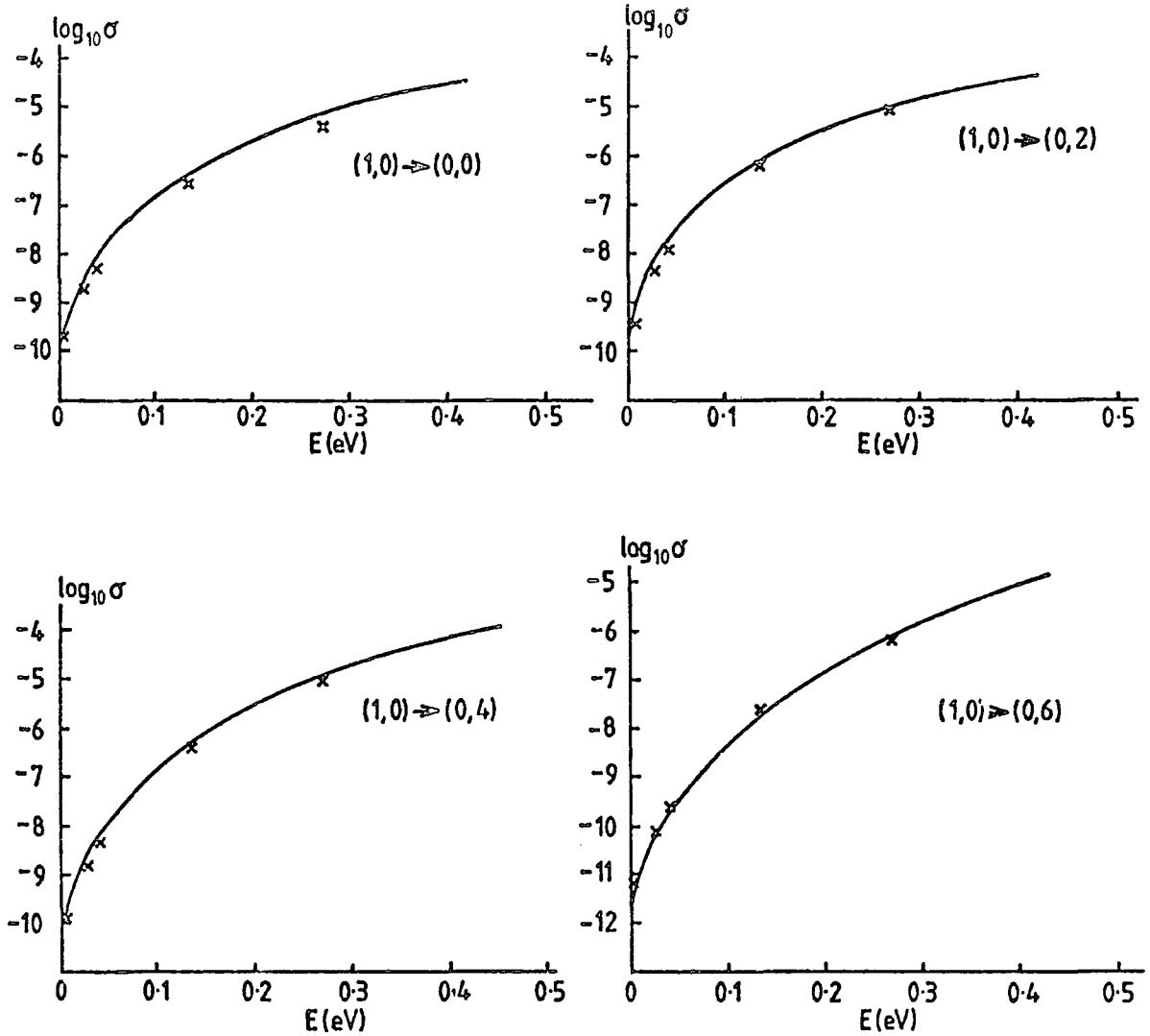


Figure 5 A comparison of the present CC calculations (x) with the CS results of Alexander and McGuire (1976). Cross-sections in units of $\mathring{A}^2$, energies in eV relative to the (1,0) state.

(Section 2). The agreement is extremely good over the energy range considered. Good agreement would be expected, since the Gordon-Secrest interaction potential is purely repulsive and short ranged, which is ideally suited to the coupled states approximation.

Values of the vibrational excitation cross sections are plotted over a wider energy range in Figure 6. Figure 6 contains results from the present CC and IOS calculations, the CS results of Alexander and McGuire and the CC results of Raczkowski et al. (1978). The calculations of Raczkowski et al. employ the Gordon-Secrest interaction potential with exact numerical $H_2$ basis wavefunctions. The present CC results are seen to go over to those of Raczkowski et al. at higher energies. The apparent discrepancy for the v = 1, j = 0$\rightarrow$v' = 0, j' = 6 transition probably arises from the exclusion of the v = 0, j = 8 state from our basis set, whereas it was included in that of Raczkowski et al.

Although the energy variation of the CC results is satisfactorily reproduced by the IOS calculations, there are substantial discrepancies at lower energies. The agreement between IOS and CC results is seen to improve with increasing energy, as would be expected. Given the good agreement between the CS and CC results, it is clearly the energy sudden component of the IOS approximation which is failing at low energy.

The experimental data available (Audibert et al. (1974, 1976)) is in the form of vibrational relaxation rate coefficients. For a gas in translational equilibrium, the rate coefficients for individual processes vj$\rightarrow$v'j' are

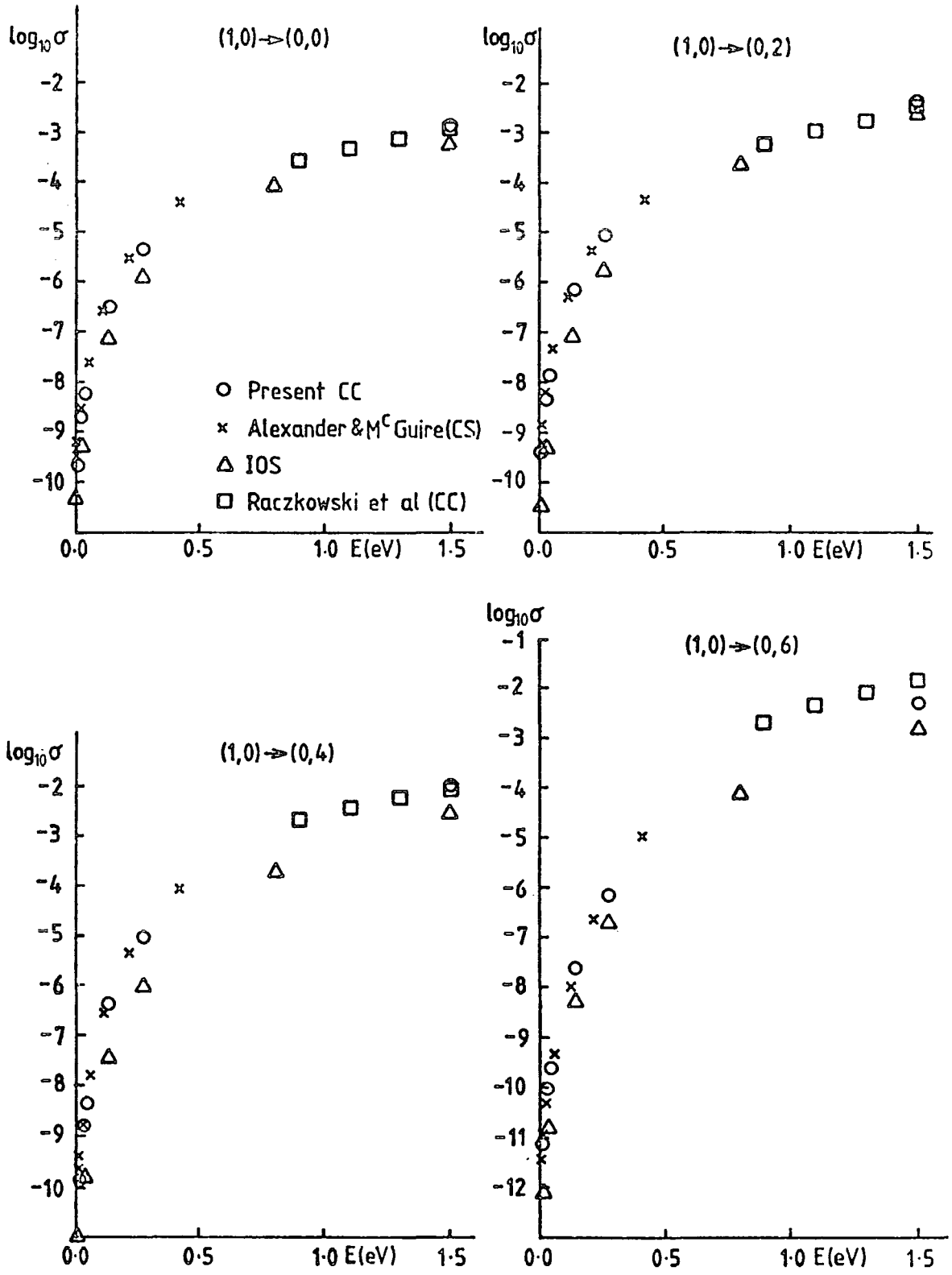


Figure 6 A comparison of the present CC and IOS results with the CC calculations of Raczkowski et al.(1978); the CS results of Alexander and McGuire (1976) are also plotted for reference. Cross-sections in units of $\AA^2$ and energies in eV relative to the (1,0) state.

are related to the corresponding cross sections by averaging over a Maxwellian velocity distribution (see Chapter I).

$$k_{vj \to v'j'}(T) = \int_0^\infty v\, \sigma(vj \to v'j'; v)\, f(v,T)\, dv \qquad \text{IV.4.1}$$

where $$f(v,T) = 4\pi\left(\frac{\mu}{2\pi kT}\right)^{3/2} v^2 \exp\left(-\mu v^2/2kT\right) \qquad \text{IV.4.2}$$

$\mu$ is the reduced mass of the system, $v$ the initial relative velocity of the atom and molecule, k Boltzmann's constant and T is the temperature. Using $E' = \frac{1}{2}\mu v^2$ we can obtain the expression in terms of an averaging over E', the initial collision energy of the system in molecular state (v,j).

$$k_{vj \to v'j'}(T) = \left(\frac{8kT}{\mu\pi}\right)\left(\frac{1}{kT}\right)^2 \int_0^\infty E'\, \sigma(vj \to v'j'; E') \exp\left(-E'/kT\right) dE' \qquad \text{IV.4.3}$$

Pure rotational relaxation ($\Delta v = 0$) is extremely rapid (Alexander (1975)) and consequently the relaxation process observed experimentally is the overall relaxation of the rotational states of the v = 1 manifold to the v = 0 manifold. The rate coefficient for this vibrational relaxation is obtained by averaging over the rotational states.

$$k_{1 \to 0}(T) = Z^{-1} \sum_{jj'} (2j+1) \exp\left[-(\varepsilon_{1j} - \varepsilon_{10})/kT\right] k_{1j \to 0j'}(T) \qquad \text{IV.4.4}$$

where $Z$ is the rotational partition function and a Boltzmann distribution among the rotational states in the v = 1 level has been assumed (Alexander (1975)).

The v = 1, j = 2 state lies approximately 500K above

v = 1, j = 0 and is therefore much more sparsely populated at the low temperatures considered. For $T \lesssim 300K$ the contribution from states v = 0, $j \gtrsim 2$ will be negligible, therefore only transitions from the v = 1, j = 0 state were included in the calculation, i.e. IV.4.4 becomes

$$k_{1\to 0}(T) = \sum_{j'} k_{10\to 0j'}(T) \qquad \text{IV.4.5}$$

The variation of $\log \sigma(1,0\to 0,4)$ with $\log E'$ is shown in Figure 7. As can be seen, this variation is extremely smooth. Therefore, the interpolation of the available results, required to evaluate the integral in IV.4.3, was performed over $\log\sigma$ as a function of $\log E'$. A spline interpolation procedure was employed to obtain values of the cross section to evaluate the integral by a Gauss-Laguerre quadrature.

The values of the vibrational relaxation rate for para-$H_2$ dilute in He evaluated from the present CC calculation are presented in Figure 8. Also plotted are the experimental points of Audibert et al., the CC results of Raczkowski et al. and the CS results of Alexander and McGuire. The present results are seen to agree well with those of Alexander and McGuire, as would be expected in view of the good agreement between the corresponding cross sections (Figure 5). The dominant contributions to $k_{1\to 0}(T)$ come from $k_{10\to 00}(T)$ and $k_{10\to 02}(T)$, and the present CC cross sections are slightly smaller than the CS for these transitions. This is reflected in the corresponding values of the vibrational relaxation rates.

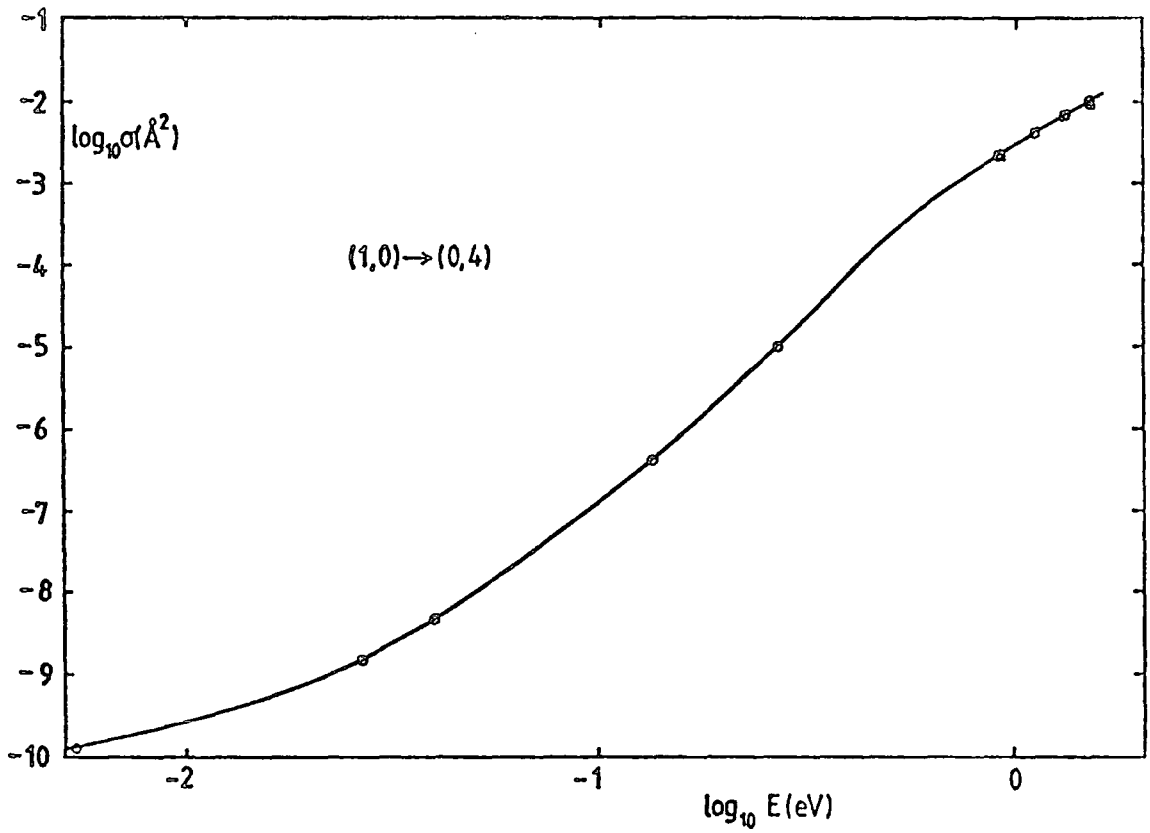


Figure 7 A log-log plot of the energy variation of $\sigma(10 \rightarrow 04)$ ($\mathring{A}^2$) demonstrating departures from a power law. The circles (C) denote the present CC results and the squares ( □ ) denote the CC results of Raczkowski et al. (1978). Energy in units of eV.

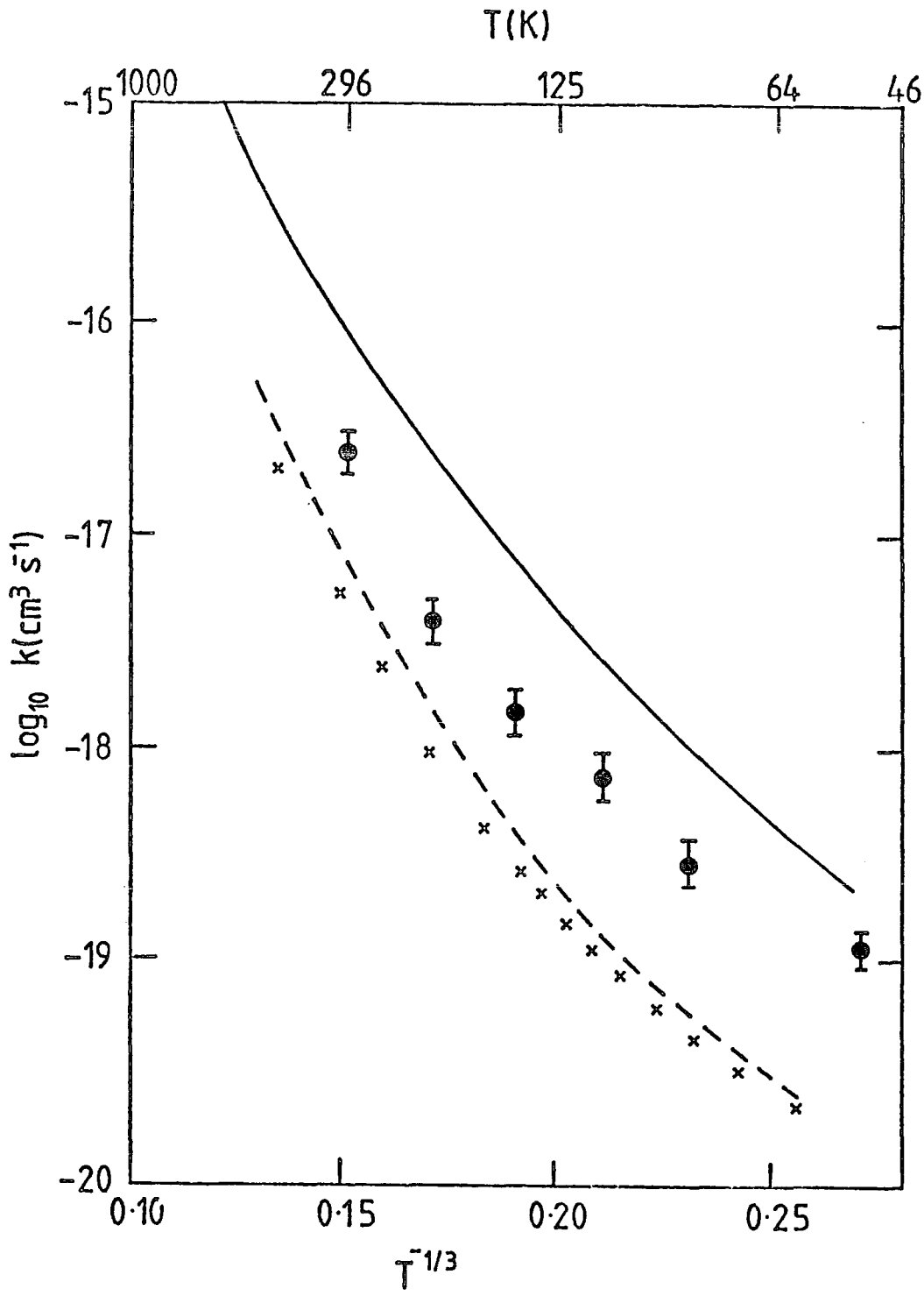


Figure 8 The temperature variation of the n = 1 → 0 vibrational relaxation rate coefficient. Continuous line : CC calculations of Raczkowski et al. (1978); dashed line: CS calculations of Alexander and McGuire (1976). Results obtained from our own CC calculations are also plotted (x), as are the experimental points (Audibert et al. 1976).

To evaluate the integral in IV.4.3, Raczkowski et al. assume a power law dependence of the cross section on collision energy

$$\sigma(v_j \rightarrow v'_{j'}; E') = A (E')^p \qquad \text{IV.4.6}$$

where A and p are constants for a given transition. This allows analytic evaluation of the integral giving a relaxation rate which varies as $T^{p + \frac{1}{2}}$. However Figure 7 demonstrates that this dependence is not accurately respected, particularly near threshold, i.e. at low temperature. Figure 7 also shows that the assumption of a power law dependence will overestimate $k_{10\rightarrow 04}(T)$, resulting in the overestimation of $k_{1\rightarrow 0}(T)$ as displayed in Figure 8. Raczkowski et al. are aware of the possible inaccuracy of this assumption and consider their calculated values of the vibrational relaxation rates to be "dubious indeed" below 200K.

As can be seen in Figure 8, large discrepancies exist between the experimental and theoretical values of the vibrational relaxation rate. This is almost certainly due to deficiencies in the description of the system, in particular, the interaction potential. In addition to performing calculations employing the present Gordon-Secrest (GS) potential, Alexander and McGuire (1976) studied various other interaction potentials and $H_2$ basis wavefunctions. They report that the use of Morse (see e.g. Mies (1964)) rather than harmonic oscillator vibrational wavefunctions produces large changes in the individual inelastic rovibrational cross sections. However, the total de-excitation cross sections (defined as $\sum_j \sigma(10\rightarrow 0j)$), and hence vibrational relaxation

rates, differ by only $\lesssim 20\%$. Modification of the GS potential by the addition of a long range, attractive, isotropic term (which varies as $R^{-6}$) increases the relaxation rates. However, these rates still lie considerably below the experimental values. The best quantative agreement with experiment is obtained by replacing the GS diagonal potential matrix elements by the semi-empirical potential of Shafer and Gordon (1973). This is attributed to the fact that the classical turning point of the Shafer-Gordon potential is considerably closer to R = O than that of the GS potential for all the energies considered. The Shafer-Gordon potential, therefore, allows closer approach of the collision partners and hence stronger coupling. The cross sections are also reported to be insensitive to the presence of a long range anisotropic term.

It is worth repeating that the GS potential is ideally suited to the CS approximation. Where the potential has been modified to include long range terms, the CS approximation would be expected to be less accurate.

Raczkowski et al. also perform CC calculations using the potential of Tsapline and Kutzelnigg (1973). However, they again assume a power law dependence of the cross sections on collision energy (IV.4.6), and hence their comparison with experiment will be misleading at low temperatures. More recent CC calculations by Orlikowski (1981), employing the Tsapline-Kutzelnigg potential and extending much closer to threshold, show better agreement with experiment than is found by Raczkowski et al. Furthermore, the results of Orlikowski lie above those of the present calculations. The results of Alexander and McGuire suggest that this is due to

the Tsapline-Kutzelnigg potential allowing closer approach of the collision partners and the presence of a shallow Van der Waal's minimum, as compared with the purely repulsive GS potential.

Bieniek (1980) has performed calculations for the $H_2$ + He system within the framework of the adiabatic distorted wave IOS approximation (ADWIOS) of Eno and Balint-Kurti (1979). The description of the system is identical to that used in the present calculation. Table 13 contains a comparison between the ADWIOS $\sigma(00 \rightarrow vj)$ results of Bieniek and the present CC and IOS calculations. The present IOS and ADWIOS results are in poor agreement with the CC calculations due to the failure of the IOS approximation. However the comparison between IOS and ADWIOS is a direct test of the efficiency of distorted wave techniques with adiabatic wavefunctions, relative to employing diabatic wavefunctions with a close coupled treatment of the vibrational degree of freedom. The $\Delta v = 2$ results are in extremely poor agreement. As discussed by Bieniek this is most probably due to the failure of the distorted wave approximation. A study by Thiele and Weare (1968) indicates that, in a distorted wave calculation, one must go to the $v^{th}$ order in the expansion to obtain reasonably accurate cross sections for a v quantum transition. They found that a first order treatment gives fairly accurate results for $\Delta v = 1$ transitions but was in error by several orders of magnitude for $\Delta v = 2$ transitions. The results of Table 13 are consistent with this, since the ADWIOS is a first order distorted wave technique.

TABLE 13 A comparison of vibrationally inelastic cross sections $\sigma(00 \to vj)(\mathring{A}^2)$. (a) ADWIOS results of Bieniek (1980); (b) present IOS results; (c) present CC results.

| E(ε) | (v,j) | | | | | | |
|---|---|---|---|---|---|---|---|
| | (1,0) | (1,2) | (1,4) | (1,6) | (2,0) | (2,2) | (2,4) |
| 2.5 | a) 1.302-8 | 1.618-8 | | | | | |
| | b) 1.433-8 | 1.708-8 | | | | | |
| | c) 5.584-8 | 5.615-9 | | | | | |
| 3.0 | 3.678-7 | 4.806-7 | 2.923-7 | | | | |
| | 3.973-7 | 6.031-7 | 3.171-7 | | | | |
| | 1.399-6 | 5.321-7 | 6.741-9 | | | | |
| 5.0 | 8.950-5 | 1.050-4 | 6.342-5 | 4.954-5 | 2.299-13 | 1.600-13 | 9.333-14 |
| | 5.335-5 | 1.570-4 | 1.246-4 | 4.448-5 | 4.288-11 | 8.597-11 | 4.518-11 |
| | — | — | — | — | — | — | — |

The IOS and ADWIOS results for $\sigma(00 \rightarrow 1j)$ are presented graphically in Figure 9. Although there are few data points, it appears that the ADWIOS is incorrectly predicting the degree of curvature of $\log\sigma$ as a function of E. The ADWIOS curvature underestimates that of the IOS results for j = 0, and increases with j, with overestimation for j = 2 and 4. As previously discussed, the present IOS results approach the CC values as the energy increases. Figure 9 suggests that this will not be true for the ADWIOS cross sections. Figure 6 demonstrates that for $\sigma(10 \rightarrow 00)$ and $\sigma(10 \rightarrow 02)$ the IOS results are reaching satisfactory agreement with CC calculations at energies $\simeq$ leV above the first vibrational threshold, whereas the agreement between IOS and ADWIOS is deteriorating at $E \simeq 5.0\mathcal{E}$ which corresponds to $\simeq 0.8$eV above threshold. This disagreement at high energy is possibly due to the use of adiabatic wavefunctions in the ADWIOS. It appears that at energies sufficiently high for the IOS approximation to be valid the use of adiabatic distorted wave (ADW) techniques is not. Eno and Balint-Kurti (1981) have performed calculations of fixed-angle S-matrices employing both CC and ADW techniques over a wide range of total angular momenta and energies, up to 4.2eV. The report that the CC and ADW values of the modulus of the v = 0 to v = 1 S-matrix element agree everywhere to within 15%. As noted by Eno and Balint-Kurti, the IOS cross sections also depend on the phase of the S-matrix. For the partial wave and energy reported (J = 11 and E = 1.2eV), the CC and ADW values of the phase are in perfect agreement. However, if this agreement between the values of the phase is not quite

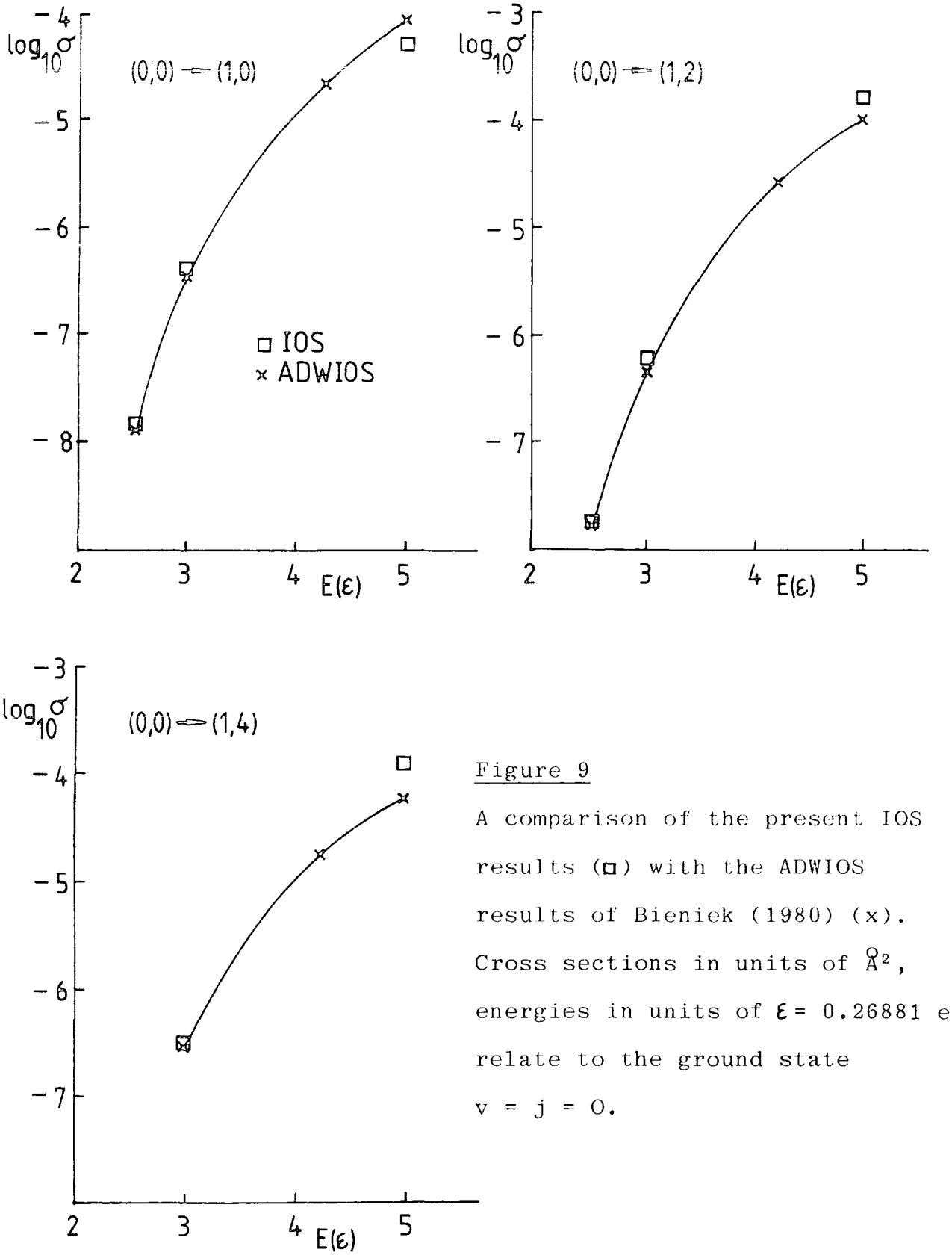


Figure 9

A comparison of the present IOS results (□) with the ADWIOS results of Bieniek (1980) (x). Cross sections in units of $\mathring{A}^2$, energies in units of $\varepsilon$ = 0.26881 eV relate to the ground state v = j = 0.

as exact for other partial waves and energies, it may be possible that the relatively small discrepancies between CC and ADW values of the modulus and phase may combine to produce much larger discrepancies in the final IOS cross-sections. Although Eno and Balint-Kurti employed the Gordon-Secrest potential they used the $H_2$ energy levels quoted by Lester and Schaefer (1973), compared with the harmonic oscillator energy levels used in the present calculations and in the work of Bieniek (1980). As discussed by Bieniek, this difference in energy levels has an extremely large effect on the rovibrational cross-sections. Although the energy separation between the v = 0 and v = 1 vibrational states used by Eno and Balint-Kurti (1979) differs by only 4% from that of Bieniek, the cross sections for E = 2.5$\varepsilon$ are reduced by 75%. However, the use of different energy levels is unlikely to effect the overall comparison between ADW and CC techniques. Bieniek also calculates cross-sections using the energy levels of Lester and Schaefer and finds discrepancies of up to 40% between his results and those of Eno and Balint-Kurti. He attributes this to the different methods of evaluating the distorted wave integrals. Eno and Balint-Kurti employed piecewise fits of the potential to evaluate the integrals analytically while Bieniek used "brute-force numerical methods". Although the results of Eno and Balint-Kurti (1981) suggest that the ADWIOS should be in much better agreement with CC / IOS calculations, any of the points discussed above, or a combination of them, could account for the apparent discrepancies between the present IOS calculations and the ADWIOS results of Bieniek.

Even if these discrepancies are due to the failure of ADW techniques, this may not be the case for systems other than the $H_2$ + He currently under investigation. Adiabaticity and the validity of the IOS approximation are both determined by the relative times of processes, rather than energy considerations. However, in the ADWIOS, the IOS component is approximating the rotational degree of freedom and the ADW, the vibrational. For heavier molecules than $H_2$, the rotational states are much more densely packed within the vibrational manifolds. It may well be true that, for such systems, the relative velocity of the collision can be sufficiently large for the IOS to be valid, yet also suitable for the use of ADW techniques for the vibrational coupling.

An attractive feature of all energy sudden (ES) approximation is the prediction of factorisation and scaling relations between cross sections (for example IV.3.6). The possibility exists of calculating only a few cross sections explicitly and obtaining the remaining results via such relations derived in an ES framework. There have been several studies in recent years exploring such possibilities (Goldflam et al. 1977a,b) and improved versions of ES factorisations have been proposed (Depristo et al. 1979, Hoffman et al. 1979). ES factorisations which include off-energy-shell effects have also been investigated by Gerber et al. (1981), Beard et al. (1982) and Beard and Kouri (1982). All such factorisations not only interlink para-$H_2$+ He results, but also facilitate the calculation of ortho-$H_2$+He cross sections from para $H_2$ + He results. In the work of Gerber et al. (1981), dealing with a combined distorted wave - ES treatment of rovibrational transitions in molecule-

surface scattering, they derive an ES scaling expression which includes, approximately, off-shell effects. This scaling relation is appropriate to vibrational de-excitation for an interaction potential of the form

$$V(\underset{\sim}{R},\underset{\sim}{r}) = A(r,\gamma)\exp(-\alpha R) \qquad \text{IV.4.7}$$

Beard and Kouri (1982) argue that this scaling relation can also be used for cross sections calculated using the GS potential by identifying $\alpha$ of IV.4.7 within $\alpha_0$ of IV.2.1 and obtain

$$\sigma(vj\rightarrow v'j') = (2j'+1)\left(\frac{k_{vo}}{k_{vj}}\right)^2 \sum_{j''} \begin{pmatrix} j' & j & j'' \\ 0 & 0 & 0 \end{pmatrix}^2 B(k_{v'j'},k_{vj}|k_{v'j''},k_{vo})\,\sigma(vo\rightarrow v'j'') \qquad \text{IV.4.8}$$

where

$$B(k_{v'j'},k_{vj}|k_{v'j''},k_{vo}) = \left(\frac{k^2_{v'j'}-k^2_{vj}}{k^2_{v'j''}-k^2_{vo}}\right)^2 \left(\frac{\cosh\left[(2\pi/\alpha_o)(k_{v'j''}-k_{vo})\right]-1}{\cosh\left[(2\pi/\alpha_o)(k_{v'j'}-k_{vj})\right]-1}\right)$$

Table 14a,b contains a comparison between the present CC results and the predictions of two factorisation schemes (SC1 and SC2) for para-$H_2$ and ortho-$H_2$ for $E = 3\varepsilon$. The SC1 results were obtained by using CC $\sigma(vO\rightarrow v'j')$ in IV.3.6 and SC2 are the results of Beard and Kouri from IV.4.8. Both SC1 and SC2 use the present CC para-$H_2$ + He results and the same rovibrational eigenvalues (IV.2.7).

As can be seen, the factorisations do not obey detailed balance for $\Delta v \neq 0$. For any factorisation of this form to exhibit exact detailed balance requires a rigorous relation between $\sigma(vO\rightarrow v'j'')$ and $\sigma(v'O\rightarrow v\ j'')$, since $\sigma(vj\rightarrow v'j')$ is constructed from the former and $\sigma(v'j'\rightarrow vj)$ from the latter. In the IOS approximation it is easily shown (II.3.22).

Table 14a Integral cross sections $\sigma(i \rightarrow f)$ (in units of $\mathring{A}^2$) for $E = 3\varepsilon$. (a) Present CC results; (b) results of Beard and Kouri (1982) (SC2); (c) SC1. (* All (a), (b), and (c) agree since detailed balance from input $\sigma(v0 \rightarrow vj)$, v=0,1).

| i \ f | (0,0) | (0,2) | (0,4) | (0,6) | (1,0) | (1,2) | (1,4) |
|---|---|---|---|---|---|---|---|
| | | a)4.195+1 | 1.395+0 | 2.875-2 | 6.375-7 | 9.931-7 | 1.555-8 |
| (0,2) | * —— | b)4.081+1 | 1.540+0 | 2.022-2 | 1.502-6 | 1.703-6 | 1.058-8 |
| | | c)4.274+1 | 2.368+0 | 1.822-1 | 1.125-7 | 1.641-6 | 2.911-7 |
| | | 8.936-1 | 4.334+1 | 3.368-1 | 4.317-7 | 2.599-6 | 7.508-8 |
| (0,4) | —— | 9.866-1 | 4.060+1 | 4.757-1 | 1.306-5 | 7.391-6 | 1.263-7 |
| | | 1.517+0 | 4.910+1 | 2.400+0 | 9.130-10 | 1.865-7 | 1.875-6 |
| | | 1.679-2 | 3.072-1 | 4.561+1 | 2.836-8 | 5.443-7 | 1.019-6 |
| (0,6) | —— | 1.181-2 | 4.338-1 | 4.055+1 | 0.0 | 1.979-4 | 4.133-6 |
| | | 1.064-1 | 2.189+0 | 6.463+1 | 0.0 | 1.892-9 | 2.704-7 |
| | 3.789-7 | 3.345-6 | 1.366-5 | 3.138-6 | | 4.935+1 | 1.124-1 |
| (1,2) | 1.609-7 | 2.908-6 | 9.742-6 | 3.775-5 | —— | 4.791+1 | 2.077-1 |
| | 2.147-6 | 1.129-5 | 8.727-6 | 5.367-6 | | 5.642+1 | 1.360+0 |
| | 4.727-9 | 5.160-8 | 3.887-7 | 5.784-6 | | 1.107-1 | 5.270+1 |
| (1,4) | 1.562-10 | 8.802-9 | 3.939-7 | 6.170-6 | - — | 2.046-1 | 4.779+1 |
| | 2.235-6 | 8.594-6 | 1.723-5 | 1.293-5 | | 1.340+0 | 9.989+1 |

| i \ f | (0,1) | (0,3) | (0,5) | (0,7) | (1,1) | (1,3) | (1,5) |
|---|---|---|---|---|---|---|---|
| (0,1) | 4.137+1 a) | 2.315+0 | 1.113-1 | 5.237-4 | 1.469-6 | 1.453-7 | 6.424-11 |
| | 4.102+1 b) | 2.435+0 | 9.826-2 | | 2.033-6 | 1.449-7 | 3.761-11 |
| | 4.155+1 c) | 2.714+0 | 2.154-1 | | 1.641-6 | 3.281-7 | 3.813-9 |
| | 4.037+1 d) | 3.452+0 | 5.797-1 | | 6.502-7 | 5.120-7 | 2.093-7 |
| (0,3) | 1.092+0 | 4.237+1 | 7.800-1 | 5.485-3 | 1.962-6 | 3.995-7 | 2.703-10 |
| | 1.149+0 | 4.069+1 | 9.109-1 | | 6.467-6 | 6.007-7 | 1.924-10 |
| | 1.280+0 | 4.519+1 | 2.316+0 | | 1.548-7 | 1.728-6 | 2.856-7 |
| | 1.628+0 | 4.391+1 | 2.897+0 | | 2.415-7 | 7.068-7 | 4.146-7 |
| (0,5) | 4.081-2 | 6.062-1 | 4.441+1 | 1.117-1 | 6.089-7 | 2.178-6 | 2.508-9 |
| | 3.602-2 | 7.079-1 | 4.056+1 | | 5.822-5 | 7.041-6 | 5.992-9 |
| | 7.895-2 | 1.800+0 | 5.511+1 | | 1.398-9 | 2.220-7 | 2.103-6 |
| | 2.125-1 | 2.252+0 | 5.351+1 | | 7.674-8 | 3.222-7 | 8.338-7 |
| (0,7) | 2.069-4 | 4.594-3 | 1.204-1 | 4.685+1 | 2.556-8 | 4.234-7 | 9.222-8 |
| (1,1) | 4.568-6 | 1.293-5 | 5.164-6 | 2.012-7 | 4.880+1 | 6.102-1 | 1.433-4 |
| | 4.672-6 | 9.093-6 | 1.635-5 | | 4.818+1 | 7.762-1 | 1.431-4 |
| | 8.248-6 | 1.021-5 | 5.943-6 | | 5.044+1 | 1.413+0 | 6.790-3 |
| | 2.022-6 | 1.592-6 | 6.509-7 | | 4.912+1 | 2.573+0 | 1.826-1 |
| (1,3) | 2.677-7 | 1.561-6 | 1.095-5 | 1.975-6 | 3.617-1 | 5.064+1 | 4.498-3 |
| | 5.696-8 | 1.370-6 | 9.179-6 | | 4.600-1 | 4.782+1 | 1.733-2 |
| | 6.054-6 | 1.242-5 | 9.535-6 | | 8.375-1 | 6.932+1 | 1.549+0 |
| | 9.434-7 | 2.761-6 | 1.620-6 | | 1.525+0 | 6.726+1 | 2.769+0 |
| (1,5) | 2.423-10 | 2.162-9 | 2.580-8 | 8.805-7 | 1.739-4 | 9.207-3 | 5.680+1 |
| | 4.698-12 | 3.989-10 | 3.762-8 | | 1.736-4 | 3.548-2 | 4.777+1 |
| | 7.210-6 | 1.952-5 | 3.789-5 | | 8.237-3 | 3.170+0 | 2.229+2 |
| | 7.897-7 | 3.316-6 | 8.580-6 | | 2.216-1 | 5.668+0 | 2.161+2 |

Table 14b Integral cross-sections $\sigma(i \rightarrow f)$ (in units of $\mathring{A}^2$) for $E = 3\varepsilon$ ($\varepsilon = 0.16881$ eV). (a), present CC calculations; (b) results of Beard and Kouri (1982) (SC2); (c) results predicted by equation IV.3.6 of text (SC1); (d) present IOS results.

$$k^2_{v0}\,\sigma(v0 \rightarrow v'j'') = k^2_{v'0}\,\sigma(v'0 \rightarrow vj'') \qquad \text{IV.4.9}$$

These are not reciprocal processes and this detailed balance type condition is imposed by the IOS approximation. This is true only for v = v' or j'' = 0. Such a relationship is not unreasonable in the IOS, where the rotor states are considered degenerate. Only by virtue of IV.4.9 do the cross sections calculated from IV.3.6 exhibit detailed balance.

$$(2j+1)\,k^2_{vj}\,\sigma(vj \rightarrow v'j') = (2j'+1)\,k^2_{v'j'}\,\sigma(v'j' \rightarrow vj) \qquad \text{IV.4.10}$$

If $\sigma(v0 \rightarrow v'j'')$ is not calculated using the IOS approximation, but by CC calculations, the resultant $\sigma(vj \rightarrow v'j')$ obtained from IV.3.6 will not, in general, satisfy detailed balance for $\Delta v \neq 0$.

The failure of SC1 to obey detailed balance is mainly due to the failure of IV.4.9 for CC cross sections. It is also partially due to different summations of j'' in IV.3.6 since v = 0, j = 6 is open yet v = 1, j = 6 is closed. The SC2 scheme also has this problem of different summations over j''. This is emphasised by $\sigma(06 \rightarrow 10)$, where only the j'' = 6 term is included, due to the properties of the 3-j coefficients. However, since v = 1, j = 6 is closed, $\sigma(00 \rightarrow 16) = 0$, and hence both factorisations predict $\sigma(06 \rightarrow 10) = 0$. As noted by Goldflam et al. (1977a) (and by Secrest (1975)), the IOS approximation analytically sums over all, open and closed, rotor states. This is possible since the rotational energy levels are assumed degenerate. The effect is that there is incorrect coupling to closed channels, giving the result that the IOS will be inaccurate

for transitions in which closed channels play an important role.

The derivation of IV.4.8 (Gerber et al.) requires the ES condition that $\alpha_o/k_{vj}$ and $\alpha_o/k_{v'j'} \ll 1$. For v = 1, j = 0 the wavevector $k_{10} = 1$, in the units of Section 2, hence $\alpha_o/k_{10} = 0.2792$. The failure of this ES condition will result in SC2 being inaccurate for this system at $E = 3\mathcal{E}$, just as the ES component of the IOS fails. As the total energy increases SC1 and SC2 would be expected to give better agreement with CC results. Also, the problem concerning the summation over $\sigma(v0 \rightarrow v'j'')$ would be alleviated, since many more rotor states would be available.

The SC2 scheme, as emphasised by Beard and Kouri (1982), compensates for the progressive overestimation of the elastic cross sections by SC1 caused by the increase of the $(k_{v0}/k_{vj})^2$ factor in IV.3.6 as $k_{vj}$ decreases towards threshold. Overall, SC2 is in much better agreement with the CC results, and does not violate detailed balance for $\Delta v \neq 0$ as severely as SC1. Both SC1 and SC2 are in better agreement with CC results than the IOS calculations.

Several ES factorisations, including SC2, are derived for de-excitation transitions only (see e.g. De Pristo et al. (1979), Gerber et al. (1981)) i.e. $\mathcal{E}_{vj} \geq \mathcal{E}_{v'j'}$. It therefore appears reasonable to use the ES scheme only for such de-excitation cross sections. The remaining excitation results can then be obtained by assuming detailed balance. If this procedure is employed, using SC2 to predict the de-excitation cross section, the overall agreement between SC2 and CC results would be improved. Consider vibrationally inelastic transitions between the states v = 0, j = 2,4,6 and

v' = 1, j' = 2,4. The de-excitation cross-sections, $\sigma(v'j' \rightarrow vj)$, are in better agreement with the CC results, than the corresponding excitation results, $\sigma(vj \rightarrow v'j')$ in 5 out of 6 cases. Similarly for vibrationally inelastic transitions between v = 0, j = 1,3,5 and v = 1, j = 1,3,5, the de-excitation results agree better than the excitation cross sections with CC values, in 6 out of 9 cases. The vibrationally elastic results would be unchanged since they obey detailed balance.

Alexander (1976) has performed CS calculations for ortho-$H_2$ + He using the GS potential with the diagonal matrix elements replaced by the semi-empirical potential of Shafer and Gordon (1973). As discussed previously, this modification of the GS potential produces large changes in the cross sections and vibrational relaxation rate coefficients for para-$H_2$ + He. The discrepancies between the present ortho-$H_2$+He results and those of Alexander are of the same order and sign as the changes produced in para-$H_2$ + He cross sections by this modification of the GS potential. In view of the good agreement between the CS results of Alexander and McGuire (1976) and the present CC results for para-$H_2$ + He, it is almost certain that these discrepancies are almost entirely due to the form of interaction potential employed. Alexander notes that, at a given collision energy, $\sigma(10 \rightarrow 0j)$ is always smaller than $\sigma(11 \rightarrow 0,j+1)$, resulting in a greater relaxation rate for ortho-$H_2$ + He than for para-$H_2$ + He, as observed experimentally (Audibert et al. (1976)). The present CC ortho and para-$H_2$ + He results, calculated at the same total energy, E = 3$\varepsilon$, also display

this behaviour. This total energy E = 3$\varepsilon$ correpsonds to a collision energy of E' = $\varepsilon$ for $\sigma(10 \rightarrow 0j)$ and E' = $\varepsilon - \varepsilon_{11}$ for $\sigma(11 \rightarrow 0, j + 1)$. As can be seen from Figure 5, $\sigma(10 \rightarrow 0j)$ increases monotonically with energy. Therefore if the CC ortho and para-$H_2$ + He results had been calculated at the same collision energy, E' = $\varepsilon - \varepsilon_{11}$ they would still maintain $\sigma(10 \rightarrow 0j)$ smaller than $\sigma(11 \rightarrow 0, j + 1)$, in agreement with Alexander and experiment. This would be expected from simple energy considerations which predict the larger cross sections for $\sigma(11 \rightarrow 0, j + 1)$ since such transitions are characterised by smaller energy defects. For example $(\varepsilon_{11} - \varepsilon_{05})$ = 2698 $cm^{-1}$, whereas $(\varepsilon_{10} - \varepsilon_{04})$ = 3168 $cm^{-1}$.

## 5. Summary

We have performed CC and IOS calculations of cross sections for rovibrational excitation of $H_2$ by He, using the potential of Gordon and Secrest (1970) with the $H_2$ basis states approximated by rotating harmonic oscillators, as described by Eastes and Secrest (1972).

We find large discrepancies between our own CC results and those of Lin and Secrest (1979) and Lin (1979). These discrepancies are present in both vibrationally elastic and inelastic cross sections and increase towards the v = 1 vibrational excitation threshold. We attribute this to an error in the computer program used by Lin (1981). This error not only effects the numerical values of the cross sections, but also their physical interpretation, since the structures in the energy variation of the cross sections, apparent in the results of Lin, and Lin and Secrest, are absent in the present calculations.

The present CC results are found to be in good quantitative agreement with the CS calculations of Alexander and McGuire (1976). The agreement with the IOS calculations is only qualitative but improves with increasing collision energy; this is consistent with the progressive failure of the "energy sudden" component of the IOS approximation as the collision energy falls.

Our CC calculations extend to lower energies than those of Raczkowski et al. (1978) and consequently yield more accurate values of the vibrational relaxation rate coefficients at low temperatures. We find that the computed values of the rate coefficient fall below the experimental points of Audibert et al. (1976). This can be attributed to deficiencies in the Gordon-Secrest interaction potential. The CC calculations of Orlikowski (1981), based upon the potential of Tsapline and Kutzelnigg (1973), and the CS results of Alexander and McGuire (1976), based upon a modified Gordon-Secrest potential, are in better agreement with experiment. The results of Alexander and McGuire suggest that the improved agreement may be due to these potentials allowing closer approach of the collision partners and the presence of minima, as compared with the purely repulsive Gordon-Secrest potential.

The present IOS calculations are in good agreement with those calculated by Bieniek (1980), using the adiabatic distorted-wave IOS approximation, at low energies. However as the collision energy increases, significant discrepancies appear. For the $H_2$ + He system under discussion, it appears

that at energies sufficiently high for the IOS approximation to be valid, the use of adiabatic wavefunctions with distorted wave techniques is not.

We have also investigated the accuracy of two energy sudden factorisation relationships (SC1 and SC2). The SC1 results were obtained by using CC $\sigma(v0 \rightarrow v'j')$ in the familiar IOS factorisation (IV.3.6). This factorisation includes contributions only from on-energy-shell T-matrices. SC2 are the results of Beard and Kouri (1982), employing a factorisation which includes off-shell effects (Gerber et al. (1981)). Neither SC1 nor SC2 produce cross sections which exhibit detailed balance for vibrationally inelastic transitions. Overall, SC2 is in better agreement with the CC results and does not violate detailed balance for $\Delta v \neq 0$ as severely as SC1. However the derivation of SC2 (Gerber et al. (1981)) assumes de-excitation cross sections. If SC2 is used to predict only de-excitation cross sections, and the excitation results are obtained by assuming detailed balance , the agreement with CC calculations improves.

A comparison between the present CC ortho and para-$H_2$ + He results reveals that $\sigma(11 \rightarrow 0, j+1)$ is larger than $\sigma(10 \rightarrow 0j)$ for the same collision energy. This is in agreement with the CS calculations of Alexander (1976) and with the experimental values of the vibrational relaxation rate coefficient (Audibert et al. (1976)).

# CHAPTER V

# ROVIBRATIONAL EXCITATION OF $H_2$ BY $H^+$

## 1. Introduction

As demonstrated in Chapter IV in calculations of rovibrational excitation of $H_2$ by He, the relatively large energy spacing of the $H_2$ rotational states provides a stringent test of the IOS approximation. The same will be true for the $H_2 + H^+$ system. However, in contrast to $H_2$ + He, the interaction potential for $H_2 + H^+$ contains long range isotropic and anisotropic terms due to the charge on the proton. The presence of such terms tends to reduce the accuracy of the coupled-states component of the IOS approximation. The accuracy of the energy sudden component will also be reduced, since the proton will spend a comparatively longer time in the interaction region. Both of these points have been discussed in Chapter II.3(a) and (b). One aspect of the $H_2 + H^+$ system which makes it more suitable than $H_2$ + He for the application of the IOS approximation is that $H^+$ is lighter than He. Hence, for a given collision energy, the validity of the energy sudden component will be greater for $H^+$ than He. The presence of long range interaction terms also makes the $H_2 + H^+$ system a more difficult calculation, computationally, since large integration ranges will be required. This will require a large number of steps in the integration algorithm, which in turn may necessitate small step sizes. The small step sizes may be required to reduce the error in each step and hence prevent the accumulation of round-off error reducing the accuracy of

the final result.

Giese and Gentry (1974) have compared and discussed three ab initio calculations of the $H_2 + H^+$ interaction potential by Csizmadia et al. (1970), Bauschlicher et al. (1973) and Carney and Porter (1974). The SCF-MO-configuration interaction calculations of Csizmadia et al. are by far the most extensive and cover a comprehensive range of nuclear geometries. Giese and Gentry conclude that an analytic fit to a restricted set of these points, suitably adjusted, is the best representation of the $H_2 + H^+$ potential surface for the purposes of collision calculations.

Giese and Gentry (1974) have performed semiclassical calculations of vibrational excitation of $H_2$ by $H^+$, employing their DECENT model (Distribution (among quantum states) of Exact Classical Energy Transfer). In this model, exact classical trajectories are used to obtain the classical energy transfer as a function of angle. Vibrational excitation probabilities can then be calculated by employing the correspondence between a classical and quantum forced harmonic oscillator. They report good arreement with the experimental results of Udseth et al. (1973). To obtain a better determination of quantum features such as rainbow structures, Schinke (1977) has performed time dependent close coupling calculations which employ an energy sudden treatment of the rotation. The overall agreement with the results of Giese and Gentry is satisfactory and, in addition, the results of Schinke contain additional rainbow structures. However, Schinke estimates that the use of a straight line trajectories restricts the time dependent close coupling method to

collision energies $\gtrsim$ 15 eV.

McGuire (1976) has performed CC and CS calculations treating the $H_2$ molecule as a rigid rotor by employing the Giese-Gentry potential with the internuclear separation set at its equilibrium value. Schinke and McGuire (1978a) have performed similar IOS calculations and, by comparison with CS results, conclude that the IOS approximation is valid for $H_2 + H^+$ at collision energies $\gtrsim$ 3.7 eV. Schinke and McGuire (1978b) have extended these IOS calculations to include the vibrational degree of freedom, which is treated by close coupling techniques.

As discussed in Chapter I.3, the $H_2 + H^+$ system is ideally suited to molecular beam experiments and experimental values of rovibrational cross sections have been reported by several authors (Udseth et al. (1973), Schmidt et al. (1976) Schinke et al. (1977), Hermann et al. (1978) and others). Schinke and McGuire (1978b) compare rovibrational state to state differential cross sections from their IOS calculations with the experimental values of Hermann et al. (1978) and find "not completely satisfactory" agreement. The discrepancies between theoretical and experimental cross sections are attributed to deficiencies in the interaction potential.

In view of these discrepancies, Schinke et al. (1980) performed configuration interaction calculations of the potential energy surface of $H_2 + H^+$ over an extensive range of nuclear geometries. In total, the potential surface was calculated at 650 points. Schinke et al. also report an analytic expression of the $H_2 + H^+$ interaction, derived from their ab initio points and the long range multipole

interaction of the system calculated by perturbation theory (Kolos and Wolniewicz (1965, 1967)). IOS calculations of rovibrational cross sections employing this new potential (Schinke et al. (1980), Schinke (1980)), are in much better agreement with the experimental values than the cross sections calculated using the Giese and Gentry (1974) potential. However, the bound state vibrational wavefunctions used in these studies (and also in the calculations of Schinke (1977) and Schinke and McGuire (1978b)) are incorrect for highly excited states, although Schinke claims that this error does not significantly effect the results of interest (private communication). This error is discussed in detail in Section 3. In view of the availability of highly refined experimental data it appears worthwhile to investigate the extent to which this error in the vibrational wavefunctions effects the rovibrational cross sections.

## 2. Interaction Potential

The analytic $H_2 + H^+$ potential of Giese and Gentry (1974) (GG) is a fit to 138 ab initio configuration interaction energies of Csizmadia et al. (1970). In contrast, the configuration interaction calculations of Schinke et al. (1980) (hereafter referred to as SDL) used a larger atomic basis set and configuration basis, and covered 650 nuclear geometries, specifically chosen to obtain an accurate potential for use in calculations of rovibrational cross sections. Therefore, the potential of SDL is certainly the more reliable description of the $H_2 + H^+$ interaction. However, the GG potential is the total potential of the $H_2 + H^+$

system, whereas SDL report only the interaction potential. Therefore, exact vibrational wavefunctions of the isolated $H_2$ molecule can be calculated only from the former, but not from the latter. In all the IOS calculations employing both the GG potential (Schinke and McGuire (1978b))and the SDL potential (Schinke et al. (1980), Schinke (1980)), the vibrational wavefunctions used were calculated from the GG potential. However, the method used by Schinke (1977) to determine these wavefunctions destroys their orthonormal properties, essential to the derivation of the fixed angle coupled equations, and produces unphysical behaviour for highly excited states (see Section 3).

We are primarily interested in the extent to which the errors in these wavefunctions effect the rovibrational cross sections. The inconsistent use of such basis functions, obtained from the GG potential, in calculations employing the interaction potential of SDL (as in Schinke et al. (1980) and Schinke (1980)) would obscure this goal. This point is discussed further in Section 5. Therefore, although the SDL interaction potential is certainly the more accurate, the GG potential was employed in the present calculations.

The GG potential is a fit of the ab initio points of Csizmadia et al. (1970) to the following ten parameter analytic function. All ten parameters (underlined) were optimised by an iterative least-squares fit of the function to the ab initio points. The coordinate system used is displayed in Figure 1.

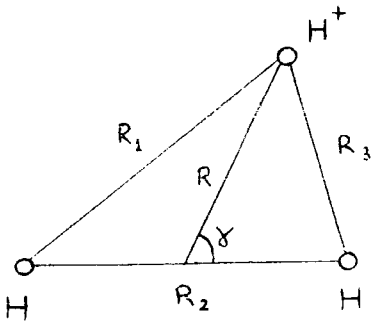


Figure 1.

$R_2$ = r, the internuclear distance of the $H_2$ molecule. The potential is expressed in terms of $R_k$ (k = 1,2,3) and is given by (in a.u.)

$$V(\underline{R},\underline{r}) = \sum_{k=1}^{3} H(R_k) + PF_1 + QF_2 + \underline{0.073225}F_3 + 0.17449 \qquad V.2.1$$

where $H(R_k) = A[-2E + E^2 - 0.1145Z^3E^2(1-Z)]$ V.2.2

with $E = e^{-Z}$ $\qquad R_e = 1.40083 + \underline{0.27923}F_4$

$Z = B(R_k/R_e - 1)$ $\qquad A = 0.17449 - (\underline{0.014665} + \underline{0.022721}R_k)F_4$

$B = 1.4426 - \underline{0.12871}F_4$

and P is the charge-induced dipole contribution

$$P = -(A_o + A_2P_2)R^{-4} \qquad V.2.3$$

$A_o$ and $A_2$ are determined from cubic fits to the spherical and angle-dependent polarisabilities versus $R_2$ as calculated by Kolos and Wolniewicz (1967) and have numerical values

$$A_o = 2.6091 + [2.246 + (0.3181 - 0.1194\varsigma)\varsigma]\varsigma$$

$$A_2 = 0.60735 + [1.3586 + (0.5573 - 0.3170\varsigma)\varsigma]\varsigma$$

where $\varsigma = R_2 - 1.40083$. The charge quadrupole contribution Q is given by

$$Q = Q_2P_2(\cos\gamma)R^{-3} \qquad V.2.4$$

where $Q_2$ is determined from a cubic fit to the quadrupole moment versus $R_2$ (Truhlar (1972), Kolos and Wolniewicz (1965))

$$Q_2 = 0.45886 + [0.53223 + (0.03234 - 0.091474\varsigma)\varsigma]\varsigma$$

Finally $F_1$, $F_2$, $F_3$ and $F_4$ are roll-off and roll-on functions given by

$$F_1 = R^5/(\underline{133.6729} + R^5) \qquad \text{V.2.5a}$$

$$F_2 = R^4/(\underline{29.6088} + R^4) \qquad \text{V.2.5b}$$

$$F_3 = 1/\{1 + \exp[\underline{2.1135}\ (R - \underline{2.4421})]\} \qquad \text{V.2.5c}$$

$$F_4 = 1/(1 + \underline{0.000164189}R^6) \qquad \text{V.2.5d}$$

The use of the summation over the diatomic potential functions $H(R_k)$ allows the width, depth and position of the potential minima to vary smoothly as the proton approaches. This gives a good representation of the true potential, but also causes numerical difficulties, since it is impossible to separate the variables R and r to any large degree since

$$R_1,\ R_3 = \left| \sqrt{R^2 + (r/2)^2 \pm Rr\cos\gamma} \right| \qquad \text{V.2.6}$$

Therefore large scale initialisation of the matrix elements, as performed in the $H_2$ + He calculation, is not possible. Some initialisation can be performed, such as the integrals over P and Q. However, the computationally expensive tasks such as exponentiation, are contained in $H(R_k)$. At each point in the integration range these matrix elements must be evaluated numerically. However, this evaluation is required only in the calculation for the initial partial wave. The generation of results for subsequent values of J does not require any explicit reference to the potential.

The awkward form of the potential is a more serious problem in CC and CS calculations, since it is not in the form of a single centre expansion. Therefore, the angular integrals over spherical harmonics contained in the CC and

CS matrix elements cannot be expressed analytically as Percival Seaton coefficients. In the CC and CS calculations of McGuire (1976) the interaction potential was fitted to a single centre expansion to overcome this difficulty.

The GG potential (V.2.1) is the total potential of the system, including that of the isolated $H_2$ molecule. The potential of the isolated molecule is given by V.2.1 with $R = \infty$ .

$$V_{H_2}(r) = A'[-2E' + (E')^2 - 0.1145(Z')^3(E')^2(1-Z')] + 0.17449 \qquad \text{V.2.7}$$

$A' = 0.17449$, $E' = e^{-Z'}$, $Z' = 1.4426\,(r/1.40083-1)$

Therefore, the interaction potential is given by

$$V_{int}(\underline{R},\underline{r}) = V(\underline{R},\underline{r}) - V_{H_2}(r) \qquad \text{V.2.8}$$

## 3. Choice of Basis Functions

Since the potential of Giese and Genty (1974) contains the potential of the isolated $H_2$ molecule (V.2.7), the calculation of exact basis wavefunctions is possible. To determine the exact $H_2$ bound states $\varphi_v^{Ex}$ and eigenvalues $\varepsilon_v^{Ex}$ one must solve (in a.u.)

$$\left[ -\frac{1}{2\mu_{H_2}} \frac{d^2}{dr^2} + V_{H_2}(r) - \varepsilon_v^{Ex} \right] \varphi_v^{Ex} = 0 \qquad \text{V.3.1}$$

The approach adopted by Schinke (1977) was to expand $\varphi_v^{Ex}$ as a series of normalised harmonic oscillator basis functions $\varphi_i^{HO}$

$$\varphi_v^{Ex} = \sum_i C_i^v \varphi_i^{HO} \qquad \text{V.3.2}$$

Where the harmonic basis functions are the solutions of

$$\left[ -\frac{1}{2\mu_{H_2}} \frac{d^2}{dr^2} + V^{HO}(r) - \varepsilon_i^{HO} \right] \varphi_i^{HO} = 0 \qquad \text{V.3.3}$$

with $V^{HO}(r) = \frac{k}{2}(r - r_e)^2$

given by

$$\varphi_i^{HO}(r) = \exp(-Q^2/2)\, N_i\, H_i(Q) \qquad \text{V.3.4}$$

where $Q = (\mu k)^{1/4} r$, $N_i$ is a normalisation coefficient and $H_i$ is a Hermite polynomial. Substitution of V.3.2. into V.3.1, using V.3.3. and the orthonomal properties of $\varphi_i^{HO}$ gives a set of homogeneous linear equations for the coefficients $c_i$ (in matrix notation)

$$(\underset{\sim}{V} + \underset{\sim}{\Delta})\,\underset{\sim}{C} = \underset{\sim}{0} \qquad \text{V.3.5}$$

where $$V_{ij} = \int dr\, \varphi_i^{HO} (V_{H_2} - V^{HO}) \varphi_j^{HO}$$

$$\Delta_{ij} = (\varepsilon_i^{HO} - \varepsilon_i^{EX})\, \delta_{ij}$$

The desired eigenvalues $\varepsilon_i^{EX}$ are the solutions of the secular equation

$$\left| \underset{\sim}{V} + \underset{\sim}{\Delta} \right| = 0 \qquad \text{V.3.6}$$

and the coefficients $C_i^V$, are the corresponding eigenvectors.

Schinke chose harmonic oscillator (HO) basis functions because of their simple form and, therefore, the increased possible use of his expansion in further applications. However, the use of HO wavefunctions has a severe disadvantage. A large number of basis functions is required in the expansion since the exact $H_2$ wavefunctions are sub-

stantially different from the HO functions for reasonably high vibrational quantum numbers. In itself, this is of no consequence as regards the computer time required to evaluate the exact wavefunctions. If we consider

$$N_i H_i(Q) = \sum h_j^i Q^j$$

then

$$\Phi_v^{EX} = \sum c_i^v \varphi_i^{HO} = \exp(-Q^2/2) \sum \left( \sum c_i^v h_j^i \right) Q^j \qquad \text{V.3.7}$$

The inner summation over i need be performed only once and subsequently the effort involved in calculating the exact wavefunction is identical to that required to evaluate the highest order HO basis function. The main problem is that for $i \geqslant 10$, the HO functions encroach into $r < 0$ (figure 2) corresponding, physically, to the nuclei of the $H_2$ molecule passing through one another. Therefore the integration range in the $V_{ij}$ elements must be increased to preserve the orthonormality of the HO basis functions. Although $V_{H_2}$ is not infinite for $r < 0$, it is extremely large and vastly different from $V^{HO}$. Therefore for large i,j, $V_{ij}$ is also extremely large. However, we are principally interested in the potential well, and by extending the integration range emphasis is transferred to the repulsive wall at $r < 0$. Schinke does not extend the integration range (private communication) and maintains the lower limit at $r = 0$, hence destroying the orthonormal properties of the HO wavefunctions which are employed to derive the secular equation V.3.5. This produces the result shown in figure 3. The "exact" wavefunction shows unphysical behaviours for large vibrational

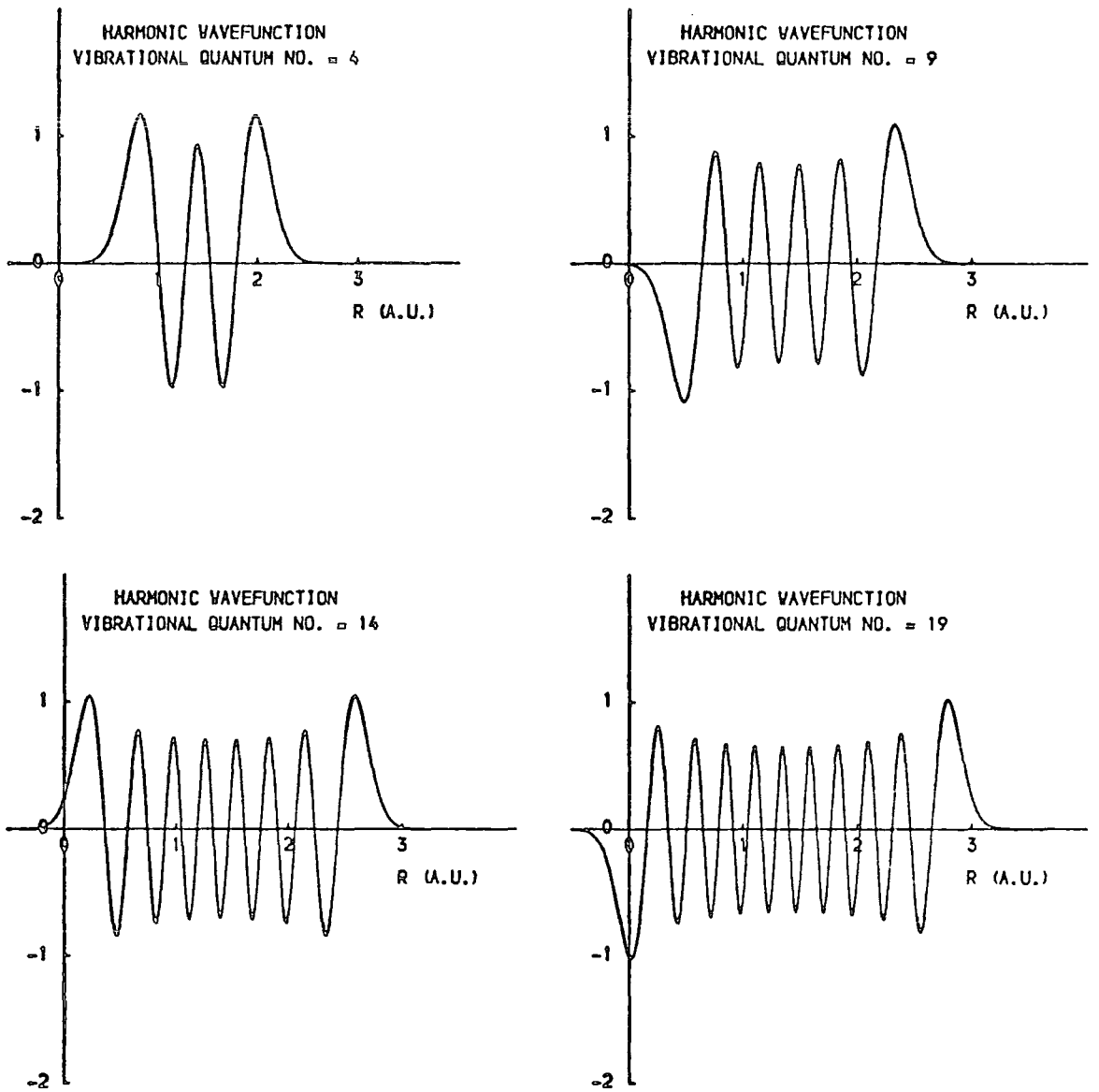


Figure 2 Harmonic oscillator wavefunction with vibrational frequency $\omega$ = 0.019 a.u. and equilibrium separation $r_e$ = 1.40083 a.u. for vibrational quantum numbers 4,9,14 and 19. Employed as expansion functions by Schinke (1977).

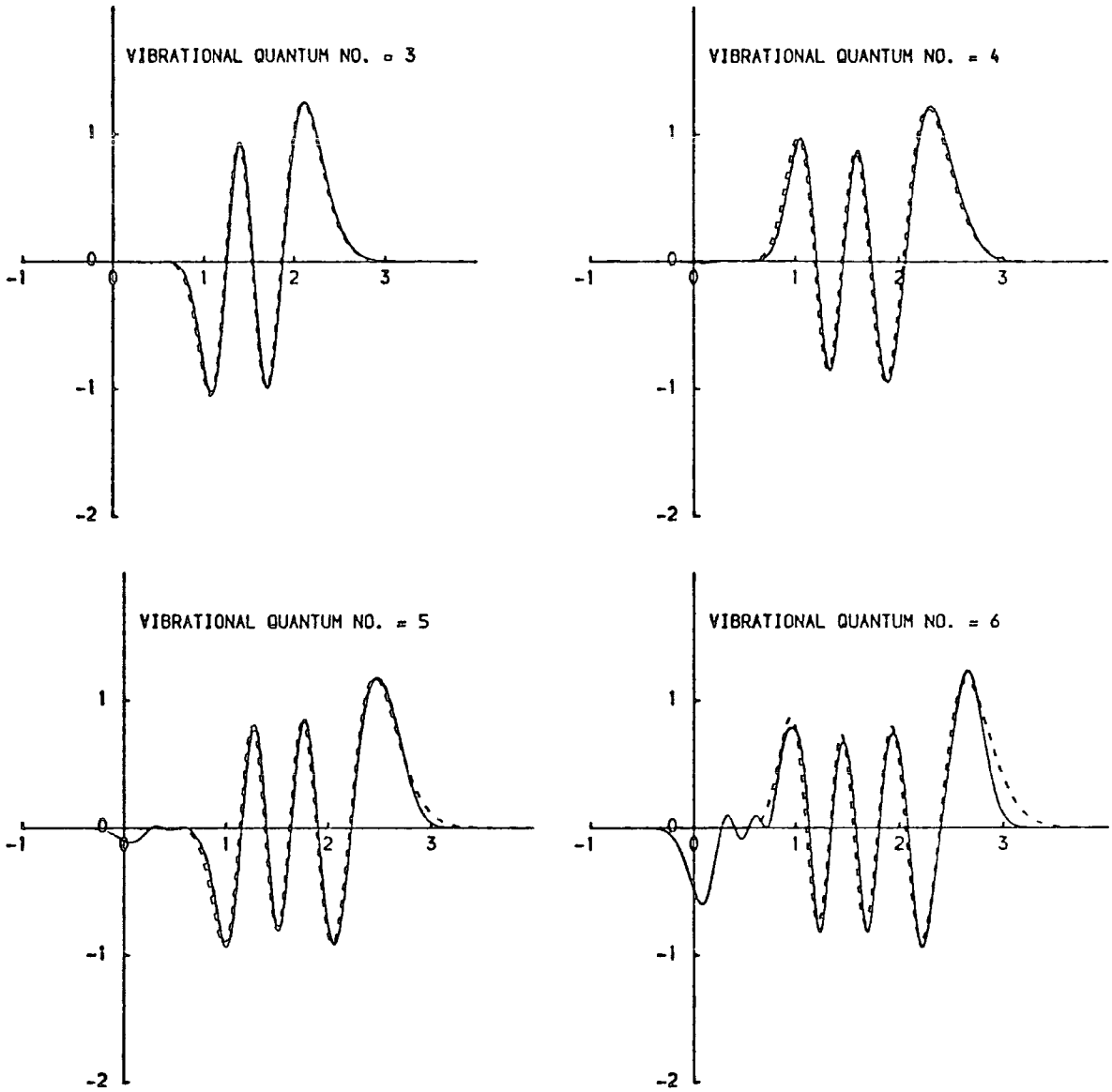


Figure 3 Comparison of vibrational wavefunctions reported by Schinke (1977) (full line) with the present Morse oscillator wavefunctions (broken line).

quantum numbers.

Twenty HO basis functions were used in Schinke's expansion. However, for v = 6 (figure 3), the highest order coefficient $C_{19}^{6}$, has a value of 0.230 which suggests that either the expansion is too small or that the difficulties discussed above are causing severe distortion. Schinke reports his expansion coefficients to only three figures. However, the orthonormality of the exact wavefunctions demands

$$\sum_i C_i^v C_i^{v'} = \delta_{vv'} \qquad \text{V.3.8}$$

Hence orthonormality can only be maintained to $\sim 10^{-3}$, due to round-off error. This is comparable to, and sometimes larger than the coupling matrix elements

$$\int \varphi_v^{Ex} V_{int}(\underset{\sim}{R}, \underset{\sim}{r}) \varphi_{v'}^{Ex} \, d\underset{\sim}{r} \qquad \text{V.3.9}$$

Although reported to only three figures, in his calculations (and in subsequent work) the expansion coefficients were specified to five figures (private communication) and are given in Table 1.

The HO wavefunctions have an equilibrium separation $r_e$ = 1.40083 a.u. and harmonic frequency $\omega$ ($=(\frac{k}{\mu_{H_2}})^{\frac{1}{2}}$) = 0.019 a.u.

In the present IOS calculations, Morse oscillator wavefunctions were chosen to represent the $H_2$ vibrational states. Although the Morse potential is not infinite for $r \leq 0$, it tends to a finite value as $r \to \infty$ , therefore only a certain number of bound states can be supported. The Morse potential and corresponding normalised eigenfunctions and

Table 1 Expansion coefficients $C_i^v$ of the vibrational basis states employed by Schinke (1977).

| i | v = 0 | v = 1 | v = 2 | v = 3 | v = 4 | v = 5 | v = 6 |
|---|---|---|---|---|---|---|---|
| 0 | 0.98924 | -0.13199 | 0.02928 | -0.03512 | 0.03022 | -0.02126 | 0.01426 |
| 1 | 0.14160 | 0.91099 | -0.34437 | 0.11093 | -0.07474 | 0.06783 | -0.05556 |
| 2 | -0.00421 | 0.37450 | 0.67933 | -0.51369 | 0.24862 | -0.14282 | 0.11137 |
| 3 | 0.03460 | 0.06605 | 0.57768 | 0.26929 | -0.50248 | 0.37348 | -0.23332 |
| 4 | 0.01112 | 0.07537 | 0.21227 | 0.60622 | -0.20469 | -0.23465 | 0.34202 |
| 5 | -0.00047 | 0.04585 | 0.14929 | 0.36869 | 0.36577 | -0.49440 | 0.17604 |
| 6 | 0.00266 | 0.01193 | 0.11484 | 0.25262 | 0.39956 | -0.05132 | -0.38364 |
| 7 | 0.00130 | 0.00918 | 0.05492 | 0.21649 | 0.32015 | 0.21168 | -0.34572 |
| 8 | -0.00006 | 0.00666 | 0.03190 | 0.14259 | 0.30800 | 0.24808 | -0.09666 |
| 9 | 0.00027 | 0.00217 | 0.02320 | 0.08986 | 0.25168 | 0.29905 | 0.03075 |
| 10 | 0.00019 | 0.00137 | 0.01262 | 0.06508 | 0.18779 | 0.31351 | 0.11111 |
| 11 | -0.00001 | 0.00111 | 0.00713 | 0.04374 | 0.14519 | 0.28292 | 0.24079 |
| 12 | 0.00003 | 0.00042 | 0.00500 | 0.02754 | 0.10864 | 0.23235 | 0.22695 |
| 13 | 0.00003 | 0.00024 | 0.00297 | 0.01920 | 0.08017 | 0.21120 | 0.31950 |
| 14 | 0.0 | 0.00020 | 0.00165 | 0.01253 | 0.05454 | 0.14742 | 0.18046 |
| 15 | 0.0 | 0.00009 | 0.00118 | 0.00858 | 0.04404 | 0.14298 | 0.32688 |
| 16 | 0.00001 | 0.00004 | 0.00068 | 0.00504 | 0.02542 | 0.07681 | 0.09873 |
| 17 | 0.0 | 0.00004 | 0.00043 | 0.00403 | 0.02301 | 0.09175 | 0.28077 |
| 18 | 0.0 | 0.00002 | 0.00022 | 0.00173 | 0.00935 | 0.02699 | 0.00861 |
| 19 | 0.0 | 0.00001 | 0.00018 | 0.00168 | 0.01132 | 0.05487 | 0.23006 |

eigenvalues are given by (Mies 1964)

$$V^{MO}(r) = D\left[ e^{-\phi(r-r_e)} - 1 \right]^2 \qquad \text{V.3.10a}$$

$$\phi_v^{MO}(r) = A_v y^{-1/2} W_{\Sigma/2, \Sigma/2 - 1/2 - v}(y) \qquad \text{V.3.10b}$$

$$\varepsilon_v^{MO} = \frac{4D}{\Sigma}\left\{ (v+1/2) - \frac{1}{\Sigma}(v+1/2)^2 \right\} \qquad \text{V.3.10c}$$

D, $\phi$ and $r_e$ are parameters of the potential chosen to approximate $V^{MO}$ as $V_{H_2}$ and

$$y = \Sigma e^{-\phi(r-r_e)} \qquad A_v^2 = \frac{\Sigma - 1 - 2v}{v!\,\Gamma(\Sigma - v)}$$

$$\Sigma^2 = \frac{8\mu_{H_2} D}{\phi^2}$$

and $W_{\Sigma/2, \Sigma/2 - 1/2 - v}(y)$ is a Whittaker function (Abramowitz and Stegun (1965)), the existence of which requires that $2v < \Sigma - 1$, which determines the number of bound states. D and $r_e$ were chosen to agree with the well depth and equilibrium separation of $V_{H_2}$; D = 0.17449, $r_e$ = 1.40083 (in a.u.). The remaining parameter, $\phi$ , was chosen by fitting the Morse eigenvalues to Schinke's energy levels. Although Schinke's expansion is incorrect, the lower eigenvalues would be expected to be close to their true values. A linear least squares fit of $\varepsilon_v^{Ex}/(v+\frac{1}{2})$ versus $(v + \frac{1}{2})$ was employed to obtain a gradient of $-4D/\Sigma^2$ and intercept $4D/\Sigma$ . Only the lower eigenvalues of Schinke were used ($\varepsilon_v^{Ex}$, v=0,1,2,3) since not only are the higher values suspect, but also because the lower wavefunctions are the ones of main interest. This gives a value of $\Sigma$ of 36.16 (dimensionless).

Employing a fit of $\mathcal{E}_v^{EK}$, v=0,1,2 and v=0,1,2,3,4 gave the values of $\sum$ = 35.44 and 37.62 respectively. However, $\sum$ can vary substantially without significantly effecting the form of $\phi_v^{MO}$ since it is a relatively small anharmonicity correction. The value of the reduced mass used by Schinke was $\mu_{H_2}$ = 918.07576 a.u. (private communication). Combining this with $\sum$ = 36.16 gives a value of $\phi$ = 0.9900134 a.u. It may seem unnecessary to specify $\phi$ to so many figures since the value of $\sum$ is only specified to four. However this is required to ensure that the parameters used in $\phi_v^{MO}$ are self consistent and maintain the orthonormality of the wavefunctions. This is extremely important since the calculation of Morse wavefunctions involves very large and very small numbers. For example $\Gamma(\sum) \sim 10^{38}$ and there is also a double exponentiation, $\exp(-\frac{1}{2}\sum e^{-\phi(r-r_e)})$.

In summary, the vibrational basis functions employed in the present calculation were Morse oscillator wavefunctions defined by V.3.10b with (in atomic units) D = 0.17449, $r_e$ = 1.40083, $\phi$ = 0.9900134, $\mu_{H_2}$ = 918.07576 and $\sum$ = 36.16. A comparison between these Morse wavefunctions and Schinke's wavefunctions is shown in figure 3. As can be seen, the Morse wavefunctions are very close to Schinke's "exact" wavefunctions but without the unphysical behaviour at high vibrational quantum numbers.

## 4. Numerical Details

Both the calculations of Schinke and McGuire (1978b) (hereafter referred to as SM) employing the GG potential, and those of SDL, employing the SDL potential, are compared with the experimental data of Hermann et al. (1978) for transitions from the ground vibrational state v = 0 to $v' = 0,1,2,3$ for E = 10 eV. Therefore, we chose to investigate the accuracy of the results of SM only for these transitions. SM report values of fixed angle S-matrix elements, $S^{L}_{0v'}(\gamma)$, as a function of angle for v' = 0,1 and L = 25,50,75 and 100 at E = 10 eV. Our preliminary calculations involved reproducing these results to verify that we had described the system accurately.

SM retained seven vibrational states in the fixed angle coupled equations, which were solved by the de Vogelaere method. The potential matrix elements were evaluated by a 28-point Gauss Legendre quadrature over the range $0.2 < r < 3.0$ a.u. As can be seen from figure 3, this restriction of $r > 0.2$ a.u. will help reduce the effect of the error in the vibrational wavefunctions. The values of $S^{L}_{0v'}(\gamma)$ obtained by SM are reproduced in figure 4.

In the present calculations the coupled equations were solved by the R-matrix propagator method employing propagators corresponding to a constant reference potential (see Chapter III). In keeping with SM, seven vibrational states were retained, Schinke's harmonic oscillator expansion (HOEX) wavefunctions and eigenvalues were used, and the potential matrix elements were evaluated in an identical manner. The reduced mass of the system was taken to be

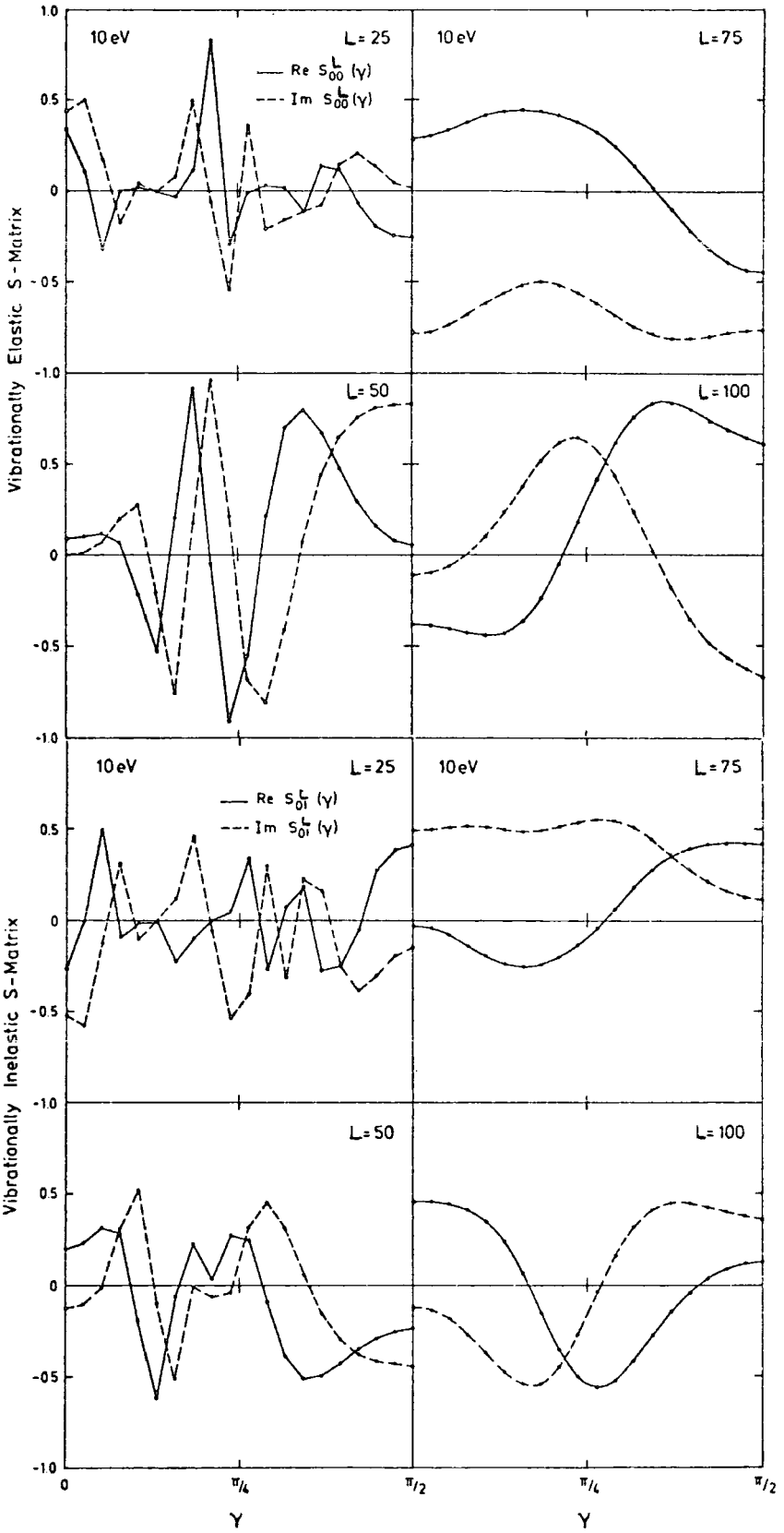


Figure 4 Results of Schinke and McGuire (1978b) of fixed angle S-matrix elements, $S^L_{0v'}(\gamma)$, as a function of $\gamma$ for v' = 0,1 and L = 25,50,75 and 100 at E = 10eV, calculated employing vibrational basis wavefunction of Schinke (1977). Real part of S-matrix, full line : Imaginary part of S-matrix, broken line.

$\mu$ = 1224.101013 a.u. as employed by SM (Schinke-private communication). After some experimentation, it was established that an integration range of $0.15 < R < 30.0$ a.u., involving $\sim$ 3000 steps of fixed length, was required to maintain the accuracy of the S-matrix elements to < 1%. In the case of very small ($< 10^{-3}$) elements, the relative error sometimes reached 10% at most. However, such small S-matrix elements represent only a small contribution to the final cross section and are therefore relatively unimportant. Using this integration range and step size, the calculation of fixed angle S-matrices required $\sim$ 100 s per orientation on the NUMAC IBM 370/168.

At this point it is convenient to introduce the notation $^{HX}S^{L}_{0v'}(\gamma)$ for S-matrix element calculated using HOEX wavefunctions, and $^{MO}S^{L}_{0v'}(\gamma)$ for elements calculated using Morse oscillator (MO) wavefunctions with parameters as detailed in Section 3. Values of $^{HX}S^{L}_{0v'}(\gamma)$ as a function of $\gamma$ for v' = 0,1 and L = 25,50,75 and 100 obtained by the present calculations are presented in figure 5. As can be seen, the agreement with the results of SM is very good, except at two values of $\gamma$ for L = 25. It appears that both the real and imaginary parts of $^{HX}S^{25}_{00}$ ($\gamma = 56.84^{\circ}$) and $^{HX}S^{25}_{01}$ ($\gamma = 42.63^{\circ}$) have opposite signs from the results of SM. This type of discrepancy does not appear for L = 50, 75 or 100, where the angle dependence of the S-matrix elements is not as strong. The real part of the S-matrix element is much smaller than the imaginary part at these two points and therefore the phase is close to an odd multiple of $\pi/2$. However, this is not unusual, and if the phase of our S-matrix disagreed with that of SM only in sign, this would

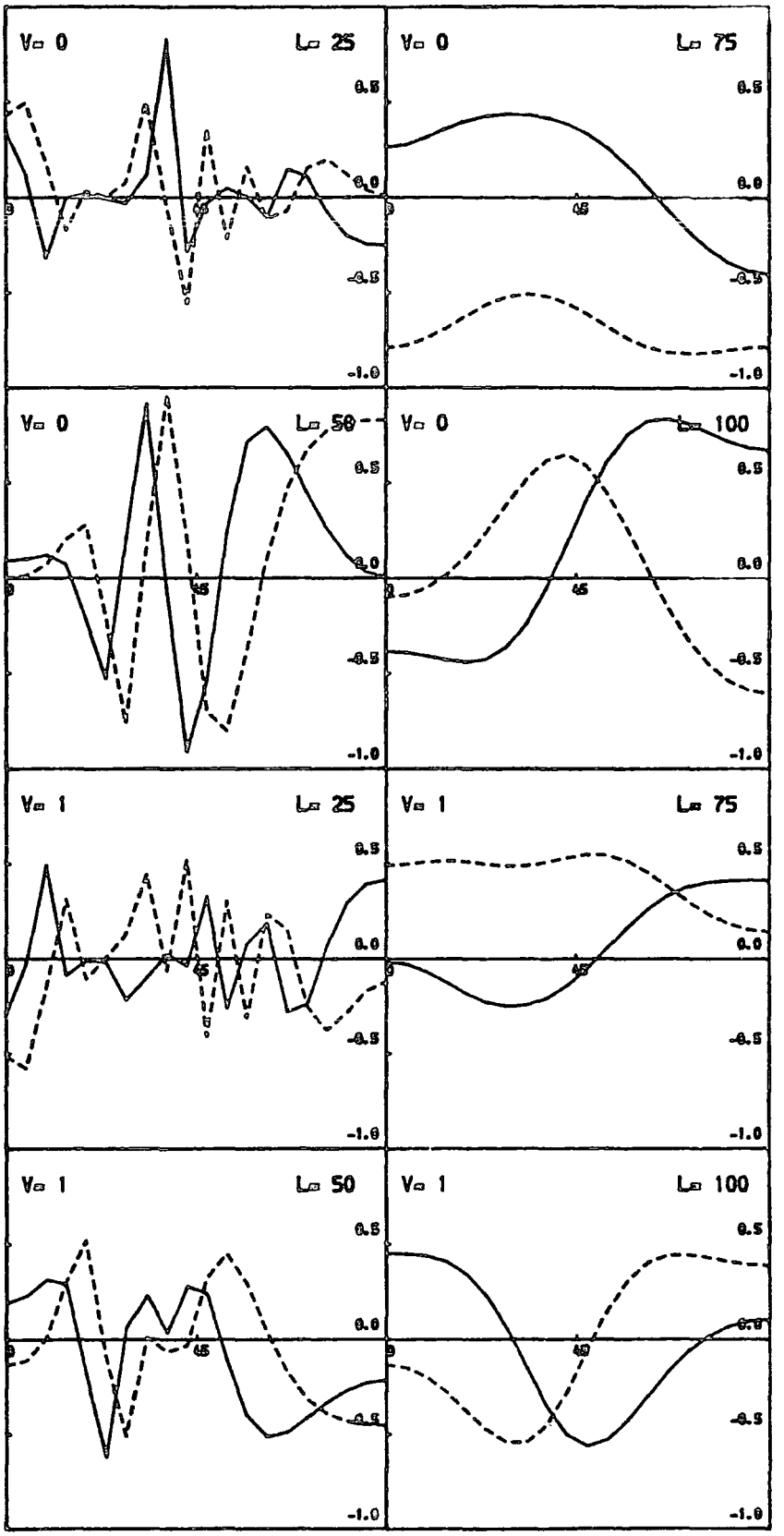


Figure 5 Results of present calculations of $S^{L}_{0v'}(\gamma)$, as a function of $\gamma$ for v' = 0,1 and L = 25,50,75 and 100 at E = 10 eV employing the vibrational basis wavefunctions of Schinke (1977). Real part of S-matrix, full line : Imaginary part of S-matrix, broken line.

change the sign of only the imaginary part. Since such discrepancies exist at only two, apparently arbitrary, points it is possible that they are merely typographical errors in the paper of SM.

There are other slight discrepancies between ${}^{HX}S^{L}_{0v'}(\gamma)$ and the results of SM. The most obvious is for $Re\left\{{}^{HX}S^{0v}_{00}(\gamma)\right\}$ at high values of $\gamma$, where the results of the present calculations are slightly lower than those of SM. In view of this, further numerical checks were performed for L = 50 at high values of $\gamma$ and the present results found to be accurate. However, we are principally concerned with the effect of the errors in the HOEX wavefunctions. For this purpose, the small discrepancies between the present ${}^{HX}S^{L}_{0v'}(\gamma)$ results and those of SM will be unimportant. The good overall agreement with the results of SM suggests that our description of the system and our numerical methods are accurate. (The accuracy and reliability of our R-matrix propagator program has been discussed in Chapter IV).

The amplitude of the MO wavefunctions is significant over a slightly different range of r (the internuclear coordinate of the $H_2$ molecule) than the HOEX wavefunctions for high vibrational states (figure 3). Therefore, potential matrix elements involving MO wavefunctions were evaluated numerically over the range $0.6 < r < 3.4$ a.u., compared to $0.2 < r < 3.0$ a.u. used with HOEX wavefunctions. Again, a 28-point Gauss Legendre quadrature was used, so as not to obscure the comparison between ${}^{HX}S^{L}_{0v'}(\gamma)$ and ${}^{MO}S^{L}_{0v'}(\gamma)$ by altering the accuracy of the matrix elements, which is

discussed later. Also, the integration ranges are both equal (= 2.8 a.u.) to maintain a similar density of quadrature points.

The vibrational energy levels enter into the coupled equations only in the wavevectors $k_v$. Since the total energy is so high, the small discrepancies between the HOEX and MO eigenvalues will have a relatively small effect. However, to obtain the best possible comparison between ${}^{HX}S^{L}_{0v'}(\gamma)$ and ${}^{MO}S^{L}_{0v'}(\gamma)$, the HOEX eigenvalues were employed in the calculation of ${}^{MO}S^{L}_{0v'}(\gamma)$ rather than the MO eigenvalues.

Values of ${}^{MO}S^{L}_{0v'}(\gamma)$ (i.e. calculated using MO wavefunctions) as a function of angle for v' = 0,1 and L = 25,50,75 and 100 are presented in figure 6. The overall agreement between ${}^{MO}S^{L}_{0v'}(\gamma)$ and ${}^{HX}S^{L}_{0v'}(\gamma)$ is quite good although there are some significant discrepancies, for example for L = 50, v' = 0 and L = 75, v' = 0 at high values of $\gamma$, and L = 25, v' = 0 and L = 75 v' = 1 at low values of $\gamma$. The discrepancies between the present results and those of SM for $S^{50}_{00}(\gamma = 56.84^{\circ})$ and $S^{25}_{01}$ ($\gamma$ = $42.63^{\circ}$) remain, adding weight to the argument that this is due to typographical errors in the paper of SM.

Table 2 contains a comparison of potential matrix elements $V_{0v'}(R, \gamma)$ using HOEX wavefunctions, for $\gamma = \pi/2$ v' = 0 to 6 and R = 3,12 and 21 a.u. calculated by 28, 32, 40 and 64-point Gauss Legendre quadratures over the range $0.2 < r < 3.0$ a.u. A 28-point quadrature, as employed by SM, is sufficient for the matrix elements of most interest ($v' \leqslant 3$). The one major exception is $V_{03}(R = 3, \pi/2)$, which is relatively small although the interaction potential

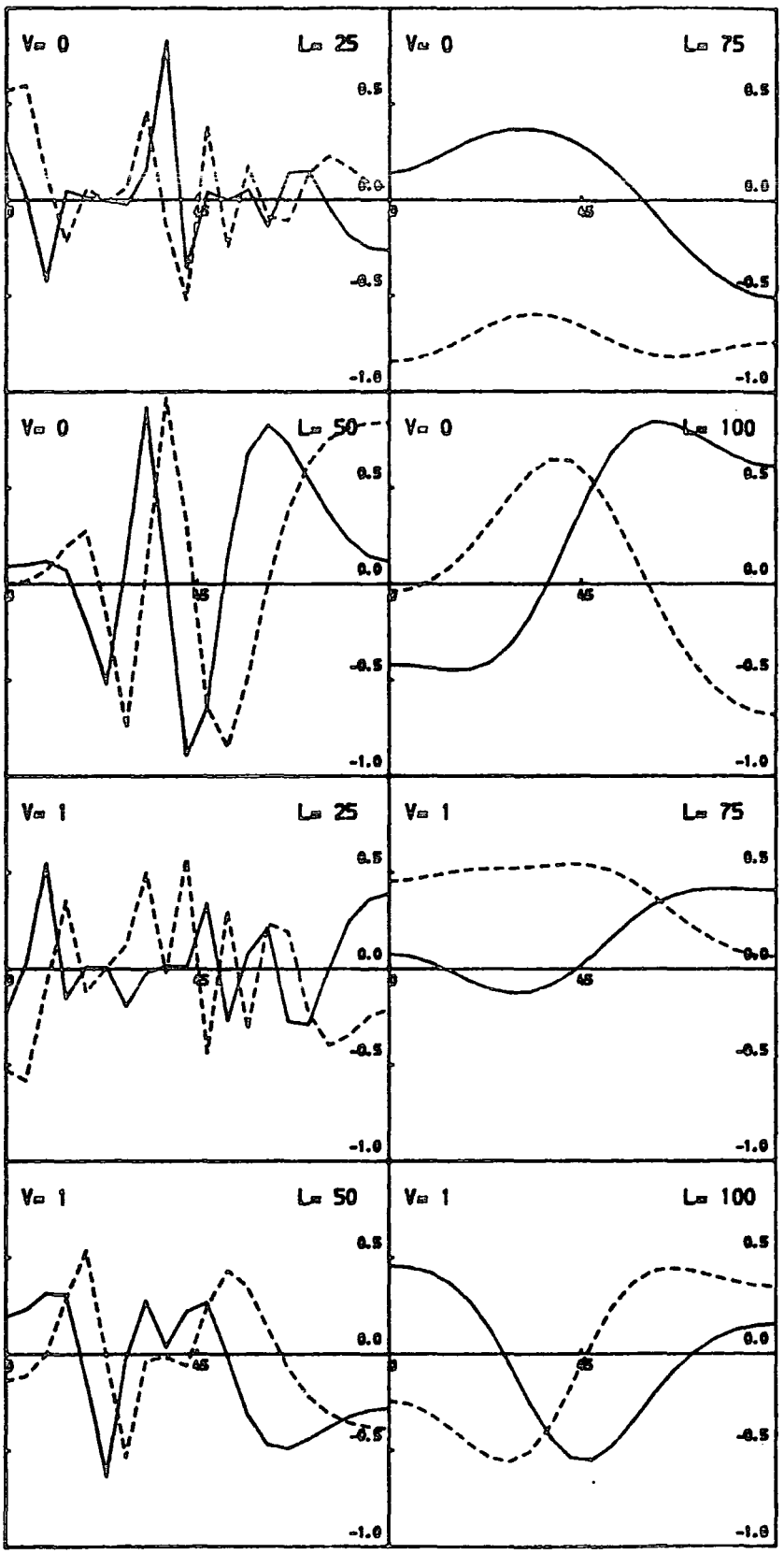


Figure 6 Results of present calculations of $S^{L}_{0v'}(\gamma)$, as a function of $\gamma$ for v' = 0,1 and L = 25,50,75 and 100 at E = 10 eV employing Morse oscillator wave-functions. Real part of S-matrix, full line : Imaginary part of S-matrix, broken line.

Table 2 Values of $V_{0v'}(R, \gamma = \pi/2)$ using HOEX wavefunctions, calculated by N-point Gauss Legendre quadrature. (a) N = 28, (b) N = 32, (c) N = 40, (d) N = 64.

| R(a.u.) | v' = 0 | 1 | 2 | 3 | 4 | 5 | 6 |
|---|---|---|---|---|---|---|---|
| 3 | (a)-0.66356271-1 | -0.81544933-2 | 0.10297962-2 | 0.90110097-5 | -0.14544774-3 | 0.12458966-3 | -0.14296324-3 |
| | (b)-0.66356273-1 | -0.81544896-2 | 0.10298287-2 | 0.93180129-5 | -0.14343215-3 | 0.13437048-3 | -0.10351576-3 |
| | (c) " | -0.81544897-2 | 0.10298284-2 | 0.93217099-5 | -0.14339751-3 | 0.13458769-3 | -0.10229989-3 |
| | (d) " | " | " | 0.93217069-5 | -0.14339753-3 | 0.13458761-3 | -0.10230013-3 |
| 12 | -0.17877312-3 | -0.63644550-4 | 0.99360236-5 | -0.19550004-5 | 0.41300750-6 | -0.59945810-7 | -0.12138375-6 |
| | " | -0.63644536-4 | 0.99361136-5 | -0.19541612-5 | 0.41794752-6 | -0.39470971-7 | -0.65210111-7 |
| | " | " | 0.99361172-5 | -0.19541359-5 | 0.41814683-6 | -0.38417857-7 | -0.60221551-7 |
| | " | " | " | " | 0.41814679-6 | -0.38417974-7 | -0.60221577-7 |
| 21 | -0.35323621-4 | -0.69829369-5 | 0.96291168-6 | -0.17082223-6 | 0.37054339-7 | -0.11865622-7 | -0.14672449-7 |
| | -0.35323622-4 | -0.69829350-5 | 0.96292682-6 | -0.17068480-6 | 0.37924655-7 | -0.79082398-8 | -0.62838157-9 |
| | " | " | 0.96292725-6 | -0.17068201-6 | 0.37947698-7 | -0.77786991-8 | 0.26030855-10 |
| | " | " | " | " | 0.37947690-7 | -0.77787266-8 | 0.25974401-10 |

is large at such small values of R. Therefore, there must be cancellation occurring in the integral and a 28-point quadrature is unable to maintain accuracy. SM report that seven vibrational states must be included to obtain reliable cross sections for $\Delta v \lesssim 3$ transitions and therefore the accuracy of high v matrix elements must also be considered. As can be seen in Table 2, a 28-point quadrature can fail badly for small matrix elements with a highly oscillatory integrand, such as $V_{06}$ $(R = 21, \pi/2)$.

The calculation of the potential matrix elements accounts for a large percentage of the total calculation ( $\sim 50\%$ for a 28-point quadrature) due to the awkward form of the potential as discussed in Section 2. Therefore, increasing the number of quadrature points will considerably increase the total computer time required. However, if an approximate potential algorithm is employed which can efficiently generate results for many partial waves, the evaluation of the matrix elements is required only in the calculation for the initial partial wave. The generation of results for subsequent values of L does not require any explicit reference to the potential matrix elements. Therefore the matrix elements can be calculated using a large number of quadrature points without significantly increasing the total time required. SM use de Vogelaere's method to solve the coupled equations, and therefore they must calculate the matrix elements for each partial wave.

We are primarily interested in the comparison between fixed angle S-matrix elements obtained using HOEX and MO wavefunctions. The slight discrepancies between our own

calculations using HOEX wavefunctions, and those of SM, and also the possible inaccuracy of using a 28-point quadrature, will not significantly effect this comparison. Therefore, in keeping with SM, all the results in the following Section 5 were obtained using a 28-point Gauss Legendre quadrature to evaluate the matrix elements.

## 5. Results and Discussion

As noted in Section 4, the results of interest are the cross sections for transitions from the ground vibrational state v = 0 to v' = 0,1,2,3. A comparison between ${}^{HX}S^{L}_{0v'}(\gamma)$ and ${}^{MO}S^{L}_{0v'}(\gamma)$ as functions of $\gamma$, for L = 25 and v' = 0,1,2,3 is presented in figure 7. The discrepancies are seen to increase with v', and for $v' \geqslant 2$ they are sufficiently large that the cross sections calculated from these fixed angle S-matrix elements will differ significantly. This is as expected, since the discrepancies between the HOEX and MO wavefunctions increase with the vibrational quantum number. A similar comparison for L = 50 is presented in figure 8. The agreement between ${}^{HX}S^{L}_{0v'}(\gamma)$ and ${}^{MO}S^{L}_{0v'}(\gamma)$ is seen to be good for all values of v' for L = 50. This improved agreement with larger L would be expected, since as L increases the $H^+$ does not approach as close to the $H_2$ molecule and the precise form of the vibrational wavefunctions will be relatively less important. Also, for large values of L the highly excited vibrational states will not play such a significant role. As noted by SM, the rapid oscillations in the S-matrix elements at L = 25 are a result of the large anisotropy of the $H_2 + H^+$ interaction potential at small values of R, and only for $L \geqslant 50$ do the

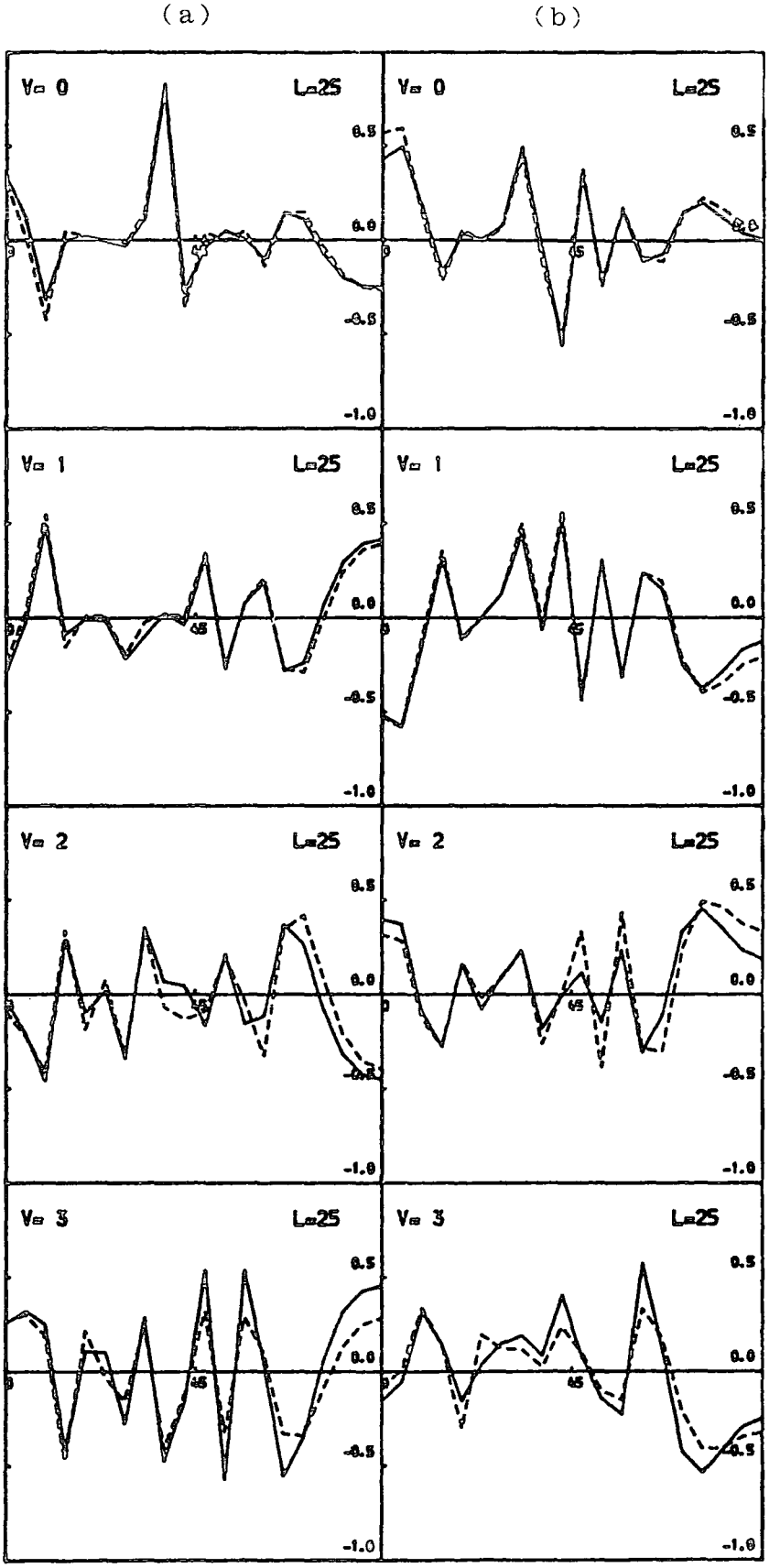


Figure 7 Comparison between $^{HX}S^{L}_{0v'}(\gamma)$ (full line) and $^{MO}S^{L}_{0v'}(\gamma)$ (broken line) as functions of $\gamma$ for L = 25 and v' = 0,1,2,3 at E = 10 eV. Column (a) real part of S-matrix : column (b) imaginary part of S-matrix.

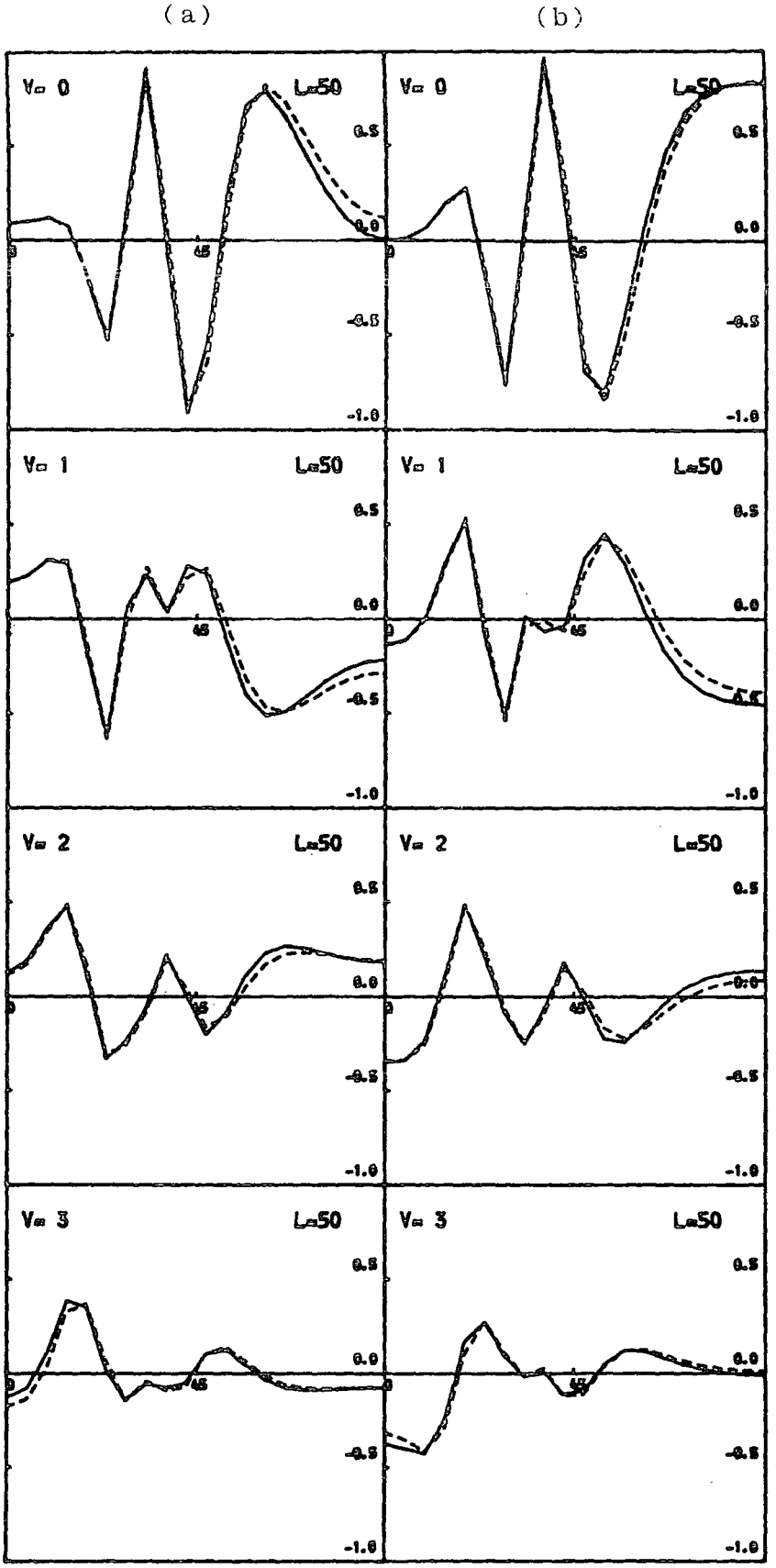


Figure 8 Comparison between $^{HX}S^{L}_{0v'}(\gamma)$ (full line) and $^{MO}S^{L}_{0v'}(\gamma)$ (broken line) as functions of $\gamma$ for L = 50 and v' = 0,1,2,3 at E = 10eV column (a), real part of S-matrix: column (b), imaginary part of S-matrix.

curves begin to take on a regular oscillatory structure. For L > 60, only the $P_o$ and $P_2$ terms of a Legendre expansion of the potential surface (McGuire (1976)) remain and the S-matrix elements become a smoother function of the orientation.

SM report plots of $\left|S^L_{0v'}(\gamma)\right|^2$ versus L at E = 10 eV for $\gamma$ = 0°, 51.43° and 90°, and v' = 1,2. These results are reproduced in figure 9. To obtain cross sections, the fixed angle S-matrix elements are multiplied by spherical harmonics and integrated over $\gamma$ (Chapter II.3(c)). Due to the $\sin\gamma$ weighting in this integral, the most important contributions to the cross sections are from high values of $\gamma$. Consider $\left|S^L_{02}(\gamma)\right|^2$. For $\gamma$ = 90° the major contribution to $\sigma$(v = 0 → v' = 2) will come from L < 50. Similarly for $\gamma$ = 51.43°, a large contribution comes from L < 50. Although $\left|S^L_{02}(\gamma)\right|^2$ is large for L > 50 at $\gamma$ = 0°, the $\sin\gamma$ weighting in the integral will make this a small contribution to the cross section. (Indeed for $\gamma$ = 0°, the contribution will be zero, but at $\gamma \gtrsim 0°$ the S-matrix elements would be expected to have a similar distribution amongst L). Therefore the major contribution to $\sigma$(v = 0 → v' = 2) comes from partial waves with L < 50. However, as demonstrated by figure 7, there are significant discrepancies between $^{HX}S^L_{02}(\gamma)$ and $^{MO}S^L_{02}(\gamma)$ for L = 25. Therefore cross sections between v = 0 and v' = 2 calculated using HOEX wavefunctions would be expected to differ significantly from the corresponding results calculated employing MO wavefunctions.

Although $\left|S^L_{03}(\gamma)\right|^2$ is not shown, it would be expected that it is largest for smaller values of L than $\left|S^L_{02}(\gamma)\right|^2$, since the $H^+$ must approach closer to $H_2$ to excite the higher v = 3 vibrational state. Also the discrepancies between

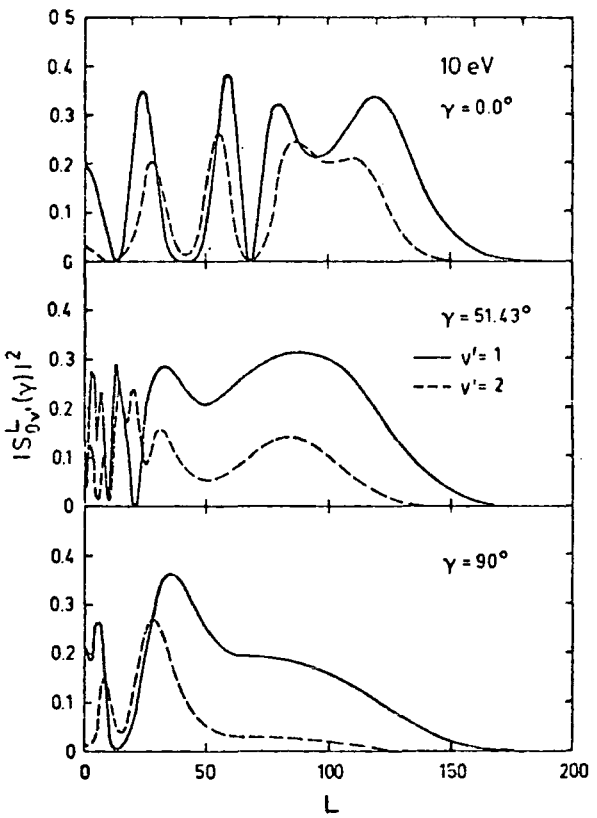


Figure 9 Results of Schinke and McGuire (1978b) of $|^{HX}S^L_{0v'}(\gamma)|^2$ versus L at E = 10 eV for $\gamma$ = 0°, 51.43° and 90°, and v' = 1 (full line) and v' = 2 (broken line).

$^{HX}S^{L}_{0v'}(\gamma)$ and $^{MO}S^{L}_{0v'}(\gamma)$ increase with v'. Therefore the values of cross sections for transitions between v = 0 and v' = 3 will differ considerably depending on whether MO or HOEX wavefunctions are employed.

Comparisons between $^{HX}S^{L}_{0v'}(\gamma)$ and $^{MO}S^{L}_{0v'}(\gamma)$ for v' = 0,1,2,3 for L = 75 and 100 are presented in figures 10 and 11 respectively. For L = 75 there are significant discrepancies for all v', including the elastic v' = 0. Also, for v' = 0,1 there are large discrepancies at high values of $\gamma$, i.e. the region which represents the dominant contribution to the corresponding cross sections. There are also significant discrepancies between $^{HX}S^{100}_{0v'}(\gamma)$ and $^{MO}S^{100}_{0v'}(\gamma)$. However they are relatively small for v' = 0, and for v' = 1,2,3 they are present mainly at low values of $\gamma$. This poor agreement is contrary to the previous agrument that the importance of the exact form of the vibrational wavefunctions, and the effect of the highly excited states are reduced at high values of L. It is generally found that the inclusion of highly excited states in calculations for high partial waves is not necessary. Indeed, SM include only five, rather than seven vibrational states at higher partial waves (although "higher" is not defined) and at even higher values of L consider the vibrational coupling to be negligible and employ WKB phase shifts to determine the vibrationally elastic S-matrix elements. Also, for low values of the vibrational quantum number the HOEX and MO wavefunctions are very similar. The good agreement between the present values of $^{HX}S^{L}_{0v'}(\gamma)$ (figure 5) and the results of SM (figure 4) would tend to rule out the deterioration of our numerical accuracy with

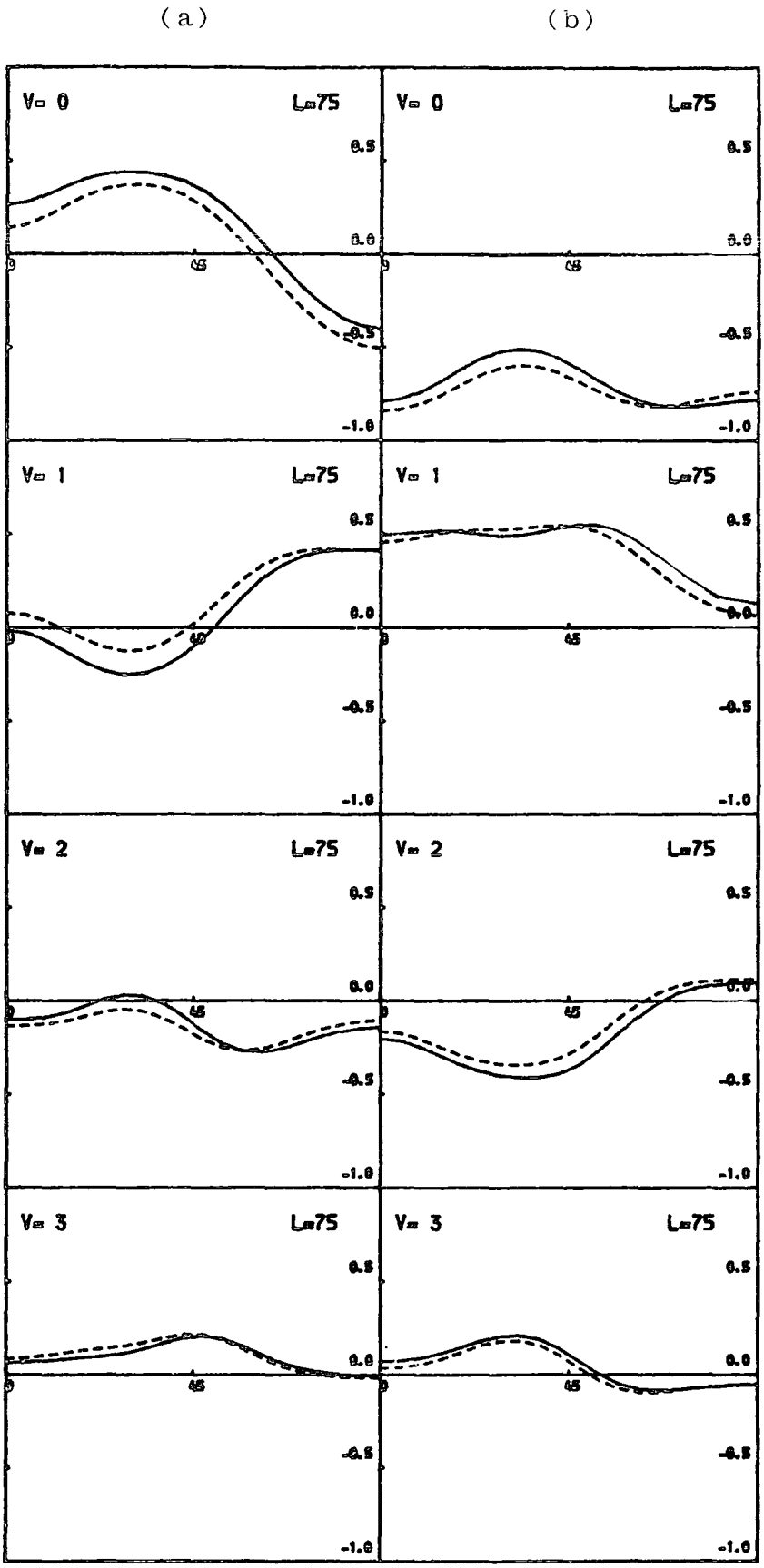


Figure 10 Comparison between $^{HX}S^{L}_{0v}(\gamma)$ (full line) and $^{MO}S^{L}_{0v}(\gamma)$ (broken line) as functions of $\gamma$ for L = 75 and v' = 0,1,2,3 at E = 10 eV. Column (a) real part of S-matrix: column (b), imaginary part of S-matrix.

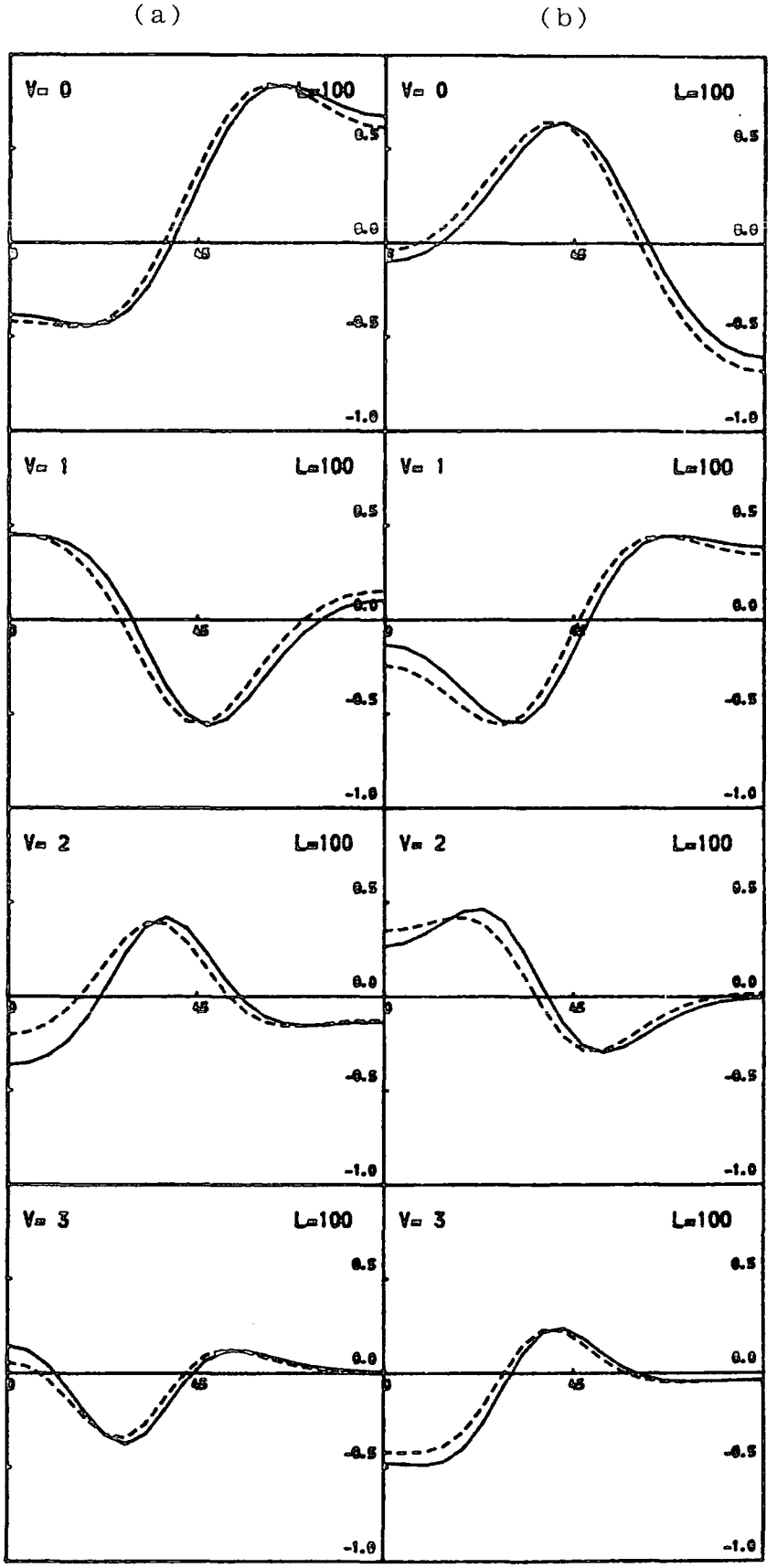


Figure 11 Comparison between $^{HX}S^{L}_{Ov}(\gamma)$ (full line) and $^{MC}S^{L}_{Ov}(\gamma)$ (broken line) as functions of $\gamma$ for L = 100 and v' = 0,1,2,3 at E = 10 eV. Column (a), real part of S-matrix: column (b), imaginary part of S-matrix.

increasing L. If such numerical problems were developing we would also expect the comparison between $^{HX}S^{L}_{0v'}(\gamma)$ and $^{MO}S^{L}_{0v'}(\gamma)$ to be significantly poorer at L = 100 than at L = 75, which is not the case. It therefore appears that the fixed angle S-matrices for L = 75 and 100 are genuinely sensitive to the exact form of the vibrational wavefunctions.

Schinke (1980) has shown that partial cross sections with $L \simeq 75$ are extremely sensitive to the form of the interaction potential. For example a plot of the vibrationally elastic partial cross section $\sigma^{L}(01\rightarrow07)$ against L at E = 4.67 eV has a large maximum at $L \simeq 75$ when the GG potential is employed. However, when the SDL potential is employed this maximum is reduced by a factor of $\gtrsim 10$. This is due to the fact that partial waves with $L \simeq 75$ sample a broad shallow well in the $P_2$ anisotropy of the interaction potential and produce a rainbow maximum in the total differential cross section. Partial waves with $L \simeq 100$ will also sample this critical region of the potential. Since the same vibrational energy levels have been used, the form of the wavefunctions and potential enter into the calculation only in the matrix elements. Therefore the use of inaccurate basis functions and an accurate potential will have a similar effect as employing accurate basis functions and an inaccurate potential. Schinke (1980) has demonstrated that a poor description of the interaction potential has a large effect for partial waves with $L \simeq 75$. It is therefore not surprising that there are significant discrepancies between $^{HX}S^{L}_{0v'}(\gamma)$ and $^{MO}S^{L}_{0v'}(\gamma)$ for L =75, 100. As can be seen from figure 9 the total cross sections for transitions

between v = 0 and v' = 1 contain a large contribution from partial waves with L > 50. The vibrationally elastic cross sections with v = v' = 0 would be expected to have a similar, or perhaps larger, contribution from high partial waves. Therefore we would expect significant differences between such rovibrational cross sections calculated employing HOEX wavefunctions, and the corresponding values calculated using MO functions.

The present conclusions have been drawn from the results of calculations employing the GG potential. Although the potential of SDL is certainly more accurate, it is qualitatively similar to the GG potential and it is therefore probable that the same conclusions would have been reached if the SDL potential had been employed. The present results suggest that all the rovibrational cross sections will be sensitive to the precise form of the vibrational wavefunctions. However, it is not clear whether the HOEX or MO wavefunctions provide the better description. Although the HOEX wavefunctions have faults, they may still be the more accurate description of the isolated $H_2$ molecule.

SM compare their calculations with the experimental data of Hermann et al. (1978) in terms of the angle dependent probabilities for vibrational transitions v = 0 $\rightarrow$ v' = 1,2,3, defined as

$$P^{v'}(\theta) = \left[\sum_{j'} \frac{d\sigma}{d\Omega}(v_j \rightarrow v'j')\right]\left[\sum_{v''}\sum_{j''} \frac{d\sigma}{d\Omega}(v_j \rightarrow v''j'')\right]^{-1} \qquad \text{V.5.1}$$

Employing the GG potential, the theoretical values of this quantity are smaller than the experimental results for all v' = 1,2,3. When the more accurate potential is employed by SDL, the theoretical values are found to be in "excellent" agreement with experiment for v' = 1,2. (The comparison for v' = 3 is not considered significant due to the small size of the transition probabilities and the associated experimental difficulties). This would appear to suggest that the HOEX wavefunctions, despite their faults, are a sufficiently accurate description of the $H_2$ molecule. However, in coupled states calculations of rovibrational excitation of $H_2$ by He, Alexander and McGuire (1976) note that the use of MO, rather than harmonic oscillator wavefunctions produces large changes in individual rovibrational cross sections, yet produces relatively small changes in rotationally summed cross sections (Chapter IV.4). This may also be true for $H_2 + H^+$, and the angle dependent transition probabilities for vibrational excitation (V.5.1) may be insensitive to the form of the vibrational wavefunctions.

This argument is strengthened by the IOS results of Schinke (1980), using HOEX wavefunctions and the SDL potential, for E = 4.67 eV. It is reported that the individual transition probabilities, defined by

$$P^{v'}(j \to j';\theta) = \left[\frac{d\sigma}{d\Omega}(o_j \to v'j')\right]\left[\sum_{j''}\frac{d\sigma}{d\Omega}(o_j \to v'j'')\right]^{-1} \qquad \text{V.5.2}$$

are "significantly below" the experimental values over the entire range of scattering angles considered for v' = 0, j = 1 and j' = 3,5,7. Note that this is a vibrationally

elastic transition. Unfortunately there are no similar comparisons with experiment for vibrationally inelastic transitions.

$H_2 + H^+$ is a very simple, two electron system and the configuration interaction calculations of SDL employ a large atomic basis set and configuration basis, and cover an extensive range of nuclear geometries, specifically chosen to produce an accurate potential for use in calculations of rovibrational excitation. With such an accurate potential, it is perhaps disappointing that the IOS calculations of Schinke (1980) are not in better agreement with experiment. As emphasised by Schinke, the IOS approximation should be accurate for E = 4.67 eV and he postulates that the disagreement between theory and experiment may be due to deficiencies in the experimental data. One of the main advantages of the SDL potential is that it is, by design, much more accurate than the GG potential for small values of r, the internuclear $H_2$ co-ordinate. There are large differences between the GG and SDL potentials in this region. (This is discussed in detail by SDL). This suggests that the HOEX wavefunctions calculated from the GG potential may be unsuitable for use with the SDL interaction potential. Therefore, although the SDL potential is certainly accurate and the IOS approximation valid, the comparison between theory and experiment presented by Schinke (1980) may be degraded by employing HOEX wavefunctions, not only because of the errors present in them, but also because they have been calculated from the less accurate GG potential.

There are two main possible sources of numerical error in the IOS calculations of SDL and Schinke (1980), which both employ the SDL potential. The present calculations using different wavefunctions differ only in the values of the potential matrix elements, since identical vibrational energy levels are used. The HOEX and MO wavefunctions are very similar, yet still produce significant discrepancies between $^{HX}S^{L}_{0v'}(\gamma)$ and $^{MO}S^{L}_{0v'}(\gamma)$. Therefore, it is possible that the relatively low accuracy of the matrix elements evaluated by a 28-point Gauss Legendre quadrature, could produce significant numerical errors in the angle fixed S-matrices. Also, SDL and Schinke (1980) calculate fixed angle S-matrices at twelve equally spaced orientations. This was not considered completely satisfactory, but was the maximum practicable due to the large amount of computer time required. However, for partial waves with $L < 50$, the fixed angle S-matrices are highly oscillatory functions of the orientation angle, $\gamma$. This is demonstrated in figure 7 for the GG potential and will certainly also be true when the SDL potential is employed. It is probable that twelve orientations will be insufficient to give an accurate integration of these S-matrix elements over $\gamma$, especially for IOS transitions involving high rotor states, j, where the elements are multiplied by a highly oscillatory $Y_{j0}(\gamma,0)$ in the integrand.

The results and discussion presented in this Chapter are preliminary and inconclusive. For example, it is not obvious what effect differences in fixed angle S-matrices will have on cross sections. Perhaps the integration over

orientation will produce cross sections which are less sensitive than the fixed angle S-matrices to the form of the vibrational wavefunctions. Despite such uncertainties and speculations, we believe that there is sufficient evidence to consider that the comparison between theoretical and experimental values of rovibrational cross sections presented by SDL and Schinke (1980) may be misleading, due to the use of HOEX wavefunctions and the restrictions imposed on their numerical techniques by the large amount of computer time required for the calculation.

In view of the highly refined experimental data (Hermann et al. (1978)) and accurate interaction potential (SDL) available, we consider it worthwhile to pursue this problem further. Additional calculations required to resolve the apparent discrepancies between theoretical and experimental values of rovibrational cross sections for the $H_2 + H^+$ system are discussed in Chapter VI.

# CHAPTER VI

# FUTURE WORK

The main results contained in this thesis are the close coupling (CC) and infinite order sudden (IOS) approximation calculations of rovibrational excitation of $H_2$ by He (Chapter IV). Due to the relatively poor description of the system employed (principally the inaccuracy of the interaction potential of Gordon and Secrest (1970)), the agreement between the values of the vibrational relaxation rate computed from the present CC cross sections, and the experimental values of Audibert et al. (1976) is poor. However, the main value of the CC calculations is as "benchmark" results with which to compare approximation schemes and energy sudden factorisations. In this context, the set of CC results is essentially complete, although rovibrational cross sections for ortho $H_2$ + He at another energy may be of value. Such results would further test proposed energy sudden factorisation schemes and also their energy range of validity.

In contrast to the calculations for $H_2$ + He, the calculations for $H_2$ + $H^+$ are preliminary and incomplete (Chapter V). However, the results suggest that the comparison between theory and experiment reported by Schinke (1980) may be false. There are two courses of action which can be pursued to attempt to resolve the apparent discrepancies between theoretical and experimental values of rovibrational cross sections. The first is to continue with the philosophy of Chapter V by determining to what extent the

restricted numerical methods and inaccurate wavefunctions employed by Schinke et al. (1980) and Schinke (1980) effect the accuracy of their calculated cross sections. By precisely establishing the errors produced in the cross sections it would be possible to determine whether the inaccurate wavefunctions or numerical techniques are responsible for the discrepancies with experiment. The second course of action is to perform full IOS calculations for $H_2 + H^+$ employing accurate numerical techniques, interaction potential and vibrational basis states, and compare directly with the experimental data. This would be an extremely expensive task computationally, but would be required anyway if the former approach revealed significant errors in the cross sections. This would entail performing IOS calculations with highly accurate matrix elements and a large number of orientations. The optimum choice of interaction potential is certainly that of Schinke et al. (1980). The choice of vibrational basis states is not so clear cut, however the bound state wavefunctions calculated by Lester and Schaefer (1973) from the isolated $H_2$ potential of Kolos and Wolniewicz (1965) are probably a good choice.

The $H_2$ + He interaction potential of Gordon and Secrest (1970) is purely repulsive and short ranged. With this potential, the use of propagators appropriate to a constant reference potential in the R-matrix propagator method is sufficient, and there is little advantage to be gained by employing the more cumbersome Bessel function propagators (see Chapter III.4(c)). In contrast, the

$H_2 + H^+$ interaction is long ranged and has a deep well, and at the energies of interest large numbers of partial waves are required (up to 200 for E = 10 eV). Also the evaluation of the potential matrix elements is an expensive task, and it is therefore imperative that results can be generated efficiently and reliably for partial waves over a large range of L values. Therefore, the $H_2 + H^+$ system is ideally suited as a test case with which to investigate the efficiency of Bessel function propagators, and their use may provide substantial savings in computer time in IOS calculations. It is important that the efficiency of Bessel function propogators be established quantitatively and we have at our disposal an ideal test case with which to achieve this goal.

REFERENCES

Aannestad, P.A., and Field, G.B. (1973),
Astrophysical Journal letters 186, 29.

Abramowitz, M., and Stegun I.A. (1965),
Handbook of Mathematical Functions (New York : Dover).

Alexander, M.H. (1974),
J. Chem. Phys. 61, 5167.

Alexander, M.H. (1975),
Chem. Phys. 8, 86.

Alexander, M.H. (1976),
Chem. Phys. Letters 38, 417.

Alexander, M.H., and McGuire, P. (1976),
J. Chem. Phys. 64, 452.

Arthurs, A.M., and Dalgarno, A. (1960),
Proceedings of The Royal Society A256, 540.

Audibert, M.M., Joffrin, C., and Ducuing, J. (1973),
Chem. Phys. Letters 19, 26.

Audibert, M.M., Joffrin, C., and Ducuing, J., (1974)
J. Chem. Phys. 61, 4357.

Audibert, M.M., Vilaseca, R., Lukasik, J., and Ducuing J (1976),
Chem. Phys. Letters 37, 408.

Balint-Kurti, G.G., (1975),
International Review of Science, Vol. 1 of Physical Chemistry, Series II, edited by A.D. Buckingham and C.A. Coulson (London : Butterworths).

Bauschlicher, C.W., O'Neil, S.V., Preston, R.K., Shaefer, H.F., and Bender, C.F. (1973),
J. Chem. Phys. 59, 1286.

Beard, L.M., Kouri, D.J., and Hoffman, D.K. (1982),
J. Chem. Phys. 76, 3623.

Beard, L.M., and Kouri, D.J. (1982)
J. Chem. Phys. 78, 220.

Bieniek, R.J., (1980),
J. Chem. Phys. 73, 851.

Black, J.H., and Dalgarno, A. (1976),
Astrophysical Journal 203, 132.

Bowman, J.M., and Leasure, S.C. (1977),
J. Chem. Phys. 66, 288.

Bunker, D.L. (1971),
Methods in Computational Physics 10, 287.

Carney, G.D., and Porter, R.N. (1974),
J. Chem. Phys. 60, 4251.

Chase, D.M., (1956),
Physical Review 104, 838.

Chu, S.I., and Dalgarno, A. (1975a),
Proceedings of The Royal Society A342, 191.

Chu, S.I., and Dalgarno, A. (1975b),
J. Chem. Phys. 63, 2115.

Clark, A.P. (1977),
J. Phys. B. 10, L389.

Clark, A.P., Dickinson, A.S., and Richards, D. (1977),
Advances in Chemical Physics 36, 63.

Collins, L.A., and Norcross, D.W. (1978),
Physical Review A 18, 467.

Csizmadia, I.G., Kari, R.E., Polanyi, J.C., Roach, A.C.,
and Robb, M.A. (1970),
J. Chem. Phys. 52, 6205.

Dalgarno, A., and McCray, R.A., (1972),
Ann. Rev. of Astron. and Astrophys. 10, 375.

Dalgarno, A. (1975),
Atomic and Molecular Processes in Astrophysics : Course at
SAAS-FEE, edited by M.C.E. Huber and H. Nussbaumer
(Geneva : Geneva Observatory).

DePristo, A.E., and Alexander, M.H. (1975),
J. Chem. Phys. 63, 3552.

DePristo, A.E., and Alexander, M.H. (1976),
J. Chem. Phys. 64, 3009.

DePristo, A.E., Augustin, S.D., Ramaswamy, R., and Rabitz, H.
(1979).
J. Chem. Phys. 71, 850.

de Vogelaere, R. (1955),
Journal of Research of the N.B.S. 24, 119.

Dickinson, A.S. (1979),
Comp. Phys. Comm. 17, 51.

Dove, J.E., and Teitelbaum, H. (1974),
Chem. Phys. 6, 431.

Eastes, W., and Secrest, D. (1972),
J. Chem. Phys. 56, 640.

Eno, L., Balint-Kurti, G.G., and Saktreger (1978),
Chem. Phys. 29, 453.

Eno, L., and Balint-Kurti, G.G. (1979),
J. Chem. Phys. 71. 1447.

Eno, L., and Balint-Kurti, G.G. (1981),
J. Chem. Phys. 75, 690.

Field, G.B., (1974),
Atomic and Molecular Physics and the Interstellar Medium : Course at Les Houches, edited by R. Balian, P. Encrenaz and J. Lequeux (Amsterdam : North Holland).

Flower, D.R. (1983),
NATO ASI "Diffuse Matter in Galaxies", (Dordrecht:Reidel).

Ford, K.W., and Wheeler, J.A. (1959),
Annals of Physics 7, 259.

Gautier, T.N., Fink, U., Treffers, R.P., and Larson, H.P. (1976),
Astrophysical Journal Letters 207, L129.

Gerber, R.B., Beard, L.H., Kouri, D.J. (1981),
J. Chem. Phys. 74, 4709.

Gianturco, F.A., and Lamanna, U.T. (1977),
Chem. Phys. 25, 401.

Giese, C.F., and Gentry, W.R. (1974),
Physical Review A 10, 2156.

Goldflam, R., Green S., and Kouri, D.J. (1977a),
J. Chem. Phys. 67, 4149.

Goldflam, R., Kouri, D.J., and Green S. (1977b),
J. Chem, Phys. 67, 5661.

Gordon, M.D., and Secrest, D. (1970),
J. Chem. Phys. 52, 120.

Gordon, R.G. (1969),
J. Chem. Phys. 51, 14.

Gradshteyn, I.S., and Ryzhik, I.M. (1980),
Tables of Integrals, Series and Products (London:Academic).

Green, S. (1974),
Atomic and Molecular Physics and the Interstellar Medium : Course at Les Houches, edited by R. Balian, P. Encrenaz and J. Lequeux (Amsterdam : North-Holland).

Green, S. (1975),
Chem. Phys. 38, 293.

Green, S. (1976),
J. Chem. Phys. 65, 68.

Green, S. (1978),
Chem. Phys. 41, 425.

Hermann, V., Schmidt, H. and Linder F. (1978),
J. Phys. B 11, 493.

Hoffman, D.K., Chan, C., and Kouri, D.J. (1979),
Chem. Phys. 42, 1.

Hollenbach, D.J., and Shull, J.M. (1977),
Astrophysical Journal 216, 419.

Hunter, L.W. (1975),
J. Chem. Phys. 62, 2855.

Johnston, B.R., and Secrest, D. (1966),
Journal of Mathematical Physics, 7, 2187.

Johnston, B.R. (1973),
Journal of Computational Physics 13, 445.

Khare, V. (1977),
J. Chem. Phys. 67, 3897.

Khare, V. (1978),
J. Chem. Phys. 68, 4631.

Kinnersley, (1979),
Molecular Physics 38, 1329.

Kolos, W., and Wolniewicz, L. (1965),
J. Chem. Phys. 43, 2429.

Kolos, W., and Wolniewicz, L. (1967),
J. Chem. Phys. 46, 1426.

Kouri, D.J., and McGuire, P. (1974),
Chem. Phys. Letters 29, 414.

Kouri, D.J., Heil, T.G., and Shimoni, Y. (1976),
J. Chem. Phys. 65, 1462.

Kouri, D.J. (1979),
Atom-Molecule Collision Theory : A Guide for the Experimentalist, edited by R.B. Bernstein (New York : Plenum).

Krauss, M., and Mies, F. (1965),
J. Chem. Phys. 42, 2703.

Lester, W.A., and Schaefer, J. (1973),
Chem. Phys. Letters 20, 575.

Lester, W.A. (1976),
Modern Theoretical Chemistry, Vol. 1, edited by W.H. Miller, (New York : Plenum).

Light, J.C. (1971),
Methods of Computational Physics, Vol. 10, edited by B. Alder, S. Fernbach and M. Rotenberg (New York : Academic).

Light, J.C., and Walker, R.B. (1976),
J. Chem. Phys. 65, 4272.

Lin, C.S., and Secrest D. (1977),
J. Chem. Phys. 67, 1291.

Lin, C.S., and Secrest, D. (1979),
J. Chem. Phys. 70, 199.

Lin, C.S., (1979),
J. Chem. Phys. 70, 1791.

Lin, C.S.,(1980a),
J. Chem. Phys. 73, 1138.

Lin, C.S., (1980b),
J. Chem. Phys. 73, 1159.

Lin, C.S., (1981),
J. Chem. Phys. 74, 5928.

Marcus, R.A. (1972),
J. Chem. Phys. 56, 3548.

McGuire, P., and Micha, D., (1972),
International Journal of Quantum Chemistry, 6, 111.

McGuire, P., and Kouri, D.J. (1974),
J. Chem. Phys. 60 , 2488.

McGuire, P., and Toennies, J.P., (1975),
J. Chem. Phys. 62, 4623.

McGuire, P. (1976),
J. Chem. Phys. 65, 3275.

Mies, F.H, (1964),
J. Chem. Phys. 40, 523.

Miller, W.H. (1971),
J. Chem. Phys. 54, 5386.

Miller, W.H. (1974),
Advances in Chemical Physics 25, 69.

Oka, T. (1973),
Advances in Atomic and Molecular Physics 9, 127.

Orlikowski, T. (1981),
Chem. Phys. 61, 405.

Pack, R.T. (1974),
J. Chem. Phys. 60, 633.

Percival, I.C., and Seaton, M.J. (1957),
Proceedings of the Cambridge Pilosophical Society 53, 654.

Percival, I.C., and Richards, D. (1970),
J. Phys. B, 3, 1035.

Rabitz, H. (1972),
J. Chem. Phys. 57, 1718.

Rabitz, H., and Zarur, G. (1974),
J. Chem. Phys. 61, 5076.

Rabitz, H. (1976),
Modern Theoretical Chemistry, Vol. 1, edited by W.H. Miller (New York : Plenum).

Raczkowski, A.W., and Lester, W.A. (1977),
Chem. Phys. Letters 47, 45.

Raczkowski, A.W., Lester, W.A., and Miller, W.H. (1978),
J. Chem. Phys. 69, 2692.

Rose, M.E. (1957),
Elementary Theory of Angular Momentum (New York : John Wiley).

Sams, W.N., and Kouri, D.J. (1969),
J. Chem. Phys. 51, 4815.

Schaefer, J., and Lester, W.A. (1973),
Chem. Phys. Letters 20, 575.

Schaefer, H.F. (1972),
The Electronic Structure of Atoms and Molecules : A Survey of Rigorous Quantum Mechanical Results (Reading, Mass. : Addison-Wesley).

Schinke, R. (1977),
Chem. Phys. 24, 379.

Schinke, R., Kruger, H., Hermann, V., Schmidt, H., and Linder, F., (1977),
J. Chem. Phys. 67, 1187.

Schinke, R., and McGuire, P. (1978a),
Chem. Phys. 28, 129.

Schinke, R., and McGuire, P. (1978b),
Chem. Phys. 31, 391.

Schinke, R., Dupuis, M., and Lester, W.A., (1980),
J. Chem. Phys. 72, 3909.

Schinke, R., (1980),
J. Chem. Phys. 72, 3916.

Schmidt, H., Hermann, V., and Linder, F. (1976),
Chem. Phys. Letters 41, 365.

Secrest, D., and Johnston, B.R. (1966),
J. Chem. Phys. 45, 4556.

Secrest, D., (1975),
J. Chem. Phys. 62, 710.

Secrest, D., (1979),
Atom-Molecule Collision Theory : A Guide for the Experimentalist, edited by R.B. Bernstein (New York : Plenum).

Shafer, R., and Gordon, R.G. (1973),
J. Chem. Phys. 58, 5422.

Simon, M., Righini-Cohen, G., Joyce, R.R., and Simon, T. (1979),
Astrophysical Journal 230, L175.

Stechel, E.B., Walker, R.B., and Light, J.C. (1978),
J. Chem. Phys. 69, 3518.

Thiele, E., and Weare, J. (1968),
J. Chem. Phys. 48, 2324.

Toennies, J.P., (1976),
Annual Review of Physical Chemistry 27, 225.

Truhlar, D.G., (1972),
International Journal of Quantum Chemistry 6, 975.

Tsapline, B., and Kutzelnigg, W. (1973),
Chem. Phys. Letters, 23, 173.

Tsien, T.P., and Pack, R.T. (1970),
Chem. Phys. Letters, 6, 54.

Tsien, T.P., Parker, G.A., and Pack, R.T., (1973),
J. Chem. Phys. 59, 5373.

Udseth, H., Giese, C.F., and Gentry, W.R., (1973),
Physical Review A 8, 2483.

Wagner, A.F., and McKoy, V. (1973),
J. Chem. Phys. 58, 2604.

Watson, W.D., (1974),
Atomic and Molecular Processes and the Interstellar Medium :
Course at Les Houches, edited by R. Balian, P. Encrenaz
and J. Lequeux (Amsterdam : North Holland).

Wilson, D.J., and Cheung, A.S. (1969),
J. Chem. Phys. 51, 3448.

Zarur, G., and Rabitz, H., (1974),
J. Chem. Phys. 60, 2057.

Zvijac, D.J., and Light, J.C. (1976),
Chem. Phys. 12, 237.

# APPENDIX

This appendix contains all the results of the close coupling and infinite order sudden approximation calculations of cross sections for rovibrational excitation of $H_2$ by He detailed in Chapter IV.

Notes

1. Cross sections in units of $\mathring{A}^2$, energy in units of $\varepsilon$ = 0.26881eV. Cross sections accumulated from total angular momentum J = 0 to JMAX. 0.20620D + 01 denotes $0.20620 \times 10^1$.

2. Close coupling results are presented as $\sigma(i \rightarrow f)$ and the $H_2$ states are specified as (vj). Not all close coupling calculations are complete. See Chapter IV, Table 5 for details.

3. For the IOS calculations only $\sigma(v0 \rightarrow v'j')$ are reported. All other cross sections can be trivially calculated from equation IV.3.6 (page 99).

4. IOS results for E = 1.5eV + 2$\varepsilon$ are reported only for transitions between v = 0,1. Although higher vibrational states are open, the cross sections between levels with v > 1 were not saved due to lack of computer storage required to hold the partial cross sections.

5. Close coupling results at E = 3$\varepsilon$ for para $H_2$ + He and ortho $H_2$ + He are presented in Chapter IV, Tables 11 and 14b respectively.

## CLOSE COUPLING RESULTS

E=2.02 $\mathcal{E}$  JMAX=12

| F \ I | (0,0) | (0,2) | (0,4) | (0,6) | (1,0) |
|---|---|---|---|---|---|
| (0,0) | 0.20620D+01 | 0.16552D+00 | 0.83329D-02 | 0.29532D-04 | 0.20670D-09 |
| (0,2) | 0.76139D+00 | 0.17024D+01 | 0.90103D-01 | 0.03424D-03 | 0.39584D-09 |
| (0,4) | 0.54992D-01 | 0.12927D+00 | 0.21605D+01 | 0.15357D-01 | 0.12483D-09 |
| (0,6) | 0.16887D-03 | 0.78843D-03 | 0.13306D-01 | 0.34123D+01 | 0.69478D-11 |
| (1,0) | 0.20464D-11 | 0.85196D-12 | 0.18727D-12 | 0.12029D-13 | 0.69014D+02 |

E=2.10 $\mathcal{E}$  JMAX=60

| F \ I | (0,0) | (0,2) | (0,4) | (0,6) | (1,0) |
|---|---|---|---|---|---|
| (0,0) | 0.41611D+02 | 0.76950D+00 | 0.23582D-01 | 0.79970D-04 | 0.19064D-08 |
| (0,2) | 0.35514D+01 | 0.26214D+02 | 0.36693D+00 | 0.20376D-02 | 0.47724D-08 |
| (0,4) | 0.15778D+00 | 0.53197D+00 | 0.25598D+02 | 0.53813D-01 | 0.15821D-08 |
| (0,6) | 0.47947D-03 | 0.26470D-02 | 0.48221D-01 | 0.26432D+02 | 0.85587D-10 |
| (1,0) | 0.90780D-10 | 0.49242D-10 | 0.11260D-10 | 0.67976D-12 | 0.60628D+02 |

E=2.15 $\mathcal{E}$  JMAX=20

| F \ I | (0,0) | (0,2) | (0,4) | (0,6) | (1,0) |
|---|---|---|---|---|---|
| (0,0) | 0.56203D+01 | 0.37643D+00 | 0.18273D-01 | 0.80885D-04 | 0.51418D-08 |
| (0,2) | 0.17406D+01 | 0.40838D+01 | 0.20743D+00 | 0.18070D-02 | 0.13160D-07 |
| (0,4) | 0.12324D+00 | 0.30255D+00 | 0.51406D+01 | 0.40351D-01 | 0.45928D-08 |
| (0,6) | 0.49813D-03 | 0.24066D-02 | 0.36845D-01 | 0.80777D+01 | 0.24705D-09 |
| (1,0) | 0.35873D-09 | 0.19856D-09 | 0.47509D-10 | 0.27988D-11 | 0.58579D+02 |

E=2.50 $\mathcal{E}$  JMAX=60

| F \ I | (0,0) | (0,2) | (0,4) | (0,6) | (1,0) | (1,2) |
|---|---|---|---|---|---|---|
| 0,0) | 0.40258D+02 | 0.82914D+00 | 0.35273D-01 | 0.24623D-03 | 0.27920D-06 | 0.81945D-08 |
| 0,2) | 0.38777D+01 | 0.42836D+02 | 0.72098D+00 | 0.73854D-02 | 0.64767D-06 | 0.83690D-07 |
| 0,4) | 0.24904D+00 | 0.10684D+01 | 0.44727D+02 | 0.17497D+00 | 0.40529D-06 | 0.46171D-06 |
| 0,6) | 0.17522D-02 | 0.11238D-01 | 0.17636D+00 | 0.47198D+02 | 0.23170D-07 | 0.10124D-06 |
| 1,0) | 0.55840D-07 | 0.27698D-07 | 0.11461D-07 | 0.65118D-09 | 0.51732D+02 | 0.23922D+00 |
| 1,2) | 0.56149D-08 | 0.12260D-07 | 0.44809D-07 | 0.97476D-08 | 0.81958D+00 | 0.54194D+02 |

E=1.5eV+2ε  JMAX=90

| I (F) | (0,0) | (0,2) | (0,4) | (0,6) | (1,0) |
|---|---|---|---|---|---|
| (0,0) | 0.32854D+02 | 0.68347D+00 | 0.10526D+00 | 0.15[illegible]D-01 | 0.11694D-02 |
| (0,2) | 0.43232D+01 | 0.35051D+02 | 0.14889D+01 | 0.19137D+00 | 0.41803D-02 |
| (0,4) | 0.13816D+01 | 0.25437D+01 | 0.35968D+02 | 0.12777D+01 | 0.97018D-02 |
| (0,6) | 0.17196D+00 | 0.43251D+00 | 0.16902D+01 | 0.58417D+02 | 0.52245D-02 |
| (1,0) | 0.86084D-03 | 0.62978D-03 | 0.85956D-03 | 0.54772D-03 | 0.54955D+02 |
| (1,2) | 0.32772D-02 | 0.35012D-02 | 0.33405D-02 | 0.25[illegible]D-02 | 0.46750D+01 |
| (1,4) | 0.21948D-02 | 0.26592D-02 | 0.38045D-02 | 0.90539D-02 | 0.12152D+01 |
| (1,6) | 0.30402D-03 | 0.50008D-03 | 0.12048D-02 | 0.30152D-02 | 0.10036D+00 |
| (2,0) | 0.47475D-06 | 0.30099D-06 | 0.14676D-05 | 0.37415D-05 | 0.41450D-05 |
| (2,2) | 0.12954D-05 | 0.14018D-05 | 0.13097D-05 | 0.12007D-05 | 0.11096D-02 |
| (2,4) | 0.45600D-06 | 0.64707D-06 | 0.13020D-05 | 0.32186D-05 | 0.45562D-03 |
| (2,6) | 0.12887D-07 | 0.17732D-07 | 0.32169D-07 | 0.80522D-07 | 0.19747D-04 |
| (3,0) | 0.80102D-11 | 0.53739D-11 | 0.21416D-11 | 0.94279D-11 | 0.64463D-08 |
| (3,2) | 0.68049D-11 | 0.13007D-10 | 0.37437D-10 | 0.90264D-10 | 0.51651D-06 |
| (3,4) | 0.25894D-12 | 0.57131D-12 | 0.20152D-11 | 0.63383D-11 | 0.30952D-09 |

| I (F) | (1,2) | (1,4) | (1,6) | (2,0) | (2,2) |
|---|---|---|---|---|---|
| (0,0) | 0.91621D-03 | 0.36566D-03 | 0.39584D-04 | 0.10052D-05 | 0.57308D-06 |
| (0,2) | 0.47897D-02 | 0.21679D-02 | 0.31862D-03 | 0.51164D-05 | 0.30347D-05 |
| (0,4) | 0.78077D-02 | 0.52990D-02 | 0.13114D-02 | 0.25978D-05 | 0.46442D-05 |
| (0,6) | 0.39088D-02 | 0.16682D-01 | 0.43418D-02 | 0.87605D-05 | 0.53743D-05 |
| (1,0) | 0.96172D+00 | 0.14903D+00 | 0.96672D-02 | 0.94[illegible]D-03 | 0.36156D-03 |
| (1,2) | 0.37328D+02 | 0.14855D+01 | 0.13527D+00 | 0.17501D-02 | 0.20786D-02 |
| (1,4) | 0.24928D+01 | 0.38412D+02 | 0.10753D+01 | 0.45604D-02 | 0.38835D-02 |
| (1,6) | 0.29046D+00 | 0.13759D+01 | 0.40805D+02 | 0.17237D-02 | 0.35963D-02 |
| (2,0) | 0.22844D-03 | 0.35884D-03 | 0.10600D-03 | 0.37465D+02 | 0.10330D+01 |
| (2,2) | 0.13137D-02 | 0.14643D-02 | 0.10564D-02 | 0.49435D+01 | 0.40225D+02 |
| (2,4) | 0.65047D-03 | 0.12966D-02 | 0.42064D-02 | 0.81349D+00 | 0.21140D+01 |
| (2,6) | 0.32615D-04 | 0.82365D-04 | 0.23987D-03 | 0.27052D-01 | 0.99772D-01 |
| (3,0) | 0.32592D-08 | 0.17946D-08 | 0.12509D-07 | 0.11521D-04 | 0.50099D-05 |
| (3,2) | 0.11851D-07 | 0.37839D-07 | 0.89882D-07 | 0.78922D-05 | 0.19851D-04 |
| (3,4) | 0.88688D-09 | 0.45114D-08 | 0.25824D-07 | 0.11004D-05 | 0.33136D-05 |

E=1.5eV+2ε  JMAX=90  (CONTINUED)

| F \ I | (2,4) | (2,6) | (3,0) | (3,2) | (3,4) |
|---|---|---|---|---|---|
| (0,0) | 0.12515D-06 | 0.29978D-08 | 0.36404D-10 | 0.72112D-11 | 0.20163D-12 |
| (0,2) | 0.86898D-06 | 0.20185D-07 | 0.12615D-09 | 0.67449D-10 | 0.21769D-11 |
| (0,4) | 0.29872D-05 | 0.62602D-07 | 0.85390D-10 | 0.53168D-09 | 0.13119D-10 |
| (0,6) | 0.97698D-05 | 0.15519D-06 | 0.50019D-09 | 0.10579D-08 | 0.55015D-10 |
| (1,0) | 0.92050D-04 | 0.33902D-05 | 0.22772D-07 | 0.40278D-08 | 0.17742D-09 |
| (1,2) | 0.63854D-03 | 0.27139D-04 | 0.55925D-07 | 0.44923D-07 | 0.24712D-08 |
| (1,4) | 0.21359D-02 | 0.11501D-03 | 0.51675D-07 | 0.24189D-06 | 0.21066D-07 |
| (1,6) | 0.88665D-02 | 0.42857D-03 | 0.46088D-06 | 0.73150D-06 | 0.15444D-06 |
| (2,0) | 0.10609D+00 | 0.29723D-02 | 0.26102D-04 | 0.39501D-05 | 0.40478D-06 |
| (2,2) | 0.13114D+01 | 0.52463D-01 | 0.54324D-04 | 0.47502D-04 | 0.58321D-05 |
| (2,4) | 0.41876D+02 | 0.60557D+00 | 0.21240D-03 | 0.26375D-05 | 0.73545D-04 |
| (2,6) | 0.71442D+00 | 0.44342D+02 | 0.53129D-03 | 0.14174D-02 | 0.14586D-02 |
| (3,0) | 0.12151D-04 | 0.25764D-04 | 0.42861D+02 | 0.96937D+00 | 0.30069D-01 |
| (3,2) | 0.68305D-04 | 0.31116D-03 | 0.43881D+01 | 0.46198D+02 | 0.57538D+00 |
| (3,4) | 0.25921D-04 | 0.43574D-03 | 0.18524D+00 | 0.78305D+00 | 0.56501D+02 |

## IOS CROSS SECTIONS

E=2.02ε JMAX=61

| | (0,0→0,j) | (0,0→1,j) | (1,0→0,j) | (1,j→1,j) |
|---|---|---|---|---|
| j=0 | 0.40344E+02 | 0.41833E-12 | 0.42254E-10 | 0.68698E+02 |
| j=2 | 0.45392E+01 | 0.34059E-12 | 0.34402E-10 | 0.26224E+00 |
| j=4 | 0.59693E+00 | 0.91795E-13 | 0.92720E-11 | 0.10562E-02 |
| j=6 | 0.43821E-01 | 0.79356E-14 | 0.80155E-12 | 0.53074E-05 |
| j=8 | 0.20480E-02 | 0.35420E-15 | 0.35776E-13 | 0.33745E-07 |
| j=10 | 0.68016E-04 | 0.10211E-16 | 0.10314E-14 | 0.16080E-08 |
| j=12 | 0.17385E-05 | 0.19697E-18 | 0.19895E-16 | 0.98795E-08 |

---

E=2.1ε JMAX=61

| | (0,0→0,j) | (0,0→1,j) | (1,0→0,j) | (1,j→1,j) |
|---|---|---|---|---|
| j=0 | 0.40067E+02 | 0.23428E-10 | 0.49199E-09 | 0.59694E+02 |
| j=2 | 0.45908E+01 | 0.21134E-10 | 0.44381E-09 | 0.88642E+00 |
| j=4 | 0.62615E+00 | 0.66119E-11 | 0.13885E-09 | 0.93017E-02 |
| j=6 | 0.47681E-01 | 0.67737E-12 | 0.14225E-10 | 0.76678E-04 |
| j=8 | 0.23071E-02 | 0.35637E-13 | 0.74838E-12 | 0.59197E-06 |
| j=10 | 0.79149E-04 | 0.12369E-14 | 0.25975E-13 | 0.59885E-08 |
| j=12 | 0.20847E-05 | 0.32903E-16 | 0.69097E-15 | 0.14563E-08 |

---

E=2.5ε JMAX=61

| | (0,0→0,j) | (0,0→1,j) | (1,0→0,j) | (1,j→1,j) |
|---|---|---|---|---|
| j=0 | 0.38762E+02 | 0.14333E-07 | 0.71666E-07 | 0.49790E+02 |
| j=2 | 0.47945E+01 | 0.17079E-07 | 0.85395E-07 | 0.26473E+01 |
| j=4 | 0.76989E+00 | 0.73151E-08 | 0.36575E-07 | 0.10929E+00 |
| j=6 | 0.69159E-01 | 0.11136E-08 | 0.55678E-08 | 0.26656E-02 |
| j=8 | 0.39166E-02 | 0.84500E-10 | 0.42250E-09 | 0.46270E-04 |
| j=10 | 0.15567E-03 | 0.40330E-11 | 0.20165E-10 | 0.64653E-06 |
| j=12 | 0.46988E-05 | 0.13933E-12 | 0.69665E-12 | 0.82827E-08 |

---

E=3.0ε JMAX=71

| | (0,0→0,j) | (0,0→1,j) | (1,0→0,j) | (1,j→1,j) |
|---|---|---|---|---|
| j=0 | 0.37667E+02 | 0.39727E-06 | 0.11918E-05 | 0.45007E+02 |
| j=2 | 0.49533E+01 | 0.60308E-06 | 0.18092E-05 | 0.38400E+01 |
| j=4 | 0.94108E+00 | 0.31712E-06 | 0.95135E-06 | 0.30044E+00 |
| j=6 | 0.10060E+00 | 0.63728E-07 | 0.19118E-06 | 0.13281E-01 |
| j=8 | 0.67303E-02 | 0.63440E-08 | 0.19032E-07 | 0.38944E-03 |
| j=10 | 0.31301E-03 | 0.38820E-09 | 0.11646E-08 | 0.85288E-05 |
| j=12 | 0.10941E-04 | 0.16753E-10 | 0.50260E-10 | 0.15462E-06 |

E=5.0ℰ  JMAX=91

| | (0,0→0,j) | (0,0→1,j) | (0,0→2,j) |
|---|---|---|---|
| j=0 | 0.34570E+02 | 0.53353E-04 | 0.42875E-10 |
| j=2 | 0.49964E+01 | 0.15702E-03 | 0.85969E-10 |
| j=4 | 0.14897E+01 | 0.12461E-03 | 0.45176E-10 |
| j=6 | 0.26008E+00 | 0.44755E-04 | 0.13572E-10 |
| j=8 | 0.28005E-01 | 0.81502E-05 | 0.29391E-11 |
| j=10 | 0.20483E-02 | 0.88947E-06 | 0.41960E-12 |
| j=12 | 0.10994E-03 | 0.65956E-07 | 0.40158E-13 |

| | (1,0→0,j) | (1,0→1,j) | (1,0→2,j) |
|---|---|---|---|
| j=0 | 0.88921E-04 | 0.37369E+02 | 0.67437E-06 |
| j=2 | 0.26170E-03 | 0.52731E+01 | 0.11093E-05 |
| j=4 | 0.20768E-03 | 0.11405E+01 | 0.65610E-06 |
| j=6 | 0.74592E-04 | 0.13953E+00 | 0.15137E-06 |
| j=8 | 0.13584E-04 | 0.10653E-01 | 0.17200E-07 |
| j=10 | 0.14824E-05 | 0.56339E-03 | 0.11935E-08 |
| j=12 | 0.10993E-06 | 0.22333E-04 | 0.58121E-10 |

| | (2,0→0,j) | (2,0→1,j) | (1,0→2,j) |
|---|---|---|---|
| j=0 | 0.21438E-09 | 0.20231E-05 | 0.44741E+02 |
| j=2 | 0.42984E-09 | 0.33279E-05 | 0.42889E+01 |
| j=4 | 0.22588E-09 | 0.19683E-05 | 0.38484E+00 |
| j=6 | 0.67859E-10 | 0.45411E-06 | 0.19473E-01 |
| j=8 | 0.14696E-10 | 0.51599E-07 | 0.65132E-03 |
| j=10 | 0.20980E-11 | 0.35806E-08 | 0.16209E-04 |
| j=12 | 0.20079E-12 | 0.17436E-09 | 0.32926E-06 |

---

E=1.5eV+1ℰ  JMAX=131

| | (0,0→0,j) | (0,0→1,j) | (1,0→0,j) | (1,j→1,j) |
|---|---|---|---|---|
| j=0 | 0.32457E+02 | 0.43397E-03 | 0.58952E-03 | 0.33749E+02 |
| j=2 | 0.46017E+01 | 0.21100E-02 | 0.28662E-02 | 0.50244E+01 |
| j=4 | 0.18780E+01 | 0.21678E-02 | 0.29447E-02 | 0.18309E+01 |
| j=6 | 0.48655E+00 | 0.11276E-02 | 0.15318E-02 | 0.40617E+00 |
| j=8 | 0.77552E-01 | 0.31235E-03 | 0.42431E-03 | 0.55455E-01 |
| j=10 | 0.82717E-02 | 0.51855E-04 | 0.70441E-04 | 0.51051E-02 |
| j=12 | 0.63736E-03 | 0.57671E-05 | 0.78341E-05 | 0.34239E-03 |